Coupled Marine Boundary Layers and Air-Sea Interaction Initiative: Combining Process Studies, Simulations, and Numerical Models

James Edson, Terri Paluszkiewicz, Scott Sandgathe, Linwood Vincent, Louis Goodman, Tom Curtin, John Hollister, and Marie Colton

Office of Naval Research

and

Steven Anderson, Edgar Andreas, Stephen Burk, Shuyi Chen, Gennaro Crescenti, Eric D'Asaro, Kenneth Davidson, Mark Donelan, James Doyle, David Farmer, Ann Gargett, Hans Graber, Dale Haidvogel, Jeff Kepert, Larry Mahrt, Michiko Martin, Julie McClean, Wade McGillis, Sean McKenna, James McWilliams, Peter Niiler, David Rogers, Eric Skyllingstad, Peter Sullivan, Robert Weller, and James Wilczak

August 25, 1999
Revision 5.0

Table of Contents

1. Introduction

Weather, wave and ocean forecasts have a profound impact on Naval operations around the world. Beside providing information about expected changes in the battlespace environment, these forecasts are also used to provide much needed information about the visibility of the fleet and their ability to peer through the atmosphere and ocean. Increasingly, these forecasts are required to provide ever more detailed information without losing their generality, i.e., they must be applicable over much of the globe. Since many of the fleet's operations take place on or near the ocean surface, realtime information on the dynamic structure of the marine boundary layers is especially important.

The dynamics of the coupled marine boundary layers are driven by a myriad of interactive processes. For example, in *Air-Sea Interactions*, Kraus and Businger (1994) list parameters that are expected to influence the drag that the atmosphere experiences as it blows over the ocean, these include wave age, stability, gustiness, fetch, and sea-state. Kraus and Businger state that "A careful study of the interrelation between these parameters is needed, both theoretically and experimentally. It clearly must include a major systematic, well-organized observation program of sea state and the structure of the atmospheric boundary layer ..."

Over the past two decades, the Office of Naval Research has sponsored several research initiatives designed to investigate some of these processes. The initial studies generally assumed that the coupling between the ocean and atmosphere involves horizontally homogeneous processes. This was a reasonable approach since it allowed investigators to focus on 1-D processes that were most applicable to the Navy's blue water operations. In recent years, the Navy has had to focus more and more of it operations in the littoral zones surrounding regional conflicts. To better understand the environmental factors that are unique to this environment, Navy-sponsored research has focused on increasingly more complex topics, including the response of the atmosphere to strong oceanic gradients (FASINEX); the effects of sea spray on the humidity exchange (HEXOS); directional wind-wave evolution and its effect on mixed layer dynamics (SWADE/SWAPP); the modulation of short wind waves by small-scale processes (HiRes); the effect of coastal processes on momentum, mixing, and heat exchange (RASEX, CMO); and the role of coherent structures in the wind, wave, and current fields in modulating momentum and energy exchange (MBL).

In the following sections, we begin with a short description of the Navy's requirements for operations within the coupled boundary layers. We then describe in some detail our current understanding of the processes that occur within the coupled boundary layers. In these descriptions, we attempt to include what is known and unknown about each process, and include discussions about compelling research issues and research needs. The sections that follow provide examples of how these processes are included in numerical models, including some of the strengths and weaknesses of the various approaches.

2. Navy Requirements

The Navy operates over, in, and under the atmosphere-ocean interface. This interface is both the background and the lens for Navy surveillance, search, and strike operations, as well as the medium in which it must survive without damage to platforms and personnel. It is difficult to argue that the success of any other national enterprise depends more heavily on resolving the structure and understanding the behavior of the air-sea interface. When the U.S. Navy developed its post-cold-war maritime strategy and took the bold steps, "Forward—From The Sea," moving the focus of Naval operations from the blue water of the open ocean to the more turbid waters of the littoral environment, it moved into an environment of drastically increased complexity. This highly variable marine environment greatly affects Navy operations such as submarine and mine detection, moving equipment and supplies over the beach, cruise missile targeting, and aircraft carrier operations. This environment also affects the performance of the sensors and systems used by the warfighter.

Knowledge of this environment and its impact on the various sensors available to the warfighter are critical to the choice of sensors, ability to gain knowledge of the tactical battlespace, and effective delivery of weapons. Knowledge of the ocean battlespace environment is important to the Joint Warfighter S&T areas of Information Superiority, Precision Force, Combat Identification, Joint Countermine, Joint Theater Missile Defense, and Joint Readiness and Logistics. These needs translate to the requirements for understanding processes and phenomenology; measurements and mapping; nowcasts and forecasts of ocean and atmospheric variability; and translating observed environmental effects to their impacts on sensors, platforms, structures, and operations.

In addition to the change of focus environmentally, the nature of conflict has evolved to highly localized and intense, but short-lived, battles involving high-tech weaponry. This, in turn, has shifted the focus of atmospheric and oceanographic environmental support to the warfighter. This shift emphasizes the need for battlespace awareness products in greater detail, spatially and temporally, than were ever required in the strategically-driven cold war. The increasing use of weapons, intelligence, and surveillance systems operating at visible, infrared, and microwave frequencies places greater dependence on information relating to the radiative and physical characteristics of the lower atmosphere.

A. Electromagnetic Characteristics of Marine Boundary Layers

On the atmospheric side of the air-sea interface, Navy communications, electronic warfare, and electromagnetic detection (radar) are very sensitive to small changes in the atmospheric boundary layer (ABL) humidity and temperature structure. The surface-based duct, normally tied to the top of the marine ABL, acts as a wave guide for electromagnetic energy. The strength and height of the waveguide determine the frequency and degree of trapping of the energy, which can allow detection of electromagnetic energy at ranges up to a thousand miles. However, the duct can dramatically increasing radar surface clutter, and horizontal variability can cause anomalous communications due to radar holes and fades. In addition, the evaporative duct generated by the strong moisture and temperature gradients at the immediate ocean surface also acts as a wave guide for higher frequency systems. A study by Konstanzer (1994) demonstrated a change greater than 50% in the SPY-1 radar detection range of certain near-surface targets with a two meter change in evaporative duct height, a sensitivity with significant implications for ship self-defense operations.

B. Electro-Optical Characteristics of Marine Boundary Layers

The marine ABL is also optically significant for Navy operations. Fog has proven to be extremely difficult to reliably predict in the marine coastal zone, yet it has an almost insurmountable effect on some Navy operations. Although the occurrence of fog depends on very slight variations in air-sea temperature differences, moisture, and aerosol distributions, it can dramatically slow ship operations, cancel air operations, and make resupply and search and rescue operations ineffective. Beyond these safety and operations impacts, the Navy's strike and ship self-defense systems are relying much more on optical sensors whose performance degrades significantly in fog and haze. Additionally, marine aerosol, especially in the lowest 10 m above the surface, dramatically hinder the detection of small surface craft, degrade cruise missile effectiveness, and hinder the detection of low-flying threats. Finally, besides these more obvious effects on optical systems, low-level atmospheric gradients and turbulence lead to scintillation and mirages that also degrade the performance of these systems.

Often, stratus clouds cap the marine ABL. Low stratus clouds effectively block optical surveillance from satellites and aircraft. Conversely, if accurately forecast, clouds can provide Navy platforms and personnel with the tactical advantage of cover. The light rain produced by marine stratus, once considered a mere annoyance to Naval operations, now impacts both surveillance and targeting sensors as Navy systems become more sophisticated. The capability to predict fog, stratus, and EM/EO propagation characteristics is required to maximize the effectiveness of high-tech weapons, optimize the employment of surveillance assets, and ensure battlegroup safety against low-flying cruise missiles.

The Navy is also interested in ocean optics for submarine and mine detection as well as for communications. Clearly, ocean turbidity impairs optical propagation and is related to ocean mixing and wave action. Additionally, ocean biological activity, including bioluminescence, is very sensitive to changes in ocean mixing and structure brought about by processes driven by air-sea interaction. The impact of this biological activity on ocean optics can be extremely important to swimmer insertions and other Navy operations.

C. Acoustic Characteristics of the Oceanic Boundary Layer

Many of these same sensor and detection problems exist below the sea surface. The thermal and saline structure of the oceanic mixed layer can provide the similar ducting conditions for the propagation of sound as the ABL provides for the propagation of electromagnetic energy. Changes in the mean structure of the temperature and salinity fields lead to changes in the detection and counter-detection ranges of submarines and weapons (e.g., acoustic mines). The variations in the mean ocean structure combine with variations caused by ocean turbulence to produce signal fluctuations and fades in both acoustic communications and tracking.

Additionally, the ocean **surface** acoustic characteristics have become a determining factor in system performance for an increasing range of Navy interests, such as surveillance, mine countermeasures, and acoustic communication. Bubbles generated by breaking waves are the dominant scattering target at higher frequencies and can have important implications at lower frequencies. These bubbles can completely change propagation characteristics. These characteristics change over shorter time scales (i.e., hours) than other upper ocean properties such as temperature (i.e., days or weeks). As with EM/EO propagation above the surface, accurate prediction of acoustic propagation, especially at higher frequencies, requires a detailed understanding of how air-sea interaction affects near surface processes.

D. Forecasting Severe Weather

Tropical cyclones (hurricanes, typhoons, etc.) affect Navy operations around the globe, often costing many millions of dollars, either in the cost to sortie or to take evasive action or in the cost to repair equipment and structures. Improving predictions of both track and intensity should lead to reduced sortie costs and lower damage costs, as preventive measures are generally more effective when the degree of prevention required is more accurately known. Many studies (e.g., Ooyama 1969; Rosenthal 1971; Rotunno and Emanuel 1987; Bender et al. 1993; Tuleya 1994; Emanuel 1995) suggest that cyclone intensity, wind structure and track depend on the exchange of heat, moisture, and momentum between the ocean and atmosphere, particularly at very high wind speeds, where these exchanges are poorly understood.

E. Wave Dynamics and Wave Forecasts

Surface waves have traditionally been the nemesis of Navy operations. Historically, waves have damaged or destroyed ships, broken piers and logistics structures, and prevented amphibious operations. As our capabilities to predict wave and surf conditions have improved, the sensitivity of Navy operations to waves has increased. Waves directly impair swimmer and special forces operations. Wave-induced motion and wave-related processes (e.g., spray and bubble production) degrade the capabilities of new technologies used in mine warfare, ship- and submarine-based guidance systems, and communications system as described above. They are also the background field for satellite surveillance and radar periscope detection, where improved understanding of wave behavior should lead to reduced signal-to-noise ratio and thus, better detections.

F. Coupled Ocean-Atmosphere Forecasts and Guidance

Understanding the coupling of the atmosphere and ocean across the air-sea interact is essential for predicting the large-scale circulation of both media. Atmospheric forcing drives ocean currents (Ekman transport), provides mixing, and generates waves. On a larger scale, horizontal variability of the atmospheric forcing drives vertical motions in the ocean that we associate with upwelling and downwelling events. In turn, the ocean provides moisture and heat to drive the large-scale atmospheric circulation. The ocean also presents ever-changing surface drag to the atmosphere through waves and provides a source of atmospheric aerosols and gases. Both the ocean and the atmosphere interact to govern the production, movement, and decay of sea ice.

Improved understanding of the general and cumulative effect of these interactions should lead to a theater-level battlespace awareness system that can be activated on short notice to characterize and predict the natural environment anywhere and anytime warfighter requirements dictate. This system would support improved knowledge of weather conditions, acoustic conditions, EM/EO propagation, and dispersion of chemical and biological agents and aerosols. This capability will enhance Navy long-range planning and tactical execution, improve warfighter capability and the safety of the warfighters themselves, save money through improved ship and aircraft routing and energy conservation, and generally improve Navy operations.

3. General Circulation

Early in their academic careers, meteorologists and oceanographers are taught that the sun's energy ultimately drives ocean and atmospheric circulations. Differential heating of the earth's surface results in density gradients and a state of disequilibrium. The potential energy within these gradients is converted to kinetic energy in the form of atmospheric and ocean circulations that attempt to mix away these gradients to achieve a state of equilibrium. Therefore, as long as the sun continues to shine, the disequilibrium will continue to exist, and the ocean and atmosphere will remain in motion.

In the atmosphere, the conversion of the potential energy generated by the density gradient to the kinetic energy of the circulation (i.e., winds) is accomplished through two mechanisms; thermally-direct circulations and baroclinic instability (Wallace and Hobbs 1977). The thermally-direct circulations driven by the rising of warm air and the sinking of cold air are mainly responsible for the conversion of potential to kinetic energy in the tropics. Baroclinic instability is the mechanism that describes the break down of horizontal temperature gradients into synoptic-scale wave disturbances in mid and high latitudes (Wallace and Hobbs 1977). Simply stated, a baroclinic atmosphere exists whenever constant pressure surfaces intersect constant temperature surfaces, i.e., the surfaces do not neatly stack up as they do in a barotropic atmosphere. Therefore, in a baroclinic atmosphere, the geostrophic wind, defined by a balance between the pressure gradient force and the Coriolis force, can advect heat from one region to another. Thermal advection allows a synoptic-scale wave disturbance to grow by extracting potential and kinetic energy from the mean flow (Holton 1979) .

The ocean circulation is often separated into two parts; the thermohaline and wind-driven circulations (Pickard and Emery 1990). While the thermohaline circulation is also a thermally-driven circulation, the fact that the sun's energy arrives at the top of the ocean as opposed to the bottom of the atmosphere makes for a very different situation. The thermohaline circulation is primarily driven by cooling and salinization of the upper ocean due to heat loss and ice formation at high latitudes. Both processes result in denser water that sinks to considerable depth before it moves horizontally through several dynamical mechanisms. The deep currents that form in the North Atlantic and Weddel Sea through this mechanism result in average flows of 1-20 Sv.

The wind-driven circulations are generally confined to the upper few hundred meters of the ocean. However, the horizontal scale of the wind-driven motion can vary from those associated with Langmuir circulations on O(10-100 m) to mesoscale eddies on O(10-500 km) to ocean gyres. The upper-layer, wind-driven circulation is often described as Ekman flow or transport, where the frictional wind stress forces the ocean surface to more horizontally. Once in motion, the Coriolis force arising from the earth's rotation redirects the flow to the right (left) of the wind in the Northern (Southern) Hemisphere. This process continues through adjacent layers, causing a spiraling of the current vectors with depth.

On the mesoscale, horizontal variability in these locally driven circulations can generate larger-scale flow. For example, the convergence or divergence of the Ekman transport, or equivalently the curl of the wind stress, generates vertical velocities associated with upwelling and downwelling. The vertical motion associated with the curl of the wind stress field is known as Ekman pumping. The wind-driven vertical motion can be substantial in coastal regions where the wind-stress field can have strong horizontal gradients. These gradients are a result of the complicated two-way interactions that occur between the wind, wave, and current fields in regions with a lateral boundary and sloping bottom. The gradients can also be modulated by changes in the atmospheric stratification that result from changes in the sea surface temperature driven by the upwelling and downwelling.

On an even larger scale, the spatial distribution of the zonally averaged winds combined with the continental boundaries cause gyral circulations and strong western boundary currents. As a result, properly interpreting field observations generally requires observations over a range of scales. This requires some foresight in designing field experiments, which should include examining past experiments and guidance from numerical models and laboratory investigations. Therefore, we believe that successful investigations of the relationship between the various scales of motion responsible for transporting momentum, mass, and energy across the coupled boundary layers require a combination of in situ observations, laboratory and numerical simulations, and models.

4. Boundary Layer Processes

The kinetic energy of the large-scale atmospheric circulations cascades down to meso-scale and smaller motions through shear instability. In the atmosphere, it can produce smaller scale motions in the atmosphere near strong gradients (e.g., near the jet stream); however, shear instability is largely confined to the boundary layer where frictional drag generates the required shear. Boundary-layer scientist generally use the concept of turbulent eddies to describe these smaller motions. These eddies can range in size from the mesoscale eddies that span the boundary layer to microscale eddies whose kinetic energy is dissipated through viscous effects.

These eddies of various sizes fill the boundary layer, such that the boundary layer depth is often defined as the layer near the earth surface that is almost continuously turbulent (e.g., Stull 1988).

For steady, horizontally homogeneous conditions, the horizontal equations of motion within the boundary layer can be approximated by a three-way balance between the pressure gradient force, the Coriolis force, and the frictional drag:

$$fU_y - \frac{1}{\rho_a}\frac{\partial P}{\partial x} = f(U_y - U_{gy}) = -\frac{\partial}{\partial z}\left(\frac{\tau_{ax}}{\rho_a}\right) \quad \textbf{(1)}$$

$$-\frac{1}{\rho_a}\frac{\partial P}{\partial y} - fU_x = f(U_{gx} - U_x) = -\frac{\partial}{\partial z}\left(\frac{\tau_{ay}}{\rho_a}\right) \quad \textbf{(2)}$$

where x, y and z denote eastward, northward, and vertical components or gradients, respectively, U denotes the mean wind, U_g denotes the geostrophic wind (defined as shown by a balance between the pressure gradient force and Coriolis force), ρ_a is the air density (assumed constant in the boundary layer), P is the atmospheric pressure, f is the Coriolis parameter, and τ_a represents the vertical transport of horizontal momentum in the atmosphere.

The vertical transport, or flux, of momentum is a result of turbulent mixing in the boundary layer. The parameterization of this momentum flux and the specification of this flux at the boundary (i.e., its boundary condition) are of particular importance in the coupled ocean-atmosphere system. The vertical flux of momentum at a given height is closely related to the local shear, such that it is commonly referred to as the shear stress. Solution to the above set of equations can be found by assuming that the momentum flux (i.e., the shear stress) is proportional to the wind shear

$$\tau_a = K_m \frac{\partial U}{\partial z} \quad \textbf{(3)}$$

where, by analogy to molecular transfer, the constant of proportionality K_m is known as the eddy viscosity (e.g., Panofsky and Dutton, 1984). This type of relationship, which parameterizes a higher-order statistic in terms of a lower-order one, allows us to close the system of equations.

The level of complexity of the closure scheme is often what sets one type of solution apart from another. Elegant analytical solutions generally require simple closure schemes. The simplest of these solutions ignores the turbulence entirely by setting $K_m = 0$, and results in the geostrophic balance described above. The next simplest closure assumes that the eddy viscosity is constant and a linear relationship exists between the wind shear and wind stress (i.e., we can treat it as a Newtonian fluid). For example, the Swedish oceanographer V. W. Ekman assumed a constant eddy viscosity and a balance between the Coriolis force and friction to derive a solution predicting the above mentioned spiraling of the ocean currents that is now known as the Ekman spiral. An analogous solution can be found in a barotropic atmosphere where, by definition, neither the pressure gradient nor the temperature gradient varies with height, such that the geostrophic wind vector is also constant with height. Under these conditions, the ageostrophic component that arises due to the frictional coupling with the surface is also predicted to resemble an Ekman spiral.

As a result, meteorologist also call the region of the boundary layer where this three-way balance holds the Ekman layer. However, an ideal Ekman layer with its associated spiral is rarely, if ever, observed in the ABL (Holton, 1979). The effects of baroclinicity associated with frontal passages and storms invalidate this simple parameterization. Additionally, mesoscale motions can also be driven by thermally direct circulations within the boundary layer. These convectively driven motion effectively mix the boundary layer at mid-level. As a result, this portion of the convective boundary layer is commonly known as the mixed-layer (e.g., Wyngaard 1992). Entrainment at the top of the mixed-layer, which is often associated with cloud processes and gravity waves, has been found to influence the turbulence statistics well within the mixed-layer (Kaimal et al. 1976; Caughey 1982). These buoyancy-driven circulations also act to enhance the shear-driven motions under convective conditions (e.g., Serra et al. 1997) and suppress it when the flow becomes stratified (e.g., Carson and Richards 1978). Near the surface, observational studies and scaling arguments have shown that the eddy viscosity varies rapidly with height near the surface. This forms the basis for the surface layer scaling described in section **4.A** and the logarithmic wind profile described in section **6.A**.

Analogous processes take place in the ocean where the transport of heat and momentum can be driven by direct thermal circulations, which also modulates the wind-driven transport. These circulations are a result of the removal or addition of buoyancy due to cooling or heating of the surface, penetrative solar heating, and the removal or addition of fresh water due to surface evaporation, precipitation, river outflow, and runnoff. This buoyancy driven mixing combines with and modulates the shear-induced mixing associated with Ekman transport to generate an oceanic mixed layer (e.g., Price et al. 1987). Additionally, entrainment processes at the base of the mixed-layer can also affect the structure of the turbulence within the mixed-layer.

Finally, the transport of momentum and heat are strongly coupled to wave-induced processes near the ocean surface. For example, there is increasing evidence that the structure of the atmosphere and the mechanism of momentum transfer are significantly modified by surface waves. These resulting wave-induced processes invalidate many methods traditionally used to include, e.g., the effects of thermal stratification on near surface turbulence flows over land. Nonetheless, these methods provide a good starting point for our discussion of the turbulent exchange of momentum and energy exchange. Therefore, we provide a brief overview of the start-of-the-art in parameterizations of momentum and heat (energy) exchange at the air-land interface. Following this overview, we begin to explore some of the many processes that are unique to the marine boundary layers.

A. The Structure of Turbulence in the Atmospheric Surface Layer

Our understanding of the role of thermal stratification on the structure of turbulence in the atmospheric surface layer was vastly improved by a number of overland field experiments conducted during the late sixties and seventies. These include the landmark 1968 Kansas (Izumi 1971) experiment, the 1973 Minnesota (Champagne et al. 1977) experiment, and the 1976 International Turbulence Comparison Experiment [ITCE] (Dyer and Bradley 1982). These experiments led to the validation of a powerful set of statistical tools derived from Monin-Obukhov MO similarity theory, which we briefly describe below. A more detailed description of the theory can be found in a number of texts, including Lumley and Panofsky (1963) and Wyngaard (1973).

The basis of Monin-Obukhov similarity theory is the argument that the structure of the turbulent flow in the surface layer is governed by mechanical and thermal forcing. We can illustrate this argument through the turbulent kinetic energy (TKE) equation

$$\frac{dE}{dt} = \frac{1}{\rho_a}\left[\tau_{ax}\frac{\partial U_x}{\partial z} + \tau_{ay}\frac{\partial U_y}{\partial z}\right] + \frac{g}{\Theta_v}\overline{w\theta_v} - \frac{\partial}{\partial z}\left(\overline{we} - \frac{\overline{wp}}{\rho_a}\right) - \epsilon \tag{4}$$

where E is the mean TKE, ρ_a is the density of air, ϵ represents the rate of dissipation of TKE, Θ_v is the mean virtual potential temperature, g is the acceleration of gravity, and w, θ_v, e, and p are the turbulent components of the vertical velocity, virtual potential temperature, TKE, and pressure, respectively. The first term on the right-hand-side of this equation represent the production of TKE through mechanical forcing (shear production) and the second term represents the production of TKE through thermal forcing (buoyant production). The third term represents the energy and pressure transport, which neither produce nor consume TKE; instead, they act to redistribute TKE throughout the boundary layer.

Obukhov (1946) and Monin and Obukhov (1954) were the first to describe a similarity hypothesis about the statistical nature of the turbulent flow based on the relative strength of these two forcing mechanisms. Monin-Obukhov (hereafter MO) similarity theory states that the structure of turbulence is determined by the height above the surface, z, the buoyancy parameter, g/Θ_v, the friction velocity, u_*, and the surface buoyancy flux, $\overline{w\theta_{v_s}}$ (e.g., Wyngaard 1973). These last two terms are defined from the surface stress and heat fluxes as

$$u_* = \left[\frac{|\vec{\tau}_a(0)|}{\rho_a}\right]^{1/2} \tag{5}$$

$$\overline{w\theta_{v_s}} = \frac{Q_h}{\rho_a c_p} + 0.61\,T_s\frac{Q_e}{\rho_a L_e} \tag{6}$$

where $\vec{\tau}_a(0)$ is the surface stress vector (the surface value of the momentum flux), Q_h is the surface value of the sensible heat flux, Q_e is the surface value of the latent heat flux, T_s is the surface temperature, c_p is the specific heat at constant pressure, and L_e is the latent heat of vaporization of water.

These four governing parameters can be combined to form an additional velocity scale defined as

$$u_f = \left(\frac{zg}{\Theta_v} \overline{w\theta_{v_o}} \right)^{1/3} \quad \textbf{(7)}$$

whose use is restricted to positive values of the heat flux (i.e., convective conditions). The two velocity scales, u_* and u_f, are then used to define two temperature and moisture scales

$$T_* = -\frac{\overline{w\theta_s}}{u_*} \quad , \quad T_f = -\frac{\overline{w\theta_s}}{u_f} \quad , \quad \textbf{(8)}$$

$$q_* = -\frac{\overline{wq_s}}{u_*} \quad , \quad q_f = -\frac{\overline{wq_s}}{u_f} \quad , \quad \textbf{(9)}$$

and a length scale now known as the Monin-Obukhov length

$$L = -\frac{\Theta_v}{g\kappa} \frac{u_*^3}{\overline{w\theta_{v_o}}} \quad , \quad \textbf{(10)}$$

where κ is the von Karman constant. The magnitude of the MO length is determined by the relative strength of the mechanical versus thermal forcing, while its sign is determined by the sign of the buoyancy flux, i.e., it is negative in convective (unstable) conditions and positive in stratified (stable) conditions.

The various scales are not independent (Wyngaard 1973). Consequently, it is common practice to select u_*, T_*, and q_* as the velocity, temperature, and moisture scales for both stable and unstable flows. In light winds conditions with appreciable heat flux , MO similarity theory requires that the surface stress (i.e., u_*) is no longer a relevant scaling parameter and that the small-scale turbulence variables approach the convective limits (Edson and Fairall 1998). In this limit the structure of the marine atmospheric surface layer in the region between $-L < z < 0.1z_i$ should approach that of local free convection and depend only on z, g/Θ_v, and $\overline{w\theta_{v_s}}$ (Tennekes 1970). Under these conditions it is more appropriate to use the convective scaling parameters denoted by the subscript f. Additionally, above the surface layer (i.e., $z > 0.1z_i$), studies of the mixed layer have shown that many turbulent processes scale with the height of the boundary layer, z_i. In this region, z_i replaces z as the appropriate length scale and one uses the free-convective velocity scale proposed by Deardorff (1970).

The similarity hypothesis then states that various turbulent statistics, when normalized by these scaling parameters, are universal function of the stability parameter $\zeta = z/L$. For example, in Figure X we have reproduced the results from the Kansas experiment where the wind shear $\partial U / \partial z$ has been normalized by $u_*^3 / \kappa z$ and plotted and plotted versus ζ. The figure shows that the normalized shear collapses to a reasonably well-behaved function donated by

$$\phi_m(\zeta) = \frac{\kappa z}{u_*^3} \frac{\partial U}{\partial z} \qquad \textbf{(11)}$$

and parameterized by the line shown in this figure. It is worth noting that the dimensionless shear allows use to relate the stability parameter to the flux Richardson number

$$Ri_f = -\frac{\rho_a g}{\Theta_v} \overline{w\theta_v} \left[\tau_{ax} \frac{\partial U_x}{\partial z} + \tau_{ay} \frac{\partial U_y}{\partial z} \right]^{-1} \approx \frac{\zeta}{\phi_m(\zeta)} \qquad \textbf{(12)}$$

which is more commonly used in oceanic applications. The approximation sign is mainly due to the assumption of a constant flux layer in MO similarity, which is not required in the definition of the flux Richardson number.

Several decades of research using this procedure has provided parameterizations of the dimensional shear that vary only slightly from one another (e.g. Dyer and Hicks 1970; Wyngaard and Coté 1971; Kaimal et al. 1972; Champagne et al. 1977; Dyer and Bradley 1982; Frenzen and Vogel 1992; Oncley et al. 1996). As a result, the MO similarity hypothesis has provided nearly universal functions from these experiments and it is widely accepted by the atmospheric community. These semi-empirical relationships are used extensively in the lower boundary conditions of numerical forecast models where one must derive turbulent quantities from the mean variables available from the model. For example, the dimensionless shear is often used to include the effect of thermal stratification on the eddy viscosity by combining **(3)** with **(11)** to obtain

$$K_m = \frac{u_* \kappa z}{\phi_m(\zeta)} \tag{13}$$

which also parameterizes the observed height dependency of the eddy viscosity in the near surface layer. Similarly, these relationships are often used to estimate the desired turbulent quantities from mean measurements over the ocean where direct measurement of the fluxes is very difficult as described in section **6**. However, **the use of overland measurements to infer surface fluxes over the ocean is questionable**, particulary close to the ocean surface. Therefore, the universality of these relationships to all surface layers is a current topic of intense debate.

B. Surface Waves

The most obvious characteristic of a wind disturbed water surface is the complex and ever changing pattern of surface waves. In very light winds, viscous dissipation suppresses the formation of short capillary and capillary-gravity waves (Kahma and Donelan 1987) and the surface appears to be "glassy calm", perhaps disturbed by long swell from a distant storm. Once the wind speed exceeds a few meters per second, surface waves roughen the surface and affect the mechanical coupling (to a lesser extent, the thermal and material coupling also) of sea with air, alter the albedo, modify the structure of the surface boundary layers in both fluids, and change the electromagnetic and acoustic reflectivity. Increasingly high winds produce correspondingly larger responses of these types. Additionally, the phenomenon of wave breaking alters the surface and adjacent boundary layers in fundamental ways by introducing spray into the upper boundary layer and bubbles into the lower. These two-phase flows have important effects on electromagnetic (including optical) propagation, scattering and remote sensing, acoustic reverberation, propagation, scattering and remote sensing, momentum, heat and mass transfer, surface mixing, turbulence structure, wave generation, etc. It is not surprising, therefore, that one of the key issues in coupling the atmosphere and the ocean surface layers is an accurate description of the waves that travel on the interface between the two fluids, which directly influence the structure of the boundary layers above and below to a distance of the order $1/k_p$, where k_p is the wavenumber of the peak (most energetic) waves in the system.

Most estimates of the directional properties of waves are derived from point observations of time series of surface elevation and slope, or sub-surface pressure and current. These yield estimates of the frequency-directional spectra; i.e. the directional (or propagation) distribution of energy (or action) in frequency bands derived from such non-unique estimators as Maximum Likelihood (MLM) and Maximum Entropy (MEM). Unfortunately, this view of the surface is severely distorted by the Doppler shifting caused by ambient currents, wind drift, and orbital velocities of the long waves on which the short waves ride. Since wavenumber spectra are needed to elucidate the issues mentioned above and many of these issues concern very short waves (viz: momentum transfer, gas transfer, wave breaking, remote sensing), the frequency-directional spectra are inadequate to the task. By contrast, engineering studies, largely concerned with the neighborhood of the spectral peak, will generally be able to use the frequency-directional spectra, to which a transformation to wavenumber spectra based on linear theory may be applied.

More recently air-borne scanning radars (Walsh et al. 1985) and lidars (Hwang et al. 1999) have been used to map the surface in a series of "snapshots" along the flight path. These spatial pictures yield wavenumber spectra (with 180 degree ambiguity in the propagation directions). However, the horizontal resolution of these methods (3 m to 10 m) permits estimates of wavenumber directional spectra of the longer waves only. Donelan et al. (1996) have developed a new approach (using wavelet analysis methods) to obtaining wavenumber spectra directly from time series of fixed point observations from arrays of wave staffs, surface slope, or sub-surface pressure and currents. The method has been applied to tower data (Donelan et al. 1999a; 1999b) and show the very strong effect of Doppler shifting on the traditional "frequency of encounter" spectra and the inferred (by linear theory) wavenumber spectra. Among the more striking differences are: a) the spectra are substantially narrower in direction than deduced from MLM techniques; b) spectral slopes in the "equilibrium range" are greater (-4 to -5) compared to traditional estimates(-3.5 to -4).

It is possible that these new techniques of observation and analysis will yield a consistent and reliable description of the wavenumber spectra from the long energetic waves to the very short capillary waves. The need for this is fundamental to the goal of coupling oceanic and atmospheric boundary layers.

C. The Marine Surface Layers

The application of Monin-Obukhov similarity theory to the marine surface layer requires caution because the scaling parameters are derived so they only account for the influence of mechanical and thermal forcing on the turbulence. Many investigations (e.g., Geernaert et al. 1986; Rieder et al. 1992; Donelan et al. 1993; and Hare et al. 1997) have demonstrated that additional scaling parameters are required to describe turbulent variables within the wave boundary layers (WBLs). **The WBLs are defined in this overview as the region where the total momentum flux, even if assumed to be constant with height, has appreciable turbulent and wave-induced components**. Within the WBLs the momentum equation can be written as

$$\frac{\partial}{\partial z}\left(-\overline{\tilde{u}\tilde{w}} - \overline{u'w'} + \nu\frac{\partial U}{\partial z}\right) \approx 0 \qquad \textbf{(14)}$$

where primes denote turbulent fluctuations, tildes denote the wave induced fluctuations [i.e., the measured wind is broken down into mean and fluctuating parts as $U + u'(t) + \tilde{u}(t) = U + u(t)$], and the last term on the right-hand-side represents the viscous stress where ν is the kinematic viscosity. Since MO similarity theory is formulated for turbulently driven processes, it is not applicable in regions of the marine surface layer where the flow is also influenced by ocean waves.

The generation of wave-induced circulations can also invalidate MO similarity in the ocean mixed-layer. Coherent structures in the mixed layer, known as Langmuir circulations, are driven by wave-current interactions. These structures are believed to transport buoyancy and momentum and enhance the mixing. For example, subsurface observations from FLIP indicated that these coherent structures can distribute the momentum from the wind stress more rapidly than predicted from 1-D models. Additionally, intermittant turbulence and additional mixing is generated by large-scale wave-breaking. Neither of these processes is expected to obey MO similarity, which implies that simple parameterizations such as **(13)** cannot account for these processes in ocean models. Even in the absence of waves, the assumption of a constant flux layer that is driven by surface forcing breaks down under conditions of penetrative solar heating. In these instances, the penetrating shortwave radiation provides a buoyancy flux profile that is independent of turbulent mixing.

***Research Issue**: The complexity of the turbulence field in a wave-dominated environment (i.e., the WBL) motivates additional research to supplement MO similarity theory and support improved boundary layer parameterizations.*

5. Processes Within the Marine Boundary Layers

Despite many experimental and theoretical studies, we have not been able to satisfactorily explain the wind/wave/current coupling mechanisms. As a result, oceanographers and meteorologists often ignore wave-induced processes and treat the WBLs as a "black box." In most numerical and process models, the fluxes of momentum and heat enter through the top of the box and then reappear unchanged at the bottom to drive the model as shown in Fig. 1. The wave-related processes responsible for the momentum transport are generally neglected or, at best, parameterized by a poorly understood, most empirical, sea-state dependent drag coefficient. Improved forecasts of the wind, wave, and current fields require a better understanding of the processes in the marine boundary layers than is presently available. This is particularly true for forecasts in regions where advection is important (horizontally inhomogeneous regions) and during rapidly evolving events (non-stationary conditions).

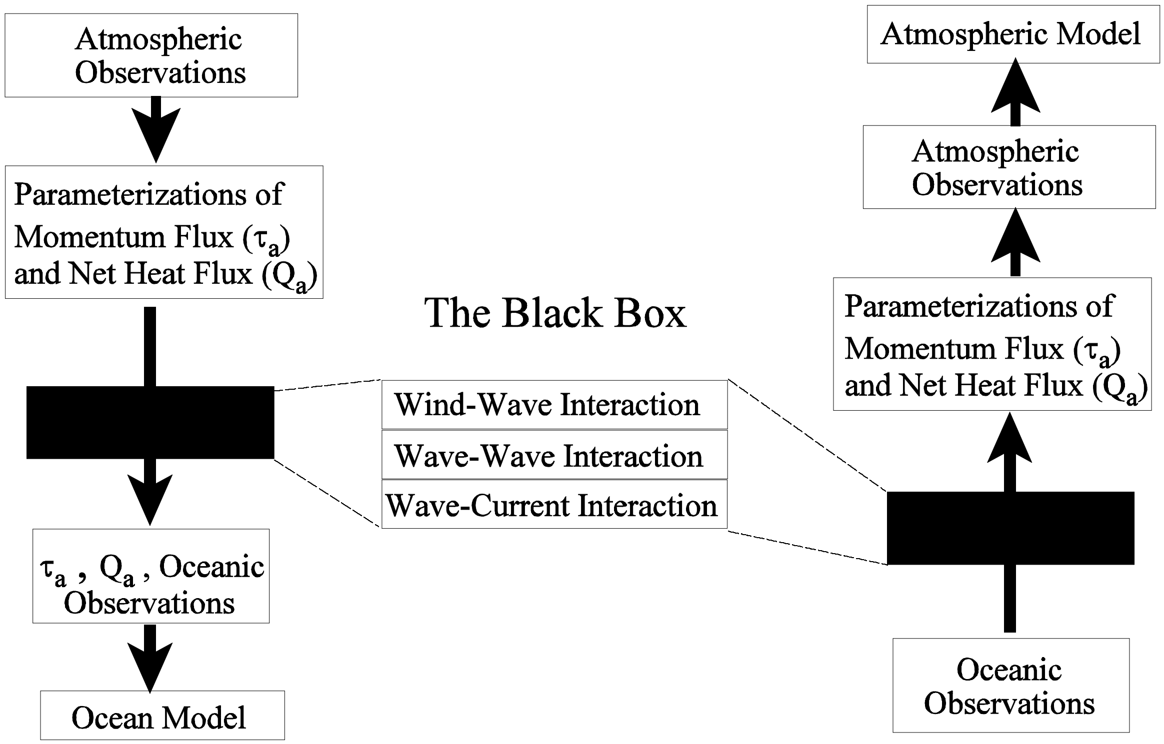

Figure 1. The commonly used approach of applying boundary conditions to drive 1-D models via one-way coupling of the atmosphere to ocean or ocean to atmosphere.

Many (but not all) of the processes that take place within this black box are shown in Fig. 2. These processes are briefly described in the following paragraphs and in more detail in the following sections, where we focus on the need for future research.

A. Momentum Exchange

Within the WBL, the vertical profile of the total momentum flux can be divided into three components: 1) the turbulent momentum flux, 2) the viscous stress, and 3) the wave-induced momentum flux. The viscous stress component is negligible except within a few centimeters of the surface. The atmospheric turbulent momentum flux dominates the total flux at the top of the WBL and decreases to zero at the surface where the turbulence vanishes. Therefore, at the surface, the total momentum flux is a combination of the wave-induced flux going into the ocean waves and the viscous stress going directly into the ocean currents.

We can illustrate this partitioning using the expression for the total momentum flux at the

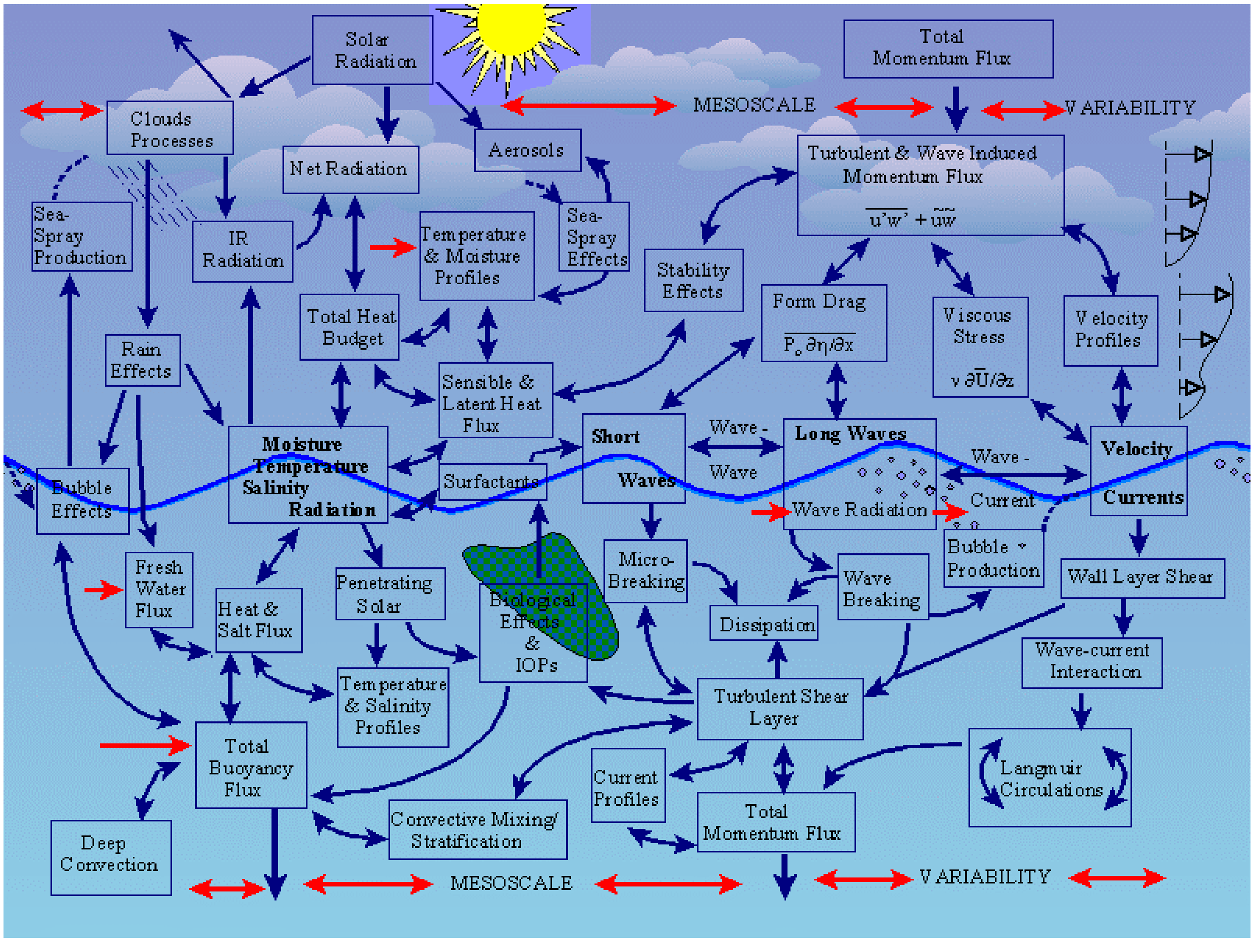

Figure 2. Some of the processes that govern the transfer of heat, mass, and momentum within the coupled boundary layers.

ocean surface (i.e., where the turbulent component becomes negligible) derived by Deardorff (1967). Deardorff (1967) derived this expression by evaluating the integrated horizontal momentum equation at the ocean surface to obtain

$$\tau_a = \rho_a \left[-\overline{\tilde{u}\tilde{w}} + \nu \frac{\partial U}{\partial z} \right]_\eta \approx \overline{p_\eta \frac{\partial \eta}{\partial x}} + \rho_a \nu \frac{\partial U}{\partial z}\Big|_\eta = \tau_{aw} + \tau_{ao} \qquad \textbf{(15)}$$

where η is the wave height, p_η is the surface pressure, and the small component of the viscous stress associated with inclinations of the interface has been neglected. The stresses given on the RHS on based on the nomenclature given in Lionello et al. (1996, 1998), where τ_{aw} represents the momentum transfer from the wind to the waves (i.e., the wave-induced flux), while τ_{ao} represents the direct momentum transfer from the wind to the ocean (i.e., **viscous stress**). This expressions shows that the wave-induced momentum flux is the correlation between the surface pressure field and wave slope, which is known as **form drag**.

The momentum transfer from the wind to waves in **(15)** represents the momentum flux supported by the entire wave spectrum. The transfer of momentum to **all** waves is accomplished through the form drag represented by the pressure-slope correlation in **(15)**. However, in the literature, the wave-induced momentum flux is often separated into the form drag due to the long gravity waves (and swell) and momentum transfer to short wind waves, which we usually think of as **roughness elements**. The transfer of momentum from wind to short waves (through pressure force on the roughness elements, i.e., form drag) and the momentum transfer from these short waves to surface currents (through the **small-scale breaking** commonly referred to as **microbreaking**) occur on much shorter time scales than the momentum transfer associated with large gravity waves. Hence, it is often considered as an almost instantaneous momentum transfer from wind to currents and is combined with the viscous stress. As such, most of the momentum flux going into the short gravity-capillary waves is quickly transferred to the current field through small scale breaking, τ_{wo}, and only a small portion of the flux goes into increasing the momentum of a growing (i.e., developing) wave field, $\tau_w = \tau_{aw} - \tau_{wo}$.

Some of the momentum retained by the wave field is returned to the ocean when **large-scale breaking** occurs. These large-scale breaking events generally entrain air and are commonly associated with whitecaps. However, it is important to note that microbreaking can occur without any air entrainment (Banner and Phillips 1974), such that whitecapping and wave breaking are not synonymous. Finally, the study by Banner (1990) has shown that form drag can be significantly enhanced over large-scale breaking waves. These studies are described in more detail in sections XXX and XXX.

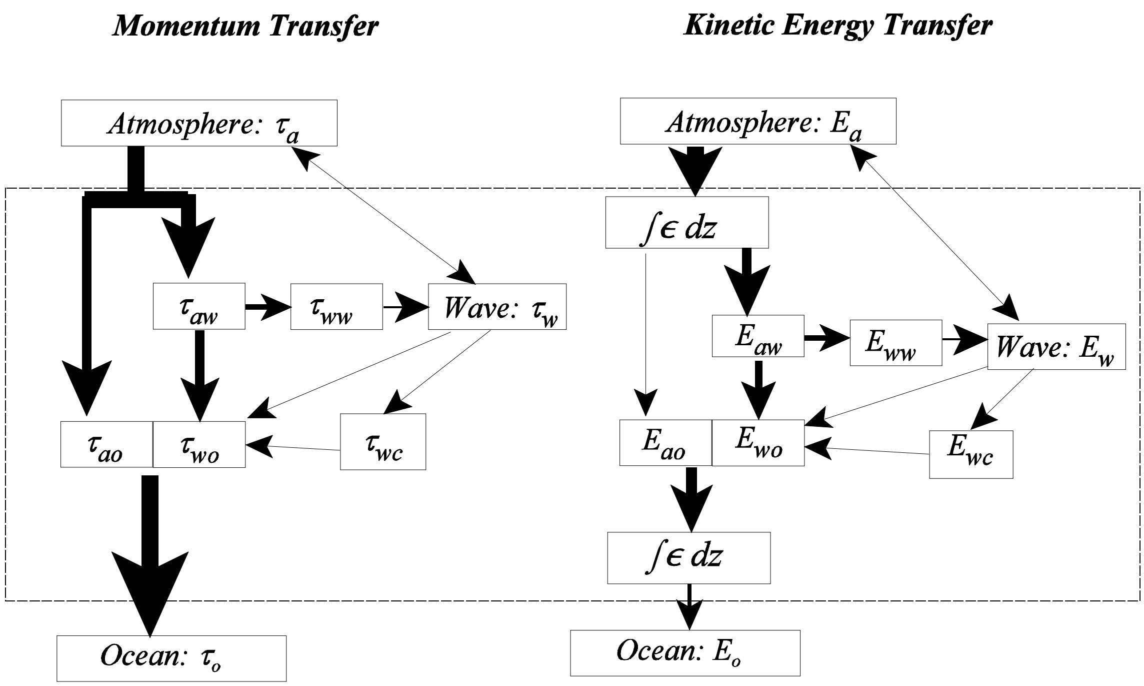

Figure 3: Conceptual exchange of momentum and energy between the atmosphere, waves, and ocean. The width of the arrows is indicative of the relative amount of the total momentum and energy in these exchanges. The broken line represents processes within the black box in Fig. 1. (modified from Lionello et al. 1996)

Lionello et al. (1996) provide a simple schematic for the various paths the momentum flux can follow that we reproduce with some modifications in Fig. 3. The arrows in this figure represent the magnitude of fluxes along the various paths. In this figure, we are attempting to show that the momentum flux that actually changes the momentum of the wave field is small compared to the total momentum flux from the atmosphere τ_a and total momentum flux going into the ocean $\tau_o = \tau_{ao} + \tau_{wo}$. Comparisons of the mixed layer models described in Price et al. (1986) and Crawford and Large (1996) show good agreement with observations when one assumes that all of the surface wind stress goes into direct forcing of the surface currents. The agreement holds in moderate wind conditions when the sea is aerodynamically rough and the momentum flux from the short waves to the ocean, τ_{wo}, is believed to dominate the momentum flux (e.g., Terray et al. 1996; Lionello et al., 1998). This indicates that the mechanism we have identified with small-scale breaking is effective at transporting momentum from the short waves to the mean currents.

As discussed earlier, the momentum flux entering the ocean surface drives Ekman transport and the curl of this quantity, $\nabla \times \tau_o$, ultimately drives vertical motions through Ekman pumping of the ocean. Therefore, the 2-D spatial structure of both the wind and wave fields play a role in the 3-D ocean circulation.

B. Mass and Heat Exchange

The exchange of momentum through Ekman transport can ultimately generate shear at the base of the mixed layer. The mixed layer deepens if the wind-driven shear is able to overcome the stratification found at the base of the mixed layer. The stratification is a result of gradients in the temperature and/or salinity structure; the gradients are generated by a combination of mechanical mixing (i.e., the momentum flux or shear stress) and the net heat flux at the surface (see Fig. 1). The net heat flux Q_a in Fig. 1 is generally approximated as a residual (i.e., the imbalance) of the measurable components of the surface heat budget (e.g., Bradley et al. 199X; Weller and Anderson 1996),

$$Q_a = Q_e + Q_h + Q_{LW}\uparrow + Q_{LW}\downarrow + (1 - \alpha_s)Q_{SW} \qquad \textbf{(16)}$$

where $Q_{LW}\uparrow$ is emission of infrared (long wave) radiation from the ocean surface, $Q_{LW}\downarrow$ is downward emission of infrared radiation from the atmosphere; and Q_{SW} is the incoming solar (short wave) radiation, where α_s is the surface albedo.

The heat flux acts to change the near surface buoyancy, i.e., the net input of heat increases the stratification by warming the upper ocean, while heat loss generates convection by cooling the surface and (potentially) increasing density. The convection driven by the latent heat loss of the ocean is further enhanced by the increased salinity of the surface water due to the evaporation. Therefore, conditions that lead to a convective atmospheric boundary layer (i.e., input of buoyancy at the surface) tend to stratify the ocean (i.e., buoyancy loss at the surface); conversely, stable atmospheric boundary layers typically form when conditions are favorable for convection in the ocean.

These generalizations may not hold for a number of reason, foremost of which include advective processes and precipitation. Lindstrom et al. (1987), Lukas and Lindstrom (1991), Anderson et al. (1996), Rogers et al. (1996), Weller and Anderson (1996), and Wijesekera et al. (1999) investigated the influence of precipitation during the WEPOCS and TOGA-COARE programs. Anderson et al. (1996) and Wijesekera et al. (1999) show that the rain water often forms a buoyant lens at the surface because the fresh water is lighter than the saltier ocean water. The salt-stratified layer has been labeled the "barrier layer" by Godfrey and Lindstrom (1989) because the stably-stratified layer resists mechanical mixing. This is often the case even when the rain is cooler than the ocean surface temperature because the salinity effect tends to dominate the change in density.

The precipitation can also impact the sensible heat flux by modifying the surface temperature and thereby the air-sea temperature difference. Evaporative cooling of rain as it falls through the atmosphere causes it to enter the ocean at or very near the ambient wet-bulb temperature a few meters above the ocean surface (Anderson et al. 1998). Since precipitation is generally associated with convective conditions, the temperature of the rain droplets (i.e., the precipitation temperature) is generally lower than the surface temperature, such that they both freshen and cool the ocean. This additional effect can have a profound impact on the surface energy budget. The cooling of the ocean reduces the sensible heat exchange (in unstable conditions) between the ocean and atmosphere. In the tropical Pacific, Anderson et al. (1996) showed that these two effects are negatively correlated; the sensible heat flux contribution tends to cool the surface while fresh water flux tends to increase stratification.

The precipitation effects can be included in the surface buoyancy flux through the expression given by Anderson et al. (1996)

$$B_{net} = \beta_T \frac{Q_a}{\rho_w c_p} + \beta_S S_o \left(P - \frac{Q_e}{\rho_a L_e} \right) \qquad \textbf{(17)}$$

where β_T and β_S are the thermal and haline coefficients of expansion, ρ_w is the water density, S_o is the reference surface salinity, and P is the precipitation rate (the second term in the parentheses equals the evaporation rate). The effect of the precipitation temperature on the sensible heat flux can be included in the net heat flux using the approach of Flament and Sawyer (1995) as described in section **6.C.1**.

When the momentum and net buoyancy (heat and/or fresh water) fluxes are directed downward (i.e., when the surface is warming and/or freshening), the mixed-layer is will deepen until the mechanical mixing balances the input of buoyancy at the surface. Conversely, surface evaporation and heat loss produces a negative buoyancy flux, which acts to destabilize the mixed-layer. This situation is analogous to the unstable conditions found in the atmosphere where mixing is driven by both buoyant and mechanical forcing. As in the atmosphere, direct thermal circulations drive the mixing when the shear stress is weak. Under these conditions the layer is convectively mixed to a depth determined by the subsurface stratification (Anderson et al. 1996).

A final process associated with stability effects is known as double diffusion (e.g., Turner 1974). This mixing process is a result of the different rates of molecular diffusion for salt and heat and can drive significant mixing on centimeter to meter scales in the absence of turbulent mixing. The process occurs because heat is diffused much more quickly than salt. For example, consider a system in static equilibrium where cooler water lies over warmer water because the cooler water is less saline. In the absence of turbulent mixing, heat will be exchanged between the two layers more rapidly than salt. As a result the lower part of the upper level will warm, become less dense, and mix upwards; conversely; the upper part of the lower layer will cool, become more dense, and mix downward. Note that this mixing occurs within their respective layers (Pickard and Emery, 1990).

Mixing can also occur through the double diffusion process when warm, less saline water lies over cooler, more saline water. In this situation the faster heat diffusion destabilizes the adjacent vertical layers and causes mixing across the interface. The mixing across the interface generates centimeter to meter scale perturbations of more saline and less saline waters in a process known as "salt fingering" (Pickard and Emery, 1990). Lateral diffusion mixes away these fingers, thereby generating two new interfaces at which double-diffusion begins anew. This process is less common in the upper open ocean, although these structures have been found in coastal areas.

***Research Issues**: 1-D models of the mixed layer that include the above processes often agree very well with observations in the open ocean. Not surprisingly, they do not perform as well when mixing at the base of the mixed layer is driven by 2 or 3-D processes associated with zonal* *currents, internal waves, Ekman pumping, and inertial-oscillations or when additional mixed layer transport is driven by wave breaking or wave-current interaction (e.g., Langmuir circulations). The determination of the relative contribution of these additional processes to the larger scale ocean circulation remains a key research objective. A generalized criteria for evaluating the role of these processes is to determine which produce significant pressure transport to the lower layer over time scales longer than an inertial period and space scales larger than the Rossby radius. A long term goal would be to simulate or parameterize the relevant processes in coupled models, thereby improving our ability to forecast ocean circulation and weather. A number of these processes are described in more detail in the following sections.*

C. Biological Effects

An area which has thus far received relatively little attention in the context of coupled ocean/atmosphere modeling is the effect of photosynthetic pigments on the penetration of shortwave radiation, hence the effects of biological productivity on the thermal structure of the upper ocean. It has long been recognized that predictive models of the near-surface ocean are sensitive to specification of the mean primary productivity of an oceanic region, incorporated in models in a gross sense by specifying the shortwave absorption coefficient according to Jerlov water type (Jerlov 1968;1976). Such sensitivity suggests that models parameterizations require more realistic descriptions of the upper ocean content of photosynthetic pigment (predominantly but not exclusively chlorophyll-a), which is known to vary on regional, meso- and seasonal scales by at least 4 orders of magnitude.

There is some evidence for substantial biological effects on sea surface temperature, particularly in the low-latitude oceans where coupling between ocean and atmosphere is strong. Lewis et al. (1990) argued that deep penetration of visible solar radiation in the relatively unproductive western equatorial Pacific distributed heat over a substantial depth range, resulting in SST which was significantly **cooler** (by a few to several degrees K) than that which would result from the very near-surface absorption typical of productive regions. In contrast, Siegel et al. (1995) found a biogeochemically mediated increase in the mixed layer radiant heating rate of 0.11 K/month) in the upper 30 m of the western Pacific warm pool after a significant phytoplankton bloom. Sathyendranath et al. (1991) demonstrated an even larger biological contribution (of order 1 K/month, with maximal values in coastal regions of 4 K/month) to the rate of mixed layer heating in the highly productive waters of the southwest monsoonal Arabian Sea. In this regional study, the surface layer was substantially **warmer** than it would have been in the absence of phytoplankton. This result has also been demonstrated on the mesoscale by the observations of Ramp et al. (1991) in the coastal transition zone off northern California.

A more speculative possibility for biological influences of the upper ocean is that of "algal-mediated convective processes" described by Lewis et al. (1983). In this process, the convection is initiated at depth within the surface layer of the ocean by shortwave absorption associated with intense subsurface maxima of Chlorophyll-A.

Given the observed sensitivity of existing ocean models to the parameterizations used for shortwave penetration, it appears possible that regional, seasonal, and mesoscale variability in biological productivity may produce significant changes in predictions of coupled ocean/atmosphere models. Changes might be expected to be particularly large in the coastal oceans which dominate global primary productivity. Estimates of potential impacts, carried out with existing coupled models, would be valuable to focus future work in this area.

D. Kinetic Energy Exchange

The significant amount of kinetic energy exchanged between the atmosphere and the ocean represents a fundamental difference between the ocean/atmosphere and land/atmosphere boundary layers. To illustrate this concept, we begin with an expression for kinetic energy flux at a given height (valid over either interface) given by

$$E_a(z) = \tau_a U(z) + \rho_a \overline{we} + \overline{wp} \tag{18}$$

where we assume horizontal homogeneity for simplicity. The first term on the right-hand-side represents the flux of mean flow kinetic energy, while the last two terms represent the rate of diffusion of kinetic energy (Townsend 19XX). Over land, we often assume that the energy flux through the ground is negligible, such that the flux entering the layer at height h can be related to the total rate of dissipation within the layer by

$$\rho_a \int_0^h \epsilon \, dz = -E_a(h) + \frac{\rho_a g}{\Theta_v} \int_0^h \overline{w\theta_v} \, dz \tag{19}$$

where the second term on the right-hand-side accounts for the generation of kinetic energy due to any buoyancy flux as shown in **(4)**. For neutral conditions, this expression states that the flux of kinetic energy into a layer is balanced by the total rate of dissipation within that layer. The dissipation can be approximated by the well known wall-layer prediction

$$\epsilon = \left(\frac{\tau_a}{\rho_a}\right)^{3/2} \frac{1}{\kappa z} = \frac{u_*^3}{\kappa z} \tag{20}$$

which is consistent with the similarity hypothesis described in section **4**. MO similarity can be invoked to include the enhanced (reduced) dissipation due to buoyancy (stratification) through the dimensionless dissipation function

$$\phi_\epsilon\left(\frac{z}{L}\right) = \frac{\epsilon \kappa z}{u_*^3} \tag{21}$$

which is described in more detail in section **7**.

1. Energy Transfer within the Atmospheric Surface Layer

Over the ocean, the surface energy flux that drives the waves and currents is no longer negligible. Expression **(19)** must be modified to take into account the total energy transfer into the ocean such that

$$E_{aw} + E_{ao} = \rho_a \int_0^h \epsilon \, dz + E_a(h) - \frac{\rho_a g}{\Theta_v} \int_0^h \overline{w\theta_v} dz \tag{22}$$

where E_{aw} and E_{ao} represents the energy flux going directly into the waves and currents, respectively. This expression implies that less (volume-averaged) dissipation is required to balance the same energy flux over the ocean versus over the land as long as there is a net flux into the ocean. Consequently, we expect the flux of energy into the ocean to cause measured dissipation rates to differ from the wall layer prediction given by **(20)** in the WBL, even if we include a means to account for stability such as **(21)**. This dissipation deficit (i.e., the imbalance between production and dissipation) was recently predicted by Janssen (1999).

Research Issues: *We would expect the dissipation deficit to be greatest over the youngest seas where the energy flux on the left-hand-side of* ***(22)*** *is largest. Evidence for this effect is given by Edson et al. (1997) and is reproduced in Fig. 4. In this figure the measured dissipation has been normalized by* ***(21)****. If the wall-layer prediction holds, we expect the normalized dissipation to equal unity at all heights. This is clearly not the case in MABL, and bin-averaging the data by the wave age,* c/u_*, *shows that the deficit appears to be a function of wave development. The*

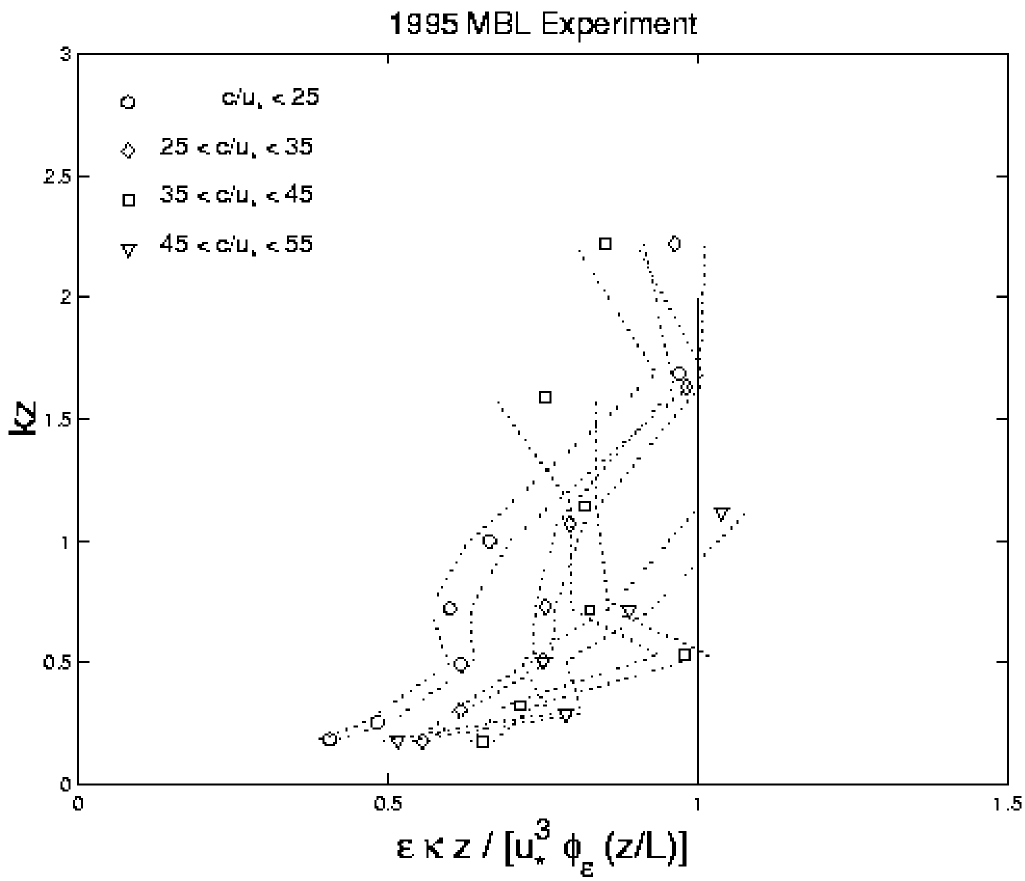

Figure 4 Normalized values of the TKE dissipation estimates. The normalized values have been bin-averaged by wave age.

results taken from this open ocean data set shows that the younger the seas the greater the deficit. In coastal zones we often find much younger seas because of limited fetch. Additionally, in these regions the energy input may also be affected by the sea state, e.g., interaction with the bottom could generate steeper waves leading to enhanced roughness, shear stress, and *dissipation. The enhanced dissipation could reduce (or eliminate) the dissipation deficit. These processes are generally not included in LES subgridscale parameterizations in the near-surface layer. These parameterizations and the physical processes are discussed further in section **8B**.*

2. Direct Energy Transfer to the Ocean Currents

Energy can be transferred between the atmosphere and ocean by either pressure fluctuations (normal stresses) or tangential stresses (Kinsman, 1965). The form that the total energy flux takes at the surface is closely related to **(15)**, and can be approximated by

$$E_{ao} + E_{aw} \approx \tau_{ao} U_s + \overline{p_\eta w_o} \approx \tau_{ao} U_s + \overline{p_\eta \frac{\partial \eta}{\partial t}} \qquad \textbf{(23)}$$

where τ_{ao} represents the direct exchange of momentum between the atmosphere and ocean through tangential stresses, U_s is the surface drift current (Stokes drift plus wind drift), η is the instantaneous wave height, p_η is the pressure at the wave surface, and w_o is the time rate of change of the surface elevation, known as the piston velocity. The surface drift arises from the combined effects of the viscous stress and short-wave momentum transfer from the atmosphere to the ocean currents (Kraus and Businger, 1994). The energy flux going directly into the ocean currents is often modeled using

$$E_{ao} = \gamma u_* \tau_{ao} \qquad \textbf{(24)}$$

where γ is the ratio of the surface drift to the friction velocity u_*. The laboratory results of Wu (1975) provide a mean value of $\gamma = 0.55$. Therefore, the energy flux from the atmosphere to ocean currents is substantially less than the energy flux entering the atmospheric surface layer because $\tau_a u_* \ll \tau_a U$.

Similar to the momentum flux, some of the wave energy, E_{wo}, is quickly transferred to the ocean. The remainder, $E_w = E_{aw} - E_{wo}$, actually goes into increasing the energy of the wave field. Although most investigators agree that the energy flux that increases the energy of the waves, E_w, is small compared to the flux entering the WBL, there is a great deal of debate about the magnitude of the two components, E_{aw} and E_{wo} that control this flux. Crawford and Large

(1996) assume that most of the energy entering the WBL is dissipated and that a negligible amount ultimately goes into the ocean, i.e., $E_{aw} \approx E_{wo} \approx 0$. They model the energy input into the ocean currents as

$$E_o = U_1 \tau_a \tag{25}$$

where U_1 is the velocity in the model's upper layer. Even if **(25)** is a good approximation of the energy input to the ocean currents, the assumption that most of the energy entering the WBL is dissipated does not agree with the findings of theoretical and experimental investigations of the energy input into the waves. This is discussed further in the following section.

3. Direct Energy Transfer to the Ocean Waves

Some of the momentum and energy going into the short-waves together with the form drag of the longer waves is retained by the wave field. The energy from the short waves is transferred between other components of the wave field by wave-wave interaction. The net result is an evolving wind wave field. The role that the two fluxes play in determining the energetics of the evolving wave field is perhaps most easily seen using the energy balance equation (WAMDI Group 1988)

$$\frac{\partial F}{\partial t} + (U(0) + c_g)\,\nabla F = S_{in} + S_{nl} + S_{ds} \tag{26}$$

where $F(\omega, \theta)$ is the frequency-direction spectrum of the waves, the total surface current $U(0)$ acts as an advection velocity, c_g is the group phase velocity of the waves and

- S_{ds} is the energy dissipation due to wave breaking and viscous damping of capillary waves. It is related to the energy flux from waves to the ocean through $E_{wo} = \rho_w g \int S_{ds} d\omega\, d\theta$, where g is the gravitational acceleration.
- S_{nl} is the non-linear exchange of energy between wave modes. This transfer can occur through wave-wave interactions, which redistribute the wave energy among wave components. Additionally, the non-linear advection term, $(U(0) + c_g)\,\nabla F$, can also

transfer energy between wave modes through wave-current interactions as the wave propagate through current gradients. This type of energy transfer also occurs when the alternating orbital velocity of the long waves generates convergence/divergence of the short waves field due to Doppler shifting (Kraus and Businger 1994). One additional source of energy associated with this term results when the wave energy entering a region is greater than that leaving the region. The resulting radiation stress divergence can be an important source of energy, particularly in shallow water where shoaling waves steepen and break more frequently as they near shore.

- S_{in} is the energy input from the wind to the waves. It is related to the energy flux from the wind to the waves through $E_{aw} = \rho_w g \int S_{in} d\omega\, d\theta$.

Both theoretical and observational investigations of the energy input term have shown that the energy flux to the waves E_{aw} is substantially larger than u_*^3 under most conditions. This can be shown with the relationship between the momentum and energy flux into waves given by

$$E_{aw}(\omega, \theta) = c(\omega)\, \tau_{aw}(\omega,\theta) \qquad \textbf{(27)}$$

where $c(\omega)$ is the frequency dependent phase speed of the waves. Therefore, the total energy flux to the waves can be determined by integrating this relationship over all frequencies and directions. The difficulty of measuring τ_{aw} over the ocean make this type of integration rather impractical. To overcome this difficulty, Terray et al. (1996) used a parameterization of S_{in} to model the flux of energy to the waves as

$$E_{aw} = \rho_w g \int S_{in} d\omega\, d\theta = \bar{c}\tau_a \qquad \textbf{(28)}$$

where $\bar{c}$ is an effective phase speed. For growing waves, Terray et al. (1996) found that the effective phase speed is approximately equal to $[0.2 - 0.6]c_p$ for fully developed to developing seas, where c_p is the phase speed of the peak of the wave spectrum. Using the approximation that $c_p \approx U \approx 30u_*$, Eqs. (3) and (4) can be combined to show that $E_{aw} \gg E_{ao}$. This result also indicates that the amount of energy going to the wave field is 20-50% of the total kinetic energy entering the surface layer. Lionello et al. (1996) point out the same fact using a slightly different set of arguments, i.e., the flux of energy to the waves (through normal stresses) is generally much greater than the flux of energy to the mean current field (through tangential stresses), and that the total is a substantial fraction of the energy entering the surface layer.

4. Energy Transfer from the Waves to the Ocean: Wave Breaking

The conclusions of the last section generates the ultimate question: Where is this energy going? The answer lies in the energy dissipation term, S_{ds}. This energy is easily accounted for by numerous observations of dissipation in the near-surface ocean that are substantially greater than the wall-layer prediction given by **(20)** (e.g., Agrawal et al. 1992; Drennan et al. 1996; Annis and Moum 1992, 1995). This enhanced dissipation was the focus of the investigation by Terray et al. (1996). These observations suggest that breaking of dominant surface waves significantly enhances surface turbulent kinetic energy, and that the near surface current profile is very different from that found in the shallow wall-layer. This view is clearly supported by time series analysis of the subsurface turbulence signals that show intermittent bursts of strong eddies due to breaking waves are larger than the background turbulence by orders of magnitude (Agrawal et al. 1992).

Additionally, measurements taken very close to the surface (approximately 40 cm) as part of the joint NSF/ONR MBL/CoOP experiment by McGillis et al. (1999) show that the normalized dissipation rates are orders of magnitude greater than unity even at low to moderate winds, when no large breaking waves are present as shown in Fig. 5. Because the characteristics of turbulence generated through shear instability are expected to produce law-of-the-wall type profiles, it is hypothesized that small-scale breaking and Langmuir circulation (discussed below) are the cause of the enhanced energy transfer from wind waves to subsurface turbulence at low to moderate winds. This is based on observations that both Langmuir circulations and the microscale breaking of wind waves readily occur at relatively moderate wave steepness without visible whitecapping.

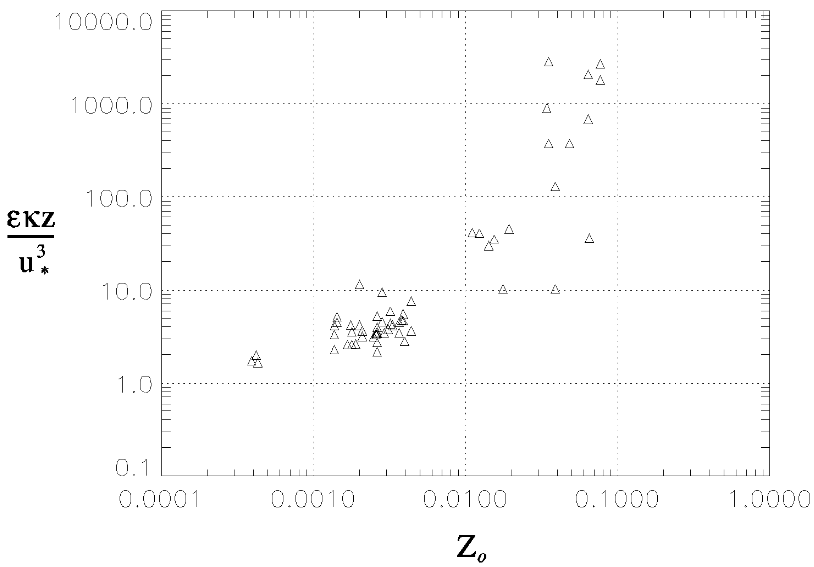

Figure 5: Non-dimensional subsurface turbulent dissipation measurements scaled with atmospheric forcing (u_*) as a function of z_o, (Charnock, 1955).

The enhanced dissipation is more or less an indirect result of the transfer of energy from the waves to the ocean. The amount of energy going into the current field (which could enhance shear production and thereby dissipation) versus the energy going into disorganized turbulent motion (which would also enhance the dissipation) has yet to be quantified. This is mainly because accurate measurements of the current shear within the wall layer are extremely difficult to obtain under the ocean due to the presence of waves. However, there is some evidence from laboratory (Cheung and Street, 1988) and field experiments (Kitaigorodskii et al. 1983; Thorpe 1984) that a nonlogarithmic velocity profile exists in the near-surface region affected by waves.

Craig (1996) used the measurements of Cheung and Street (1988) to develop a 1-D mixed-layer model of the near surface velocity and the KE profiles within the constant flux layer. This model, which is an adaptation of the open ocean formulation proposed by Craig and Banner (1994), provides good agreement with these observations. It includes wave effects through its boundary conditions for surface velocity and kinetic energy flux E_{wo}. The numerical results of both Craig and Banner (1994) and Craig (1996) suggest that the principal balance in the KE equation is between the total (pressure plus energy) transport and dispersion in the near surface layer.

Beneath this layer, a balance between production and dissipation holds such that **(20)** applies. Additionally, while the velocity profile is shown to follow a $z^{-0.8}$ power law near the surface, a logarithmic velocity profile produced very similar agreement with the measurements by adjusting the roughness length to a larger value. The larger roughness length is required to simulate the enhanced turbulence transferred from the wave field. Their results implies that 1) the near surface profile remains fairly logarithmic, 2) the energy input from the waves is simply being dissipated at the same rate that it is being transported away from the surface, and 3) the wave energy is not significantly enhancing the production term. This result is consistent with the generally good performance of simple 1-D models that assume that $\tau_a \approx \tau_o$ and ignore E_{wo} in their parameterizations of mixed-layer dynamics.

In summary, in the absence of stratification or buoyancy, the flux of kinetic energy in the marine atmospheric surface layer is either 1) converted to thermal energy through viscous dissipation, 2) directly transferred to the current field, 3) or transferred to the wave field. The transfer of some of this energy to the ocean results in less dissipation than predicted by traditional wall-layer parameterizations, in other words, a dissipation deficit. Some of the kinetic energy is consumed working against the stratification in stable conditions, whereas buoyancy will generate additional kinetic energy in unstable conditions. The effect of thermal stratification will thereby affect the amount of energy reaching the surface at a given wind speed.

The total amount of energy entering the ocean is, in general, a substantial fraction of the total energy entering the top of the atmospheric surface layer. Of this total, a much larger portion of the energy from the atmosphere is directly transferred to the wave field rather than the current field, $E_{aw} \gg E_{ao}$, once gravity-capillary waves form. However, the amount of energy **retained** by the waves is roughly the same as the energy going into the currents $E_w \approx E_{ao}$. The remainder is quickly transferred from the waves to the ocean, i.e., most of the wave energy, particularly from the short wave, is quickly dissipated and provides enhanced levels of kinetic energy to the current field.

It seems reasonable to expect that the dissipation deficit in the atmosphere due to the flux of energy to the ocean should be nearly balanced by the enhanced dissipation found beneath the waves. However, the ultimate fate of this energy remains an important research issue. For example, to properly model or simulate near surface flows we need to determine what fraction of this energy is going into the mean flow thereby enhancing the shear and momentum transport, and what fraction is going into the unorganized turbulent motion. Both of these pathways would explain the observations of enhanced dissipation, and both mechanisms would require modifications to traditional closure schemes in numerical models.

Crawford and Large (1996) state that "most of this energy is dissipated in the lower 10 m of the atmosphere." Although the claim that most of the energy entering the WBL is dissipated before reaching the ocean is generally not true, the assumption that most of the energy is dissipated in the atmosphere may not be crucial to their model because it does not require the very near surface structure for the model to simulate what they are investigating, i.e., global circulation. For example, their model may work very well because they are simply including the wave input to the ocean's kinetic energy as

$$E_o = U_1 \tau_a \approx U_1 \tau_o = U_1 \tau_{ao} + U_1 \tau_{ow} \qquad \textbf{(29)}$$

i.e., they are including energy going into the mean currents by means of the momentum flux from the short waves to the ocean. The success of this model suggests that over the open ocean, it appears that inclusion of this additional energy is generally not required to drive ocean circulation models. As a result, the assumption that most of the energy is dissipated in the atmosphere is not crucial to their model because it does not need to model the very near-surface structure for the model to simulate what they are investigating, i.e., large scale circulations.

In conclusion, the importance of accounting for E_{aw} and E_{wo} in numerical models and simulations probably depends on what you are trying to predict or simulate. Ignoring this energy may be fine for climate models, but it may be important for accurate forecasts of surface currents or waves. Additionally, the fate of this energy in coastal waters or other spatially (or temporally) varying conditions is poorly understood. However, the question of whether or when we need to include these terms is likely to remain unresolved until we have a better understanding of how this additional energy influences the near-surface flow.

5. Energy Transfer from the Waves to the Ocean: Wave-Current Interactions

In addition to transferring momentum and energy to the near-surface flow, wave-current interactions generate transient, coherent structures, known as Langmuir cells. One of the major research objectives of ONR sponsored mixed-layer research is to understand the role of the additional circulation these cells generate in the oceanic boundary layer. It is known that these circulations transfers energy from the long surface gravity waves and the near surface current profile into counter rotating roll vortices in the oceanic mixed layer (Craik and Leibovich 1976). The energy from these organized circulation cells drive additional vertical transport of heat and momentum from the air-sea interface to the base of the oceanic mixed layer. However, the exact mechanisms of these transfers are still the topics of rigorous ongoing investigation.

Historically, characterization of Langmuir circulations (LC) has proved to be difficult because it requires observation of the near-surface structure of the oceanic mixed layer on scales of 10-cm to 10-m in a variety of conditions. Measuring the horizontal and vertical velocities associated with the cells is arduous since the currents associated with the Langmuir cells are expected to be small (less than 20 cm/s) when compared to orbital velocities of the surface waves. Observations of scalars, such as temperature, does not always reveal the structure of LC. It is possible to remove much of the surface wave problem but the signature from the cells is small because the mixed-layer water is well mixed. Acoustic tracking of bubbles beneath the surface has been used to visualize the near-surface signature of cells; however, the bubbles do not passively trace the vertical circulation of the cells.

Nonetheless, a few experiment have successfully measured these circulations. For example, the observations given in Weller and Price (1988) clearly show the 3-D structure of Langmuir circulations in the mixed layer. These observations indicate that Langmuir circulations may increase the mixed-layer entrainment rate by a factor of two during convective mixed-layer deepening events. Gnanadesikan (1995) also suggests that Langmuir cells can drive mixed-layer entrainment in the presence of large, long surface waves without significant wind forcing.

E. Breaking Waves and Bubble Production

Large-scale breaking waves entrain significant amounts of air into the ocean generating bubble concentrations that extend well into the mixed layer. The residence time of the larger bubbles is mainly determined by their size-dependent rise velocity. The residence times of smaller bubbles may also be affected by the turbulent flow in the near surface layer. These bubbles may reside on the surface for a significant amount of time depending on the surface characteristics, which may be modified by the presence of surfactants. As such, these bubbles can act as tracers that map out the surface signatures of Langmuir cells (Farmer and Li 1995), or the edge of current fronts and rips (Marmorino and Trump 1996).

Bubbles produced by breaking surface waves play an important role in air-sea interaction studies, both *directly*, through the exchange of potential or kinetic energy in the breaking process, the modification of upper ocean turbulence and Langmuir circulation by a buoyant surface layer, their contribution to air-sea gas exchange and to the acoustic and optical environment; and *indirectly*, as passive tracers of upper ocean processes, including those associated with the direct effects. Additionally, the actions of breaking waves and bubble productions generates easily detectable ambient noise. This noise can strongly degrade the performance of the Navy's systems that attempt to detect unnatural acoustic signatures or map objects using acoustics. However, this noise has also been used as a signal to determine such geophysical variables as wind speed and rain rate.

It should be no surprise that acoustical methods have played a central role in observing bubble distributions. Bubbles have a very high quality factor at resonance, giving them an acoustical cross-section some three orders of magnitude greater than their geometrical cross-section. This effect typically reaches a maximum at an acoustical frequency of 30kHz, corresponding to a bubble radius of 100 µm. Different frequencies excite bubbles of different radii so that the size distribution becomes a crucial factor in acoustical measurement. But bubbles of different sizes behave differently in the turbulent surface layer. Thus measurements of bubble size distribution lead us to questions of near surface turbulence, advection and other properties central to a dynamical description of air-sea interaction.

The task of interpreting bubble measurements demands much improved models of upper ocean processes. For example, it has long been known that most of the air entrained by a breaking wave rises to the surface within a few seconds, forming the whitecaps visible whenever the wind speed rises above about $5ms^{-1}$. But wave breaking leaves a debris of smaller bubbles that can persist for minutes. These smaller bubbles are drawn into the convergence zones of Langmuir circulation (a term used here to encompass all coherent motions that tend to align with the wind), forming subsurface 'windrows' that are a characteristic feature of high frequency acoustic imaging. Their organisation in this way serves as an effective integral measure of the near surface circulation, as well as providing useful acoustical targets for deriving the instantaneous velocity field using Doppler processing. Similarly, the injection of bubbles by breaking waves provides a signal for the measurement of breaking wave distributions and properties.

Consider the life history of bubbles produced when a wave breaks. The initial air-entrainment is evidently accompanied by intense turbulence. Individual bubbles break into a spectrum of smaller bubbles as turbulent pressure fluctuations surpass the restoring force of surface tension (i.e. the turbulent Weber number exceeds unity). The break up of larger bubbles occurs rapidly, forming an initial size spectrum which appears to have a spectral slope of between -2 and -3. As each bubble is formed, it tends to revert to its lowest energy (i.e. spherical) shape, radiating acoustic waves as it does so. Surrounding bubbles may absorb much of this energy, by enough escapes to provide a very detectable signal with properties that depend on the conditions within the whitecap itself.

Gravity plays no significant role in the fracturing of air at the moment of breaking, but quickly asserts itself thereafter, sorting the bubble distribution through buoyancy: the large bubbles quickly disappear, steepening the large radius end of the spectrum. At the small radius end of the spectrum, dissolution is at work. The primary gases, Nitrogen and Oxygen, dissolve at different rates dependent on their solubilities and the partial pressure differences across the bubble skin (thus requiring measurement of dissolved N_2 and O_2 for comprehensive model analysis). Close to the surface, in supersaturated waters, the bubbles can actually grow, but they only have to penetrate a short distance for hydrostatic effects to dominate, leading to rapid dissolution of the smallest bubbles. These opposing effects, buoyancy and dissolution, tend balance at a radius of around 100mm, which explains the general shape of the resulting size distribution. Turbulence also plays a role here, and helps suspend a 'stratus' of bubbles close to the surface. Over time scales of 10-100s, advection becomes important and the bubbles drift towards convergence zones. As they descend, increased hydrostatic pressure, augmented by surface tension, further decreases the radius, thus reducing the bubble buoyancy and enhancing the dissolution, leading to their disappearance.

The bubble size distribution provides a signature that can be used to interpret the detailed physical processes at work in the upper ocean, and further motivates development of models incorporating essential elements of the factors shaping the spectrum, from initial bubble creation to loss through buoyancy or dissolution. At each step, questions arise about the magnitude of different processes. What is the wave breaking frequency? What is the depth of injection? How is turbulence within the whitecap related to the observed bubble size distribution at source? What are the characteristics of near surface turbulence outside of wave breaking? How do bubbles contribute to air-sea gas exchange and to the formation of aerosols? What role do surfactants play in inhibiting gas transfer across the bubble skin? How does the buoyant surface bubble layer affect near surface turbulence? Does it provide a significant torque in opposition to the Craik-Leibovich torque thought to drive Langmuir circulation? What is the significance of three-dimensionality and longitudinal instability in Langmuir circulation to the observed bubble distribution? What is the physical explanation of the observed sound spectrum radiated by breaking waves and how do bubble layers influence near surface acoustic propagation?

Both observations and model analysis of bubble distributions are at a relatively undeveloped stage. The techniques for observing bubble distributions using acoustical methods have been developed to the stage at which self-contained instruments can be deployed for extended periods. Passive acoustical sensing has been used to track individual breaking waves and provokes questions about the relationship of acoustical spectral shape to the initial bubble size distribution. Optical methods are essential within the whitecap, where bubble densities tend to be too high for useful acoustical measurement. Acoustic imaging techniques have provided numerous pictures of the bubble distribution and Doppler measurement has provided many insights on the dynamics, as well as contributing to measurement of the directional wave properties. But the measurement of all of the important variables and their synthesis remains an outstanding challenge, not least because of the difficulty of deploying, maintaining and recovering sensitive instruments suitable for near surface observation at high sea states. Nevertheless, it is anticipated that as progressively more comprehensive and accurate models of the ocean surface layer are sought, oceanographers will increasingly turn to the observation and interpretation of bubble distributions and properties. Bubbles are the primary target for acoustical remote sensing beneath the surface and their spatial distribution and size spectra challenge our ability to explain the crucial physical processes of air-sea interaction.

F. Sea-Spray and Marine Aerosol

Sea spray droplets form at the sea surface primarily by two processes. Waves break and engulf near-surface air. This air gets distributed into bubbles; and when these bubbles rise to the surface as a whitecap, they burst and create film and jet droplets. Film droplets form from the thin film that caps a bubble and typically have radii of a few micrometers. After a bubble bursts, the bubble cavity collapses and shoots up a jet of water from its base. Because of instabilities along this jet, it breaks up into 5-10 jet droplets with radii from a few to a few tens of micrometers.

The second main process that creates sea spray is the mechanical tearing of the wave crests by the wind: When the wind gets high enough, it can simply rip water off the wave crests and thus creates a class of sea spray called spume (Monahan et al., 1986). Spume droplets are the largest spray particles; radii are typically larger than 20 micrometers.

Rain drops striking the sea surface and large spray droplets falling back into the sea also produce spray droplets mechanically. Such sea spray particles are usually called splash droplets (e.g., Andreas et al., 1995). Although a lot of work has been done on spray generation by whitecaps (e.g., Blanchard, 1963; Monahan et al., 1986; Woolf et al., 1988), less has been done on spume production (e.g., Andreas, 1992, 1998), and still less is known about the production of splash droplets. Generally, the spume droplets account for most of the spray volume flux, while splash droplets are generally believed to be an insignificant part of the total spray volume.

All spray droplets are ejected into the WBL and there seems to be substantial evidence that wave motions are important in droplet dynamics near the surface. For instance, profiles of droplet concentrations often show a near-surface maximum at one to two metres (e.g. De Leeuw; 1986a,b, 1987, 1990). These observations prompted a mildly acrimonious controversy (Wu; 1990, De Leeuw; 1990) as to whether the cause of the maximum was transport in the wave-induced flow concentrating the droplets near the wave crest, or that it was near the crest because these were spume droplets which were produced at this height. A modelling study by Mestayer *et al.* (1996) supported the former hypothesis, although they simplified the dynamics in that the turbulent diffusion is applied separately from the wave-induced advection, neglected droplet evaporation, and presented results for only a single wave shape. Further, while Mestayer *et al.* found their droplet concentration maximum near the crest height, the relationship between the significant wave height and the height of the maximum is not so clear-cut in the observations. Similarly, Andreas *et al.* (1995) used Edson and Fairall's (1994) Lagrangian spray transport model with a wavy lower boundary to show that wave motions could substantially increase droplet concentrations above the wave height.

The wave-induced motion in the WBL and the turbulent motion throughout the ABL can prolongs the residence time of spray droplets. Therefore, these two dispersion mechanisms allow the droplets to interact more fully with their environment. These interactions have several effects on the marine boundary layer (MBL). Sea spray droplets are the source of the local marine aerosol and, thus, affect the optical properties of the MBL. When dispersed to higher altitudes, these aerosol particles also serve as condensation nuclei for marine clouds. Similarly, the evaporating sea-spray can influence the humidity and temperature profiles, particularly at moderate to high wind speeds, and therefore could affect electromagnetic propagation in the near surface layer by changing the strength of the surface-based duct. Finally, by effectively increasing the ocean's surface area, spray droplets might also modify the rates at which heat and moisture are transferred across the air-sea interface.

1. Influence on Energy Exchange

Ocean scientists have been speculating for at least 50 years that sea spray droplets can enhance the usual interfacial fluxes of heat and moisture. The community has reached no consensus, however, because our understanding of the relevant spray processes are so rudimentary; there are so many possible feedback loops among the air, the sea, and the spray; and measurements in winds high enough to see spray effects are very difficult. In fact, spray's role in air-sea transfer is so ambiguous that, in just the last six years, Ling (1993) could state unequivocally that sea spray is responsible for large air-sea latent heat fluxes in winds as low as 10 m/s, while Makin (1998) could state as emphatically that sea spray has "no impact" "on heat and moisture fluxes" for wind speeds up to 18 m/s. Three consecutive papers in the Hurricanes and Tropical Meteorology Conference at the recent annual meeting of the American Meteorological Society further highlighted this controversy. Andreas and Emanuel (1999) led off by concluding that, primarily by transferring sensible heat, sea spray could markedly increase the intensity of tropical cyclones. Wang et al. (1999) and Uang (1999) followed with presentations that focused largely on spray's ability to transfer water vapor and concluded that, though spray can effect the rate at which a cyclone develops, it cannot affect its final intensity.

There are three main issues we need to confront to progress in understanding spray's role in air-sea heat exchange. The most fundamental and most difficult is evaluating the sea spray generation function--the rate at which spray droplets are formed as a function of wind speed. The spray generation functions available in the literature span almost six orders of magnitude at any given droplet radius; but on theoretical grounds, Andreas (1998) excludes several functions and thereby reduces the range of plausible functions to a spread of about one order of magnitude.

The second issue is the residence time of spray droplets: How long do they have to exchange heat and moisture with their environment before falling back into the sea. This question couples droplet microphysics (e.g., Andreas, 1990) with the need to understand turbulence dispersion processes in the WBL (e.g., Edson and Fairall, 1994; Edson et al., 1996). In a nutshell, smaller droplets--the film and jet droplets--have relatively long residence times and exchange heat and moisture quickly. Because of the total volume of these produced, however, they do not seem to carry a lot of heat and moisture across the air-sea interface. Spume droplets, because of their size and production rate however, do carry a lot of heat and moisture but transfer both more slowly and tend to fall back into the sea before reaching thermal and moisture equilibrium with the near-surface air. In other words, there is a critical balance between a spray droplet's ability to exchange heat and moisture and the role of near-surface turbulence in suspending it long enough to accomplish this transfer. The answer to whether spray can or cannot influence the net air-sea heat flux therefore rests delicately on the interplay between residence time and droplet microphysics.

A related issue is the depth of the droplet evaporation layer. For instance, Kepert and Fairall (1999) studied spray evaporation and dispersion under conditions similar to those in a moderate tropical cyclone, with a 10 m wind speed of 25 $m.s^{-1}$. They found that although small droplets were transported to a great height, they produced a shallow DEL since they evaporated much more rapidly than they were transported. Large droplets also produced a shallow DEL, but because they were barely transported by turbulence. Interestingly, there was an intermediate range of droplet sizes that were still actively evaporating several tens of metres above the surface. These were both light enough to be transported by the turbulence, and large enough that their evaporation time scale was of similar order to their transport time scale. The radius of these droplets lies near the peak volume production in several plausible spray source functions, and so the consideration of their turbulent transport is important in calculating the droplet-mediated fluxes. Also, the fact that the DEL may be several tens of meters deep may be expected be important both to parameterization of spray fluxes, and to interpretation of flux observations at high wind speeds.

The third issue is that of feedbacks. As spray evaporates, it moistens and cools the surrounding air, which has several consequences. Firstly, this is a negative feedback on further spray evaporation, either by increasing the equilibrium radius (for small droplets) or reducing the evaporation rate (for larger ones). Kepert and Fairall (1999) showed that these processes began to have a significant impact even at quite low source rates. The boundary layer adjusts to limit this feedback by removing the excess moisture supplied by, and replenishing the sensible heat consumed by, evaporating droplets. However, its capacity to do so is limited, and so the efficiency at which droplets modify the near-surface conditions reduces dramatically at high source rates. They argued that proper assessment of this process required consideration of the whole boundary layer and showed that this adjustment placed an upper bound on the net spray evaporation. A related issue is that of how much of the droplet contribution to the fluxes is "realised" above the evaporation layer. While Fairall *et al.* (1995) assumed 0.5 was appropriate, the model simulations of Edson *et al.* (1996) and Kepert *et al.* (1999) suggest a somewhat higher figure. Further feedbacks arise due to the stability changes in the evaporation layer reducing the turbulence there. However, as the near-surface turbulence at high wind speeds is overwhelmingly generated by shear, these effects are small.

The forth issue is the lack of data necessary to evaluate spray processes in high winds. HEXOS (for Humidity Exchange over the Sea Experiment) provided excellent turbulence flux data for wind speeds less than 20 m/s (DeCosmo et al, 1996). Andreas and DeCosmo (1999) used these data to tune Andreas's (1992) spray model and therefore to partition the spray fluxes into sensible and latent heat contributions. To evaluate spray's role in generating and maintaining tropical cyclones, however, we need data in winds up to at least 35 m/s. Unfortunately, we have no proven technology for making the required direct flux measurements in such severe conditions. These issues are discussed further in section 5.G.

In summary, concern over sea spray's ability to transfer heat and moisture across the air-sea interface cannot be divorced from the more general field of air-sea interaction research. In wind speeds above about 15 m/s, sea spray droplets proliferate. The bulk-aerodynamic methods for estimating air-sea sensible and latent heat fluxes, such as the TOGA-COARE algorithm

(Fairall et al., 1996), can no longer be strictly accurate in such conditions. Modern air-sea flux estimation schemes must explicitly include a spray parameterization. Andreas and DeCosmo's (1999) solution to this problem was to complement the TOGA-COARE algorithm with a spray parameterization tuned with the HEXOS data to produce a unified air-sea flux model. Of course, this model is currently limited by the maximum HEXOS wind speed of 20 m/s.

2. Effect on Electro-Optical Properties

Although the heat and moisture exchanged by film and small jet droplets have minimal impact on the surface heat budget, the salt they leave behind is a major component of the marine aerosol and can have an impact on the radiative transfer and electro-optical properties of the marine atmosphere. They provide a component of the total aerosol spectrum as described in the Navy Aerosol Model (Gathman, 1983; Gathman and Davidson, 199X). In this model, the ...

3. Effect on the Evaporative Duct

The numerical simulations by Rouault et al. (1991) and Edson et al (1994) have shown that sea-spray can have a

G. High-Wind Issues

Tropical cyclones are the most obvious and important high-wind events over the open ocean. Although there have been impressive improvements in predicting cyclone tracks in the last several decades, there has been no noticeable improvement in predicting the change in cyclone intensity. Since the wind force on structures increases, roughly, as the square of the wind speed, the inability to predict storm winds reliably has serious implications for human safety. This forecasting problem also reflects the dearth of our understanding of what happens at the air-sea interface in winds above about 30 m/s, when the near-surface air is "too thick to breathe and too thin to swim in" (Kraus and Businger, 1994, p. 58).

There are also crucial issues at more moderate wind speeds. The drag coefficient C_D, which parameterizes the surface stress as a function of wind speed, has been measured rarely over the open ocean at 10-m winds above 20 m/s. Large and Pond's (1981) evaluation, which was for 10-m winds up to 25 m/s, is the best available data set. Smith's (1980) set of C_D measurements includes wind speeds up to 22 m/s. Both sets show a linear increase in C_D with wind speed. Geernaert (1990) reviews oceanic measurements of C_D but reports no open ocean observations of C_D in higher winds than in these two sets.

The bulk-transfer coefficients that parameterize the exchanges of sensible and latent heat, C_H and C_E, are also uncertain in high winds. The TOGA-COARE bulk flux algorithm (Fairall et al. 1996), which is generally regarded as the state of the art for parameterizing turbulent air-sea fluxes, has been tested only for 10-m winds up to about 15 m/s. Although the TOGA-COARE flux code and the analysis by Liu et al. (1979), on which that code is based, suggest the parameterization is valid for higher winds, no analysis has verified this. In fact, Andreas and DeCosmo (1999) have used the HEXOS sensible and latent heat flux data (DeCosmo et al. 1996) to test the TOGA-COARE algorithm for winds up to 20 m/s and found it to underestimate the latent heat flux, especially, in winds above 15 m/s. Andreas and DeCosmo attribute this bias to the effects of sea spray, which begins to proliferate at about 15 m/s.

Filling these knowledge gaps—i.e., knowing how to predict the surface stress for winds above 25 m/s and knowing how to predict the turbulent heat fluxes in winds above 15 m/s—is crucial if we are to make any progress in predicting the intensity of tropical cyclones. Analytic models of the maximum potential intensity of tropical cyclones (Emanuel 1986, 1991; Holland, 1997) demonstrate considerable skill at placing an upper limit on the intensity of the most severe storms. These models, however, ignore the physics of the transfers across the air-sea interface by parameterizing the near-surface meteorological conditions as simple functions of the sea surface temperature—typically as a prescribed air-sea temperature difference and near-surface relative humidity. The precise values employed tend to be treated as tuning parameters for the respective models; and, indeed, the models are quite sensitive to the exact choices made (Holland 1997). These models are thus incomplete in that they depend crucially on the near-surface physics but conceal the details of the processes that determine it within these tuning parameters.

And this neglect is not unimportant. For example, Emanuel's (1995) axis-symmetric tropical cyclone model produces a realistic storm only when the ratio C_H/C_D is in the range 1.2-1.5. Large and Pond's (1981) prediction of C_D and an extrapolation of the TOGA-COARE prediction of C_H produce a ratio that is already below this range when the wind is as low as

20 m/s. On the other hand, the operational GFDL hurricane prediction model (Kurihara et al., 1998) takes the crude approach of using equal roughness lengths for scalars and momentum, which gives C_H/C_D = 1. High-resolution regional research models, such as the Penn-State/NCAR model MM5, generally take this same approach.

Evidently, other processes come into play in high winds that tend to augment the C_H/C_D ratio. For one, sea spray could enhance the transfer of heat. Although when spray is present, the transfers of sensible and latent heat can no longer be parameterized strictly in terms of C_H and C_E (Andreas, 1994), the basic effect is the same—the turbulent heat fluxes are larger when spray is present. Other sections of this document discuss spray's role in air-sea heat and moisture transfer in more detail. But the recent simulation by Bao et al. (1999) of hurricane development with a coupled atmosphere-ocean-wave model is one example of sea spray's impact. Bao et al. find that including a sea spray parameterization can significantly increase the fluxes of sensible and latent heat and produce a much more intense storm.

Likewise, there are suggestions from wind tunnel studies that C_D does not increase without limit with increasing wind speed, as we would infer from extrapolating the Large and Pond (1981) results. Rather, on the basis of a wind-wave tunnel study, Wade McGillis (1999, personal communication) suggests that C_D seems to approach an asymptotic limit for winds over 30 m/s; and Mark Donelan (1999, personal communication) similarly finds that waves cease growing at about this wind speed range. Frank (1984) performed a budget study of the hurricane boundary layer which suggested that C_D as given by Large and Pond was too large at high winds. Shay (1999) studied the oceanic internal wave energy flux forced by Hurricane Gilbert and again found that there appeared to be an upper limit to C_D. Further, the hurricane storm surge model of Hubbert et al. (1991) also limits C_D at high wind speeds to avoid overprediction. Certainly these pieces of evidence are indirect and must be treated with caution. Nor do any of these studies direct us towards a reason for the phenomenon. But we speculate that, in high winds, perhaps the wave crests are simply sheared off such that the wind mechanically limits the wave height and thus the drag coefficient. The upshot is that there is weak evidence suggesting that C_H/C_D may remain between 1.2 and 1.5 at very high winds, as Emanuel (1995) predicts, despite extrapolations suggesting otherwise.

Because tropical cyclones can be considered to be heat engines that are driven by the enthalpy flux at the air-sea interface, models of them are very sensitive to the parameterization of that flux. Extratropical cyclones, on the other hand, are driven by synoptic scale dynamics as well as by the air-sea fluxes; therefore, models of them will be less sensitive to the air-sea flux parameterization than will hurricane models. Nevertheless, surface winds in marine extratropical cyclones can frequently reach hurricane strength, and the same uncertainties over the air-sea fluxes in hurricanes also apply to extratropical cyclones. Improving the parameterization of surface fluxes under high wind speeds should, therefore, also improve forecasts of the intensity of extratropical storms, although perhaps not to the same extent as for hurricanes.

There are a host of other scientific and observational issues when the winds get high and sea spray proliferates that range from turbulence generation and sound propagation in the oceanic mixed layer to the surface heterogeneity and associated boundary layer structure resulting in cyclonic storms. In high winds, both the near-surface air and the near-surface ocean have two phases—spray in the air and bubbles in the water. Satellite remote sensors can, thus, no longer sense the sea surface. For example, spray, foam, and bubbles confound infrared measurements of surface temperature and scatterometer measurements of surface-level wind speed.

These problems with remote sensing in high winds are examples of the difficulty in obtaining the good near-surface data that is critical for quantifying air-sea exchange processes in high winds. Katsaros et al. (1994) describe other difficulties with in situ instruments and recount some of the measures the HEXOS team took to circumvent them. Currently, though, we have no proven technology for measuring the fluxes of heat and momentum in the air near the sea surface in 10-m winds above 25 m/s. The standard turbulence wind sensors, sonic anemometers, begin to miss data when aerosols clutter the sonic paths. Since most high-frequency temperature measurements now also rely on sonic measurements of sound speed, aerosols also compromise turbulent temperature measurements. Turbulent humidity measurements—made for example with Lyman-α or infrared hygrometers—are also a problem since the contaminant (i.e., spray) has the same composition as the quantity of interest (i.e., water vapor). Clearly, advancing our understanding will require developing innovative new technologies for sampling at high winds in a two-phase environment.

6. Parameterizations of the Momentum and Energy Flux Over a Fully Developed Sea

With the myriad of physical processes taking place in the marine boundary layers, it should come as no surprise that analytical solutions of the equations of motion are rarely applicable to the real atmosphere or ocean. The modeling of the turbulent flows generally requires more realistic parameterizations of the turbulent processes and often higher order-closure schemes, neither of which is amenable to analytic solutions. Instead, the system of equations must somehow be closed, discretized, and numerically solved to arrive at a steady state solution or marched forward in time to arrive at a forecast.

In this section, we focus on some of the parameterizations of the physical processes that are used to close the system of equations. We begin our discussion by considering the flux of momentum and energy within the portion of the marine atmospheric surface layer that lies above the WBL. We further limit the discussion to situations when the ocean and atmosphere are in equilibrium, i.e., the wave-field is fully developed and stationary.

A. Momentum Flux

The bulk aerodynamic method remains the most commonly used model to estimate the fluxes of momentum and heat into the open ocean. Based on scaling arguments, Taylor (1916) suggested that drag of the atmosphere on the earth's surface should be proportional to the wind speed squared

$$\tau_a = \rho_a C_D U^2 \qquad \textbf{(30)}$$

where τ is the momentum flux (surface stress), and C_D is a constant of proportionality known as the drag coefficient. The drag coefficient can be thought of as a measure of the surface roughness and remains fairly constant for a given surface. Over the ocean, however, this quadratic relation must be modified to account for the dynamic nature of the surface.

Using the bulk aerodynamic method to estimate the momentum flux is most applicable to the fully-developed open ocean. Under these conditions the form drag is negligible, and a wind speed dependent drag coefficient is most applicable to compute the momentum flux going into the ocean currents. There are two approaches to parameterizing the drag coefficient. The first is a straightforward parameterization where the measured drag coefficient is plotted versus wind speed. Quite often, a lower limit is placed on the wind speed used in the parameterization to avoid situations when the sea surface is not aerodynamically rough. For example, a commonly used parameterization of this type is the formulation given by Large and Pond (1981)

$$C_{DN} = 1.2 \qquad 4 \leq U_{rN}(10) \leq 11 ms^{-1} \tag{31}$$

$$C_{DN} = 0.49 + 0.065\, U_{rN}(10) \qquad 11 \leq U_{rN}(10) \tag{32}$$

where C_{DN} and $U_{rN}(10)$ are the values of the drag coefficient and the 10-m wind speed (relative to the ocean surface) in the absence of any thermal stratification (N stands for neutral conditions), respectively. The effects of stability on momentum transfer are included through MO similarity theory (Obukhov, 1946), which provides stability parameters that increase (suppress) the drag coefficient under unstable (stable/stratified) atmospheric stability

$$C_D^{1/2} = C_d = \frac{C_{dN}}{1 - \frac{C_{dN}}{\kappa}\psi_m\left(\frac{z}{L}\right)} \tag{33}$$

where ψ_m is a stability function that is the integral form of ϕ_m defined by **(11)**.

The second approach is based on the assumption that a semi-logarithmic wind profile exists over the ocean. Integration of **(11)** results in

$$U(z) = U(z_o) + \frac{u_*}{\kappa}\left[\ln(\frac{z}{z_o}) - \psi_m(\frac{z}{L})\right] \tag{34}$$

where z_o is the height where the semi-logarithmic profile goes to zero. This height is a measure of the surface roughness and is commonly known as the aerodynamic roughness length, which is generally some fraction of the actual roughness elements, i.e., the gravity-capillary wave.

Combining this profile with **(30)** leads to an expression for the drag coefficient

$$C_D = \left(\frac{\kappa}{\ln\left(\frac{z}{z_o}\right) - \psi\left(\frac{z}{L}\right)} \right)^2 \qquad \textbf{(35)}$$

The momentum transfer due to short wind waves is traditionally parameterized using the roughness length introduced by Charnock (1955), which relates the equivalent roughness with the wind friction velocity as

$$z_{o_c} = \alpha \frac{u_*^2}{g} \qquad \textbf{(36)}$$

where α is an empirical constant known as the Charnock constant. The momentum supported by the viscous stress is generally modeled using a roughness length for smooth flow. Therefore, Smith (1980, 1988) combined these two parameterization

$$z_o = z_{o_c} + 0.11 \frac{\nu}{u_*} = z_{o_c} + z_{o_s} \qquad \textbf{(37)}$$

to include both viscous drag and the form drag from the gravity-capillary waves in the total roughness length. This provides a parameterization of the momentum fluxes

$$\tau_o = \tau_{ao} + \tau_{wo} = \rho C_D(z, z_o, L)\, U_r(z)^2 \qquad \textbf{(38)}$$

that has been shown to work well over fully-developed open ocean waves (Fairall et al., 1996). Smith (1980, 1988) and Fairall et al. (1996) found a value of α = 0.011 for open ocean conditions, while shallow water sites provide a higher value of α = 0.018 (e.g., Garratt 1977, Johnson et al., 1998).

Even under conditions of a fully developed sea, drag coefficient parameterizations remain uncertain in very low wind conditions. The drag coefficient is often observed to increase with weak wind conditions over the sea as well as over land, presumably due to the influence of smooth flow (viscous) effects, as noted above. The modulation of gravity-capillary waves by surfactants is expected to complicate this relationship. However, the patchy nature of surfactant slicks has made it difficult to quantify any surfactant effects in the field. Additionally, swell is rarely absent in the open ocean in low wind conditions and its effect on momentum exchange has only recently been investigated. Investigations of these processes is further complicated because of the naturally occurring variability at low wind speeds. Calculation of the drag coefficient at weak winds is an uncertain process since random flux errors become large and the calculation at weak winds becomes sensitive the exact method of calculation of the stress, such as choice of averaging time, inclusion of cross wind stress, exclusion of nonstationary cases and so forth (Mahrt et al. 1996).

The open ocean parameterizations also appear to become inaccurate at high wind speeds. Observations also show that a single value of the Charnock constant cannot parameterize the wind speeds up to the current limit of our observations (roughly 25 m/s). This implies that the gravity-capillary waves parameterized by Charnock's relationship is not the sole source of roughness in such conditions. At even higher wind speeds, hurricane models such as those proposed by Ginnis (199X) give unrealistic results if the drag coefficient continues of increase at the rate predicted by **(36)**.

An investigation by Frank (1984) of the momentum budget of the ABL over a hurricane suggested that drag coefficient did not increase forever with wind speed. Shay (19XX) investigated the internal wave energy of the OBL during the passage of Hurricane Gilbert and found a similar result. Various storm surge modelers (e.g., Hubbert et al. 1991) have also suggested that there may be an upper limit to the drag coefficient. Although we have to be cautious making too much of these indirect assessments, these results suggest that as yet to be defined processes may cause a decrease in the drag on the ocean under these extreme conditions. One explanation is the smearing of the interface due to air entrained in the water and vast amounts of sea-spray in the air. However, few, if any, measurements currently exist to investigate such hypotheses.

B. Rain-Induced Momentum Flux

Rain falling on the ocean surface directly transfers some of its momentum to the ocean surface (Caldwell and Elliot 1971) and changes the drag on the ocean surface by suppressing shorter gravity waves while generating gravity-capillary waves (Tsimplis 1992; Poon et al. 1992; Craeye and Schlussel, 1998). Caldwell and Elliot (1971) parameterized the rain-induced momentum flux using

$$\tau_R = \rho_R U_R(0) P \tag{39}$$

where ρ_R is the density of the rain drops, and $U_R(0)$ is the horizontal velocity of the rain upon impact. Caldwell and Elliot (1971) uses a simple model to show that the horizontal speed of the rain at impact was 80 to 90% of the wind speed at roughly 10-m. Using an average value of 15%, they combine **(39)** with **(30)** to obtain

$$\frac{\tau_R}{\tau_a} = 0.85 \frac{\rho_R R}{\rho_a C_D U} = 0.85 \frac{\rho_R R}{\rho_a u_*} \tag{40}$$

Using a value of the drag coefficient and precipitation rate of 1.2×10^{-3} and 20 mm/hr (5.6×10^{-6} m/s), respectively, results in a rain-induced momentum flux equal to 67% of the total turbulent flux at 5 m/s and 22% of the total flux at 15 m/s. Caldwell and Elliot (1971,1972) also showed that the 10-20 % momentum lost by droplet as it fell through the strongly sheared layer near the surface results in an equivalent gain by the atmosphere. Caldwell and Elliot (1972) also noted that the combination of the direct and indirect mechanisms ultimately means that all of the horizontal momentum of the rain drops ultimately reaches the surface, which implies that the coefficient in **(40)** is actually 1 rather than 0.85.

Clearly these results indicate that the rain-induced momentum flux can add a substantial amount of momentum to the ocean. However, the conclusions of such studies can be modified by at least three additional factors. The first involves the assumption in **(39)** that all of the momentum of the rain goes into the surface currents on impact. Tsimplis (1992) has shown that some of the kinetic energy of the rain generates small-scale turbulence that acts to suppress short waves less than 25 cm in wavelength. Houk and Green (1976) and Poon et al. (1992) also showed that some of the rain's kinetic energy goes into generation of gravity-capillary waves. This suggest that some of the rain's momentum is generating turbulence and small waves rather than contributing to the mean shear. It is interesting that this distinction is similar to the one made with the small-scale wave field, i.e., the rain be generating a significant flux of kinetic energy without enhancing the shear and, ultimately, the momentum flux.

The second, closely related, factor that can modify the transport of momentum to the ocean when it is raining involves the change of the surface roughness. If the overall effect is to reduces the surface drag, then the enhanced momentum flux from impacting rain can be offset by the reduced shear stress over the smoothed surface. Finally, the rain often generates a barrier layer that stabilizes the near surface as described above. This would act to suppress turbulent mixing and momentum exchange. Measurement of the momentum flux under a variety of wind speeds and rainfall rates are required to investigate the role of rain in momentum exchange.

C. Latent and Sensible Heat Fluxes

The bulk aerodynamic method has also been used to estimate the surface fluxes of sensible and latent heat

$$Q_h = \rho_a c_p C_H [\Theta_s - \Theta(z)] U_r \quad \textbf{(41)}$$

$$Q_e = \rho_a L_e C_E [Q_s - Q(z)] U_r \quad \textbf{(42)}$$

where c_p is the specific heat of air at constant pressure; L_e is the latent heat of vaporization; C_H and C_E are the Stanton and Dalton numbers, respectively; Θ is the mean potential temperature, Q is the mean specific humidity, and the subscript s refers to values at the ocean surface. The Stanton and Dalton numbers can be defined in terms of the drag coefficient and their respective scalar transfer coefficients

$$C_H = C_D^{1/2} C_\theta = C_d C_\theta \quad \textbf{(43)}$$

$$C_E = C_D^{1/2} C_q = C_d C_q \quad \textbf{(44)}$$

This approach is advantageous because it allows investigators to separate the drag coefficient, which is sensitive to both sea-state and wave age, from the scalar transfer coefficients, which are expected to be less influenced by the waves. Instead, these transfer coefficients may be influenced by additional processes such as wave breaking and sea spray evaporation (see below).

As with the drag coefficient, the Stanton and Dalton numbers can be parameterized as a function of wind speed (Large and Pond 1981; ...), or the transfer coefficients can be determined semi-empirically using MO similarity theory with diabatic profiles of temperature and humidity to derive the transfer coefficients as a function of their "roughness" lengths

$$C_\theta = \left[\frac{\kappa / Pr_T}{\ln(\frac{z}{z_{o\theta}}) - \psi_h(\frac{z}{L})} \right] \tag{45}$$

$$C_q = \left[\frac{\kappa / Sc_T}{\ln(\frac{z}{z_{oq}}) - \psi_q(\frac{z}{L})} \right] \tag{46}$$

where Pr_T and Sc_T are the turbulent Prandtl and Schmidt numbers under neutral conditions, respectively; and ψ_h and ψ_q are dimensionless stability corrections to the temperature and humidity profiles, respectively. Liu et al. (1979) used the laboratory results of Kondo (1975) to parameterize the thermal roughness lengths as a function of the roughness Reynold number.

Some forms of the bulk areodyanamic method lead to serious under prediction of the fluxes of heat and other scalars in weak winds. Therefore, the velocity scale for the bulk aerodynamic approach has been generalized to include the influence of ``large convective eddies" (Beljaars, 1995; Fairall et al., 1996; Grachev et al., 1998) by introducing the free convection velocity scale into the bulk aerodynamic relationship. This is asymptotically similar to modifying the stability function so that the heat flux does not vanish in the limit of vanishing wind speed (Mahrt and Sun, 1995). The velocity scale has also been generalized to include the influence of mesoscale motions that are on scales smaller than the spatial or grid-averaging scale (Mahrt and Sun, 1995; Vickers and Esbensen, 1998; Levy and Vickers, 1999). The difference between the generalized velocity scales and traditional one becomes significant for weak wind conditions. While such pragmatic generalizations improve the behavior of numerical models, the physics of the weak wind cases has not been isolated.

Fairall et al. (1996) derived dimensionless functions with the correct functional form in the convective limit and then combined these functions with the roughness length parameterizations given by Smith (1980) and Kondo (1975) to produce the TOGA-COARE bulk algorithm. The TOGA-COARE algorithm also corrects for the change of temperature from the near surface value commonly available from ships and buoys to the actual surface (or skin) temperature. The modular coding style of the TOGA-COARE uses physical models of each of the processes involved and is readily improved as new understanding of the physics is gained.

Research Issues*: Even over the open ocean, the value of the scalar transfer coefficients are not as well known as the drag coefficient. Currently, the modified Liu et al. (1979) model introduced by Fairall (1996) is represents the current state-of-the-art bulk aerodynamic code. However, the Fairall et al (1996) TOGA COARE algorithm introduced several new features which are not yet supported by measured data. For example, Fairall et al (1996) proposed modifications to the dimensionless profile functions so that they follow the correct power-law behavior in the convective limit. However, validation of these functions requires scalar profiles measurements that have yet to adequately measured over the ocean. As a result, the stability corrections commonly used in bulk parameterizations are still primarily based on overland measurements. Additionally, the maximum wind speeds experienced in TOGA COARE made it difficult to make any conclusive statements about the sheltering effect at high winds proposed by Liu et al. (1979). Finally, it is worth noting that the Stanton and Dalton numbers are a function of the drag coefficient to the half power as shown by* ***(43)*** *and* ***(44)****. Therefore, accurate parameterization of the Stanton and Dalton numbers is expected to suffer, although to a lesser extent, from the same uncertainties introduced by, e.g., sea-state, wave-age, and surfactants. Perhaps it is not surprising numerical modelers appear reluctant to include these parameterizations in their lower (upper) boundary conditions in atmospheric (oceanic) models.*

1. Parameterization of Modulation by Spray

Andreas (1992) has developed a simple model of the contribution of sea-spray to the sensible and latent heat fluxes. Andreas's (1992) model has three components. First, it predicts that rate at which sea spray droplets with initial radii between 2 and 500 μm are produced at the sea surface as a function of wind speed. This spray generation function, denoted by dF/dr_o, is derived from Miller's (1987) generation function but also has the first realistic prediction for spume production. Spume droplets are those torn directly off the wave crests by the wind, are typically 20 μm in radius and larger, and contribute most to the spray sensible and latent heat fluxes (Andreas 1992). Recently, Andreas (1998) extended the spray generation function to wind speeds up to 32 m/s.

The second component of Andreas's (1992) spray model is a complete microphysical model that computes, for droplets of arbitrary size, time scales that quantify how rapidly individual droplets exchange sensible and latent heat with their environment (Andreas 1990). By comparing these time scales with an estimate of a droplet's residence time above the sea surface, the model can estimate how much of a droplet's available heat and water it can exchange before falling back into the sea. The third component of Andreas's spray model is thus an estimate of this residence time, T_f, parameterized as the quotient of the significant wave amplitude and the droplet's settling speed in still air.

Andreas's model computes the nominal spray sensible (Q_{hd}) and latent (Q_{ed}) heat fluxes as

$$Q_{hd} = \int Q_{hd}(r_o)dr_o = \rho_s c_{ps}\int (T_s - T_{eq})\left[1 - e^{\mathrm{T}_f/\mathrm{T}_h}\right]\left(\frac{4\pi}{3} r_o^3 \frac{dF}{dr_o}\right) dr_o \qquad \textbf{(47)}$$

and

$$Q_{ed} = \int Q_{ed}(r_o)dr_o \approx \rho_s L_e \int \left[1 - \left(\frac{r(T_f)}{r_o}\right)^3\right]\left(\frac{4\pi}{3} r_o^3 \frac{dF}{dr_o}\right) dr_o \qquad \textbf{(48)}$$

where r_o is the droplet radius at formation, T_h is the time scale for sensible heat exchange, T_{eq} is the equilibrium temperature, and $r(\mathrm{T}_f)$ is the droplet radius after time T_f given by

$$r(\mathrm{T}_f) = r_{eq} + (r_o - r_{eq})\, e^{-\mathrm{T}_f/\mathrm{T}_e} \qquad \textbf{(49)}$$

where r_{eq} is the equilibrium droplet size at a given humidity and T_e is the time scale for latent heat exchange. The droplets equilibrium temperature is closely related to the wet-bulb temperature, but differs due to the effect of salinity.

Within the droplet evaporation layer (DEL), the evaporating droplets tend to cool and moisten the layer. Therefore, the effect the droplet's have on the temperature and humidity fields are closely coupled. The contribution to the sensible heat actually takes place before the droplet begins to evaporate as it surface temperature adjusts to the equilibrium temperature. Additionally, the sea spray affects the profiles of temperature and moisture in the droplet evaporation layer, which then modifies the fluxes computed strictly from bulk aerodynamic models described above. The feedback affect can be included in the parameterization of the total surface flux at the top of the DEL as

$$Q_h = Q_h^{bulk} + \beta Q_{hd} - (\alpha - \gamma) Q_{ed} \tag{50}$$

$$Q_e = Q_e^{bulk} + \alpha Q_{ed} \tag{51}$$

where α, β, and γ are small, non-negative numbers that account for any feedback effects. Andreas (1992) implicitly assumed $\alpha = \beta = 1$, $\gamma = 0$.

Fairall *et al.* (1994) modified the formulations of Andreas (1992) to study the effects on tropical cyclone development. Their improvements included a physically based extrapolation of the source function to higher wind speeds, and the use of α=β=0.5 and γ=0. They found that sea spray had a profound effect on the thermodynamics of the tropical cyclone boundary layer, and in particular could explain observations of surprisingly large air-sea temperature differences. Betts and Simpson (1987) constructed a thermodynamic budget of the tropical cyclone boundary layer based on saturation point dynamics, and found it was necessary to include droplet evaporation to achieve simultaneous closure of the sensible and latent heat budgets. Their method was, however, unable to distinguish between sea-spray and rain evaporation.

However, although these results are interesting, there are still sufficient uncertainties in the parameterizations that the scientific community is well short of achieving consensus as to the role of sea spray evaporation in boundary layer structure and thermodynamics, or in the dynamics of severe weather systems.

2. *Parameterization of the Rain-Induced Sensible Heat Flux*

The sensible heat flux associated with rain has been parameterized by Flament and Sawyer (1995) as

$$Q_R = c_{pw} \rho_R (T_R - T_s) P \qquad \textbf{(52)}$$

where c_{pw} is the specific heat at constant pressure of fresh water and T_R is the precipitation temperature. The investigation by Anderson et al. (1998) showed that the precipitation temperature is closely approximated by the ambient wet bulb temperature. Observations in the intertropical convergence zone by Flament and Sawyer (1995) showed that the sensible heat flux accounted for up to 40% of the net surface heat flux during rain events. Anderson et al. (1998) found that it accounted for 15%-60% of the net heat flux during rain events, which amount to 15% of the net surface heat flux when averaged over a 4-month period.

It is worth noting that the return of evaporatively-cooled spume-drops to the ocean surface would have a similar effect on the sensible heat flux. The magnitude of the effect would be a function of wide speed since high winds would be needed to generate a comparable amount of water. However, in term of their effect on the buoyancy flux, the return of the cooler, more saline droplets would act as a positive buoyancy flux at the surface. Therefore, the correlation between these two effects is expected to be positive and both would act to enhance mixing.

D. Scalar Profiles

The computation of scalar profiles temperature, humidity, and salinity is required for a number of Navy propagation and performance model. For example, the prediction or characterization of both EM (i.e., radar frequencies) and IR/EO propagation in the vicinity of the air-sea interface, it is necessary to generate profiles of temperature and humidity (or water vapor content). The temperature and humidity profiles are combined to generate microwave (radio) refractivity profiles as described in section **6.D.2**.

The atmospheric propagation/performance models generally rely on MO similarity and bulk aerodynamic formula (e.g., Fairall et al. 1978; Musson-Gennon et al. 1992; Babin et al.

1997). The currently accepted bulk aerodynamic formula is the modified Liu et al. (1979) algorithm described in Fairall et al. (1996). Using relationships that are similar to the velocity profiles given by **(34)**, profiles of temperature and humidity are determined by combining the MO similarity functions and bulk derived momentum, sensible heat, and moisture fluxes as

$$\Theta(z) = \Theta_s + Pr_T \frac{T_*}{\kappa}\left[\ln\left(\frac{z}{z_{o\theta}}\right) - \psi_h\left(\frac{z}{L}\right)\right] \quad \textbf{(53)}$$

$$Q(z) = Q_s + Sc_T \frac{q_*}{\kappa}\left[\ln\left(\frac{z}{z_{oq}}\right) - \psi_q\left(\frac{z}{L}\right)\right] \quad \textbf{(54)}$$

where T_* and q_* are defined by **(8)** and **(9)**, respectively. These profiles are then combined to produce the required refractivity profiles as described below.

1. Surface-based and Evaporative Ducts

The surface ducting of Electromagnetic (EM) signals occurs when the microwave/radar refractivity profile is negative near the surface. These ducts allow these signals to propagate over the horizon and are therefore beneficial to detection of low-flying and periscope threats. The microwave/radio refractivity index N_{RF} is given by (Bean and Dutton 1968; Battan 1973)

$$N_{RF} = (n - 1) \times 10^6 = \frac{77.6}{T}\left(P + 4810\frac{e}{T}\right) \quad \textbf{(55)}$$

where n is the index of refraction, e is the vapor pressure in millibars, and T and P are the temperature and pressure in Kelvin and millibars, respectively. The modified refractivity M_{RF} is often used to account for the earth's curvature

$$M_{RF} = N_{RF} + \frac{z}{10^{-6}R_e} \approx N_{RF} + 0.157z \quad \textbf{(56)}$$

where R_e is the earth's radius. Microwaves are therefore refracted downward whenever $\partial N_{RF}/\partial z$ is less than -0.157. If this gradient extends to the surface then microwaves originating within this region are trapped within this layer. This layer is known as a surface duct and acts as a waveguide (Babin et al. 1997), which can allow microwaves to propagate over the horizon if this vertical structure is maintained in the horizontal direction. These surface ducts are common features of the marine boundary layer due to the strong inversion as the top of the boundary layer. A subset of surface based ducts is the evaporative duct that is generally found near the ocean surface due to the strong humidity gradient (Cook 1991). However, the duct can be very weak in unstable conditions or greatly strengthened in stable conditions when the temperature profile is also negative.

2. EO/IR Propagation

The decay of infrared (IR) and electro-optical (EO) signal in the atmosphere are mainly to the effects of molecular, aerosol, precipitation and clouds/fog extinction. The molecular extinction is a function of temperature, pressure and humidity. Therefore, the most critical parameters for accurate nowcasts/forecasts of IR and EO propagation through the atmosphere are temperature, pressure, moisture content (vapor and liquid water), and aerosol size distribution. These extinction mechanisms are interrelated, e.g., the effect of humidity on the aerosol size distribution must be incorporated in IR/EO propagation models (Gathman 1983; Gathman and Davidson 1993). Additionally, the formation of fog is obviously related to all of the environmental variables and must be accounted for in these models. In fact, improving the Navy's ability to predict fog remains one of the top priorities of METOC officers and their staffs (personnel communications). Therefore, successful IR/EO models must also accurately reproduce the total moisture profile near the surface.

As with the EM propagation, the EO/IR signals can also be trapped with a surface duct when the refractivity profile is negative. To illustrate this we can examine the IR refractivity given by Edlén (1953)

$$M_{IR} = 23.72\left[1 + 2.2\left(1 - \frac{0.09}{\lambda}\right)^{-1} + 0.05\left(1 - \frac{0.16}{\lambda}\right)^{-1}\right]\frac{P}{T} - 0.043\left[1 - \frac{0.014}{\lambda}\right]e \qquad \textbf{(57)}$$

where λ is the wavelength in µm. This expression can be simplified to

$$M_{IR} \approx 77.19\left[1 + \frac{0.06}{\lambda}\right]\frac{P}{T} - 0.043\left[1 - \frac{0.014}{\lambda}\right]e \qquad \textbf{(58)}$$

for $\lambda > 1$ μm. Although the leading term of the IR and radio/microwave refractivities are closely related, the humidity (and wavelength) dependence makes it inaccurate to infer the refractivity profile for IR propagation from the EM refractivity profile. Therefore, separate profiles of temperature and humidity are required to compute the refractivity profiles in both EM and EO/IR models.

Research issues: *The Navy's ongoing research is aimed at determining how best to measure/model the surface layer refractivity profile for use in system performance assessment and optimization. Current theory shows considerable skill over the standard atmosphere at predicting representative evaporation ducting conditions for propagation paths typical of tactical problems. The bulk algorithms (e.g., Liu et al. 1979; Fairall et al., 1996) implementing the theory differ somewhat in predictive skill but are comparable.*

In the case of EM refractivity, the model should generate a complete vertical profile, calculated with stability effects included, rather than simply providing the duct height described below. This allows the user to either deduce a duct height from the profile for reference to existing data bases, or use an accurate profile in propagation calculations. As stated above, these profiles are typically provided by bulk aerodynamic formula that require the sea surface temperature and the air temperature, moisture (dew point temperature, wet bulb temperature, or relative humidity), and wind speed at a given height above the surface. Therefore, the same research issues that affect the accurate parameterization of the heat fluxes and scalar profiles apply to refractivity profiles.

Substantial increases in sensor accuracies are required to drive the bulk techniques. Based on the analysis given by Dockery (1991) for the unambiguous range/propagation factor in AEGIS, the following accuracy limits have been proposed: 0.25 deg temp, 2% relative humidity, and 10% wind speed. However, measurement accuracies needed to drive bulk aerodynamic models differ depending on the atmospheric thermal stability. In very unstable conditions (water warmer than overlying air), accuracies of 1 degree for temperature and dew point, and 2-3 m/s for wind don't change the calculated duct profiles significantly. In near neutral conditions, the *temperature and wind are much more critical, and basically should be as accurate as available. Uncertainties of more than one degree for temperature and dew point and 2 m/s for wind result in unacceptable errors.*

Because the propagation models are most concerned with horizontal propagation, horizontal variability of the temperature and moisture profiles are an issue. Therefore, the value added by increased accuracy is impossible to determine until the determination of the amount of error involved in using point meteorological measurements to characterize a path (horizontal homogeneity). Until the effects caused by turbulence and range varying ducting can be quantified, current existing models are adequate for refractivity profile estimation under neutral and unstable conditions. Additionally, a significant shortcoming of the bulk models exist with regards to stable conditions, i.e., profiles extrapolated from single level measurements cannot detect a subrefractive environment. Measurements up to several hundred meters may be needed for stable conditions resulting in ducting versus in subrefraction. Therefore, a sounding of some sort is certainly required to determine the top of the surface-based trapping layer.

Perhaps an even better alternative involves the assimilation of sounding and surface data into high resolution models. Even if these models are used only as interpolators in a nowcast mode, they could ultimately provide a much more useful 3-D picture of the environment. For example, recent efforts have been made to compute the refractivity profiles using mesoscale model output from COAMPS (Burk and Thompson 1997). The use of mesoscale models in these efforts is particularly important in regions where we cannot assume spatial homogeneity.

If accuracy considerations were extended to what measurements are needed but not presently available; one is sea state, including wave period and height. Most persons presently involved in air-sea interaction studies believe there is possibly some profile dependence on wave state as well as on stability given the same air-sea differences. The effect of spray as well as waves is an important open question at this time. Andreas et al (1995) have reviewed studies, that are just beginning to consider what happens to the profiles as spray-droplets are introduced. The impact of sea spray on the water vapor profile during high winds (>25 knots) could turn out to be more important for the purpose of determining the refractive profile than for water vapor flux.

7. Wave Growth Parameterizations

We now turn our attention to the more interesting, and certainly more commonplace, situation where the wave field is developing or decaying. Processes that foster growth or decay include time-varying winds due to frontal passages, wave shoaling in coastal zones, waves propagating across current fronts such as the Gulf stream, and enhanced wave damping due to the presence of surfactants. Our understanding of how the physical processes associated with these situations affect wave growth varies considerably from process to process.

Many of the current theories that attempt to explain the transfer of atmospheric energy to the wave field, i.e., S_{in}, have been around for over 40 years. Still, there is no one theory capable of describing the process of wave generation. Instead, different stages of wave growth are thought to be best described by different theories. All of these models attempt to describe how the ocean extracts energy from the atmosphere through, ultimately, the surface pressure-slope and surface pressure-piston velocity correlations in **(15)** and **(23)**.

A. Phillip's Resonance Model

The initial stages of wave-growth are generally attributed to the resonance mechanism described by Phillips (1957, 1977). Deformations at an initially undisturbed ocean can be generated by tangential (shear stress) or normal (pressure) stress fluctuations. Phillips (1957) considered only the turbulent pressure distribution that remain coherent over some finite time as they are advected over the surface. Phillips (1957) showed that the wavelengths contained in the advected pressure field are capable of generating waves of equal wavelength. Therefore, those waves's whose phase speed matches the advection velocity of the pressure distribution are expected to grow. In principle, this process can excite any wave that matches the wavelength of the pressure disturbance. However, this mechanism is too slow for longer waves and is most effective for initiating short gravity-capillary waves. Once these waves have formed, the mechanism is too weak to account for observed wave growth and must be supplemented by some other mechanism.

B. Jeffreys' Wave Sheltering Model

Jeffreys (1924, 1925) appears to be the first fluid dynamicist to consider the out-of-phase pressure-height variations that could lead to wave growth (Kraus and Businger, 1994). This out-of-phase component is equivalent to energy input provided by the pressure-piston velocity correlation given in **(23)** (or equivalently the pressure-slope term in the momentum equation **(15)**). Jefferys postulated that air moving faster than the phase speed of the wave separates from the surface as it overtakes the wave. The separation causes a sheltering effect that generates a pressure surplus on the upwind side of the wave and a deficit on the lee. Jeffreys theorized that the energy transferred to the ocean by the normal pressure forcing could be expressed as

$$E_{aw} = \frac{1}{\lambda}\int_0^{\lambda} p_\eta w_o dx \qquad \textbf{(59)}$$

where he assumed that the surface pressure could be modeled as

$$p_\eta = \bar{p} + s\rho_a(U - c)|U - c|\frac{\partial\eta}{\partial x} \qquad \textbf{(60)}$$

where $\bar{p}$ is the mean atmospheric pressure and s is the sheltering coefficient. Integrating **(59)** using the surface pressure and the simple waveform $\eta = a\cos(kx - \omega t)$ provides

$$E_{aw} = \frac{1}{2}s\rho_a(U - c)|U - c|k^2a^2c \qquad \textbf{(61)}$$

where we have used the deep-water relationship $c = \omega / k$.

Recall that if the flow were perfectly irrotational, then the pressure field would be $180°$ out of phase with the vertical velocity, which is inconsistent with **(60)**. The sheltering coefficient thereby parameterizes the out-of-phase fraction of the pressure variations that contribute to wave growth (or decay). Jeffreys theory did not take into account the nonlinear change of wind with height, i.e., the semi-logarithmic wind profile. Therefore, his theory fell out of favor with many scientists because the wind profile lead to near surface winds that are slower than the phase propagation of most waves (Krauss and Businger). This argument suggests that flow separation is a relatively rare event that is generally associated with the flow over large-scale breaking waves.

Recent investigations, however, have begun to focus on the role of microbreaking in momentum and energy transfer. These short waves may well be traveling slower than the near surface velocity. This raises the question: could this sheltering model be used to parameterize the momentum transfer supported by these waves? LINWOOD???

C. Miles' Critical Layer Model

The critical layer model proposed by Miles (1958) is probably the most widely cited model for developing waves and perhaps the least well understood of the theories because of the less-than-intuitive nature of the theory. In fact, a number of articles have been written that attempt to place the mathematical concepts of the model into a more physical basis. The discussion provided by Lighthill (1962) and Komen (199X) are probably the most successful.

The model assumes that the wave-induced perturbations in the air can be treated as small perturbations of the mean shear flow one would find in the absence of waves. The perturbation analysis of the resulting equations of motion reveal a singular behavior at a critical height where the phase speed of the wave equals the wind speed. The vorticity perturbation at the critical height induces a perturbation of the horizontal velocity and pressure fields. This results in a resonant interaction between the wave-induced pressure fluctuations and free-surface waves, i.e., a shift in the pressure field that is 90° out of phase with the elevation and in phase with the slope. The net result is a loss of momentum and energy from the airflow at the critical layer that must be accompanied by a growth of the waves (Janssen 1991). The energy flux to the waves at the critical height is given by (Miles 1957; Lighthill 1962)

$$E_{aw}(\omega) = c(\omega)\,\tau_{aw}(\omega) = \frac{c(\omega)\rho_a\lambda}{4}\,\frac{U''(z_c)}{U'(z_c)}\,W^2(z_c) \tag{62}$$

where U' and U'' represent the vertical wind profile and its derivative, respectively, W represents the amplitude of the wave-induced vertical velocity fluctuations, and wind z_c is the critcal height defined as the height where $U(z_c) = c(\omega)$.

The mechanism that allows perturbations at the critical layer to result in a momentum transfer at the surface is the wave-induced momentum flux $\tilde{u}\tilde{w}$. Lighthill (1962) states that the singular behavior at the critical layer implies that the wave-induced momentum flux is zero above the critical layer and constant below. Since the actual wavefield over the ocean is not monochromatic, the profile of the wave induced momentum flux represents the sum of these constant/null profiles, each representing a step function at a different critical height. The sum of these profiles at the surface would equal the total wave-induced momentum flux. At least that's how I interpret it!

8. Sea-State Dependent Parameterizations

The open ocean parameterization works well for a fully developed sea with little or no swell. However, the results from a number of ONR-sponsored field programs, including SWADE and MBL, indicate that the momentum flux is a function of sea-state and wave-age (e.g., Donelan, 1982, 1990; Geernhaert 1990), even over the open ocean. The wave-age is defined as the developmental stage of the sea relative to the current state of wind-forcing. Additionally, under conditions of decreasing winds, the slowly decaying wave field can add momentum to the atmosphere when the waves are propagating faster than the wind speed (Holland 1981). Secondly, the modulation of the short wind waves by longer waves may also be responsible for a sea-state dependancy. The sea-state is defined from the physical characteristics of the wave field, such as wave height or wave steepness (wave slope).

A. The Drag Coefficient

Observations have shown that the drag coefficient over the ocean is a function of wind speed, and that the drag coefficient increases with increasing wind speed. This should not be too surprising to anyone having spent time at sea. Over the open ocean, this increase is mainly due to the increase in amplitude of the short gravity waves rather than the growing long waves. However, when the waves are actively growing (or slowly decaying), form drag from these longer waves can also contribute to the total drag, thereby affecting the momentum exchange. These conditions exist when the wind increases (or decreases) more rapidly than the adjustment time of the wave field, e.g., during frontal passages or under gusty winds. Additionally, interaction of the waves with the bathymetry and the fetch dependence of wave development can also affect how rough the sea appears to the wind in coastal waters. Lastly, the physical characteristics of the ocean surface and near-surface thermal properties can also affect the wave-state, particularly at low wind speeds. Therefore, it should not be surprising that plots of the measured drag coefficient versus wind speed generally exhibit a great deal of scatter (e.g., see the review by Garratt 1977).

Model simulations require parameterizations derived from experimental studies to simulate various processes involved in wind-wave-current coupling. However, the goal of directly relating the sea surface drag coefficient to sea state remains elusive (Smith et al., 1992; Dobson et al., 1994). Donelan (1982) was one of the first to present field data which showed a strong relationship between wave parameters and wind stress. His research demonstrated the breakdown of Charnock's relation between the aerodynamic roughness length and the friction velocity in all but fully-developed wave conditions. Since this pioneering work, other researchers have attempted to define a quantitative relationship between the wind and wave fields. Smith (1991) demonstrated a drag coefficient anomaly, a departure of the drag coefficient from values expected through the use of Charnock's expression, which was significantly correlated with wave age

$$10^3 C_{DN} = 1.85 - \frac{2.24 c_p}{U_{10N} \cos\theta} \qquad \textbf{(63)}$$

where c_p and U_{10N} are expressed in ms^{-1} and θ is the difference between the wind and wave directions. Geernaert et al. (1986) proposed an empirical relation between wind stress and wave age; however, lacking wave spectral data, they were forced to estimate the wave field from wind data and may have predetermined their results on account of this circular argument.

1. Wave-age Dependent Charnock Relationship

Following the ideas of Kitaigorodskii (1973), Geernhaert et al. (1987), Janssen (1989), and Nordeng (1991) proposed a wave age dependent Charnock parameter

$$\alpha = \frac{z_{o_c} u_*^2}{g} = f\left(\frac{c_p}{u_*}\right) \quad \textbf{(64)}$$

which states that the normalized roughness length associated with the wave field is a function of wave age. Since this investigations, Smith et al. (1992), Johnson and Vested (1992), Martin (1998), and Johnson et al. (1998) have all attempted to account for the wave age dependence by an empirically derived wave-age-dependent Charnock parameter in the general form

$$\alpha = A\left(\frac{c_p}{u_*}\right)^B \quad \textbf{(65)}$$

where the coefficients A and B are summarized in Table 1 and the resulting form of α plotted in Fig. 6.

Chalikov and Belevich (1993) obtained a similar parameterization for the roughness length using

$$\alpha = \mathrm{X}\sqrt{\alpha_p} \quad \textbf{(66)}$$

where X is a universal constant and α_p is the Phillips' parameter, which is used to determine the wave-age dependence of the wave spectrum. Jannsen (1982) suggested

$$\alpha_p = 0.57\left(\frac{u_*}{c_p}\right)^{3/2} \quad \textbf{(67)}$$

where we have used the dispersion relationship for deep water waves. If we combine this parameterization with X = 0.10 (Chalikov and Belevich 1993) we obtain

$$\alpha = 0.08\left(\frac{c_p}{u_*}\right)^{-3/4} \quad \textbf{(68)}$$

which is very similar to the formulation given by Nordeng (1991).

Since u_* appears in both α and the wave age in **(64)**, these investigations acknowledged the possibility that self-correlation could give rise to spurious results (e.g., Hicks 1978; Dobson et al. 1994). Johnson et al. (1998) argued that this effect could be reduced by comparing the mean results from several sites with different fetches. Their coefficients are actually derived from a fit to the mean phase speed and Charnock parameters from a number of different field experiments. It is interesting to note that the Charnock parameter represents the ratio of gravitational accelerations to inertial accelerations, which is analogous to an inverse Froude number. The wave Froude number can be expressed in terms of the wave slope (Kraus and Businger, 1994)

$$Fr_w = (Ak)^2 \qquad \textbf{(69)}$$

where A is the wave amplitude. Therefore, it may be more appropriate to parameterize the Charnock parameter as a function of wave slope. This is discussed in the following two sections.

Investigator(s)	A	B
Geernhaert et al. (1987)	0.015	-0.74
Nordeng (1991) for $c_p/u_* > 15$	0.11	-0.75
Smith et al. (1992)	0.48	-1
Johnson & Vested (1992) for $c_p/u_* > 10$	0.06	-0.52
Martin (1998)	0.68	-1.24
Johnson et al. (1998)	1.89	-1.59

2. Wave Height Scaling

To avoid the problems with self-correlation, Donelan et al. (1993) present an alternative approach where the aerodynamic roughness length is scaled by the rms amplitude σ_H of the waves or alternatively the significant wave height, *H*, defined as $4\sigma_H = H$. Similar analysis have been conducted by Smith et al. (1992); Dobson et al. (1994), and Martin (1998).

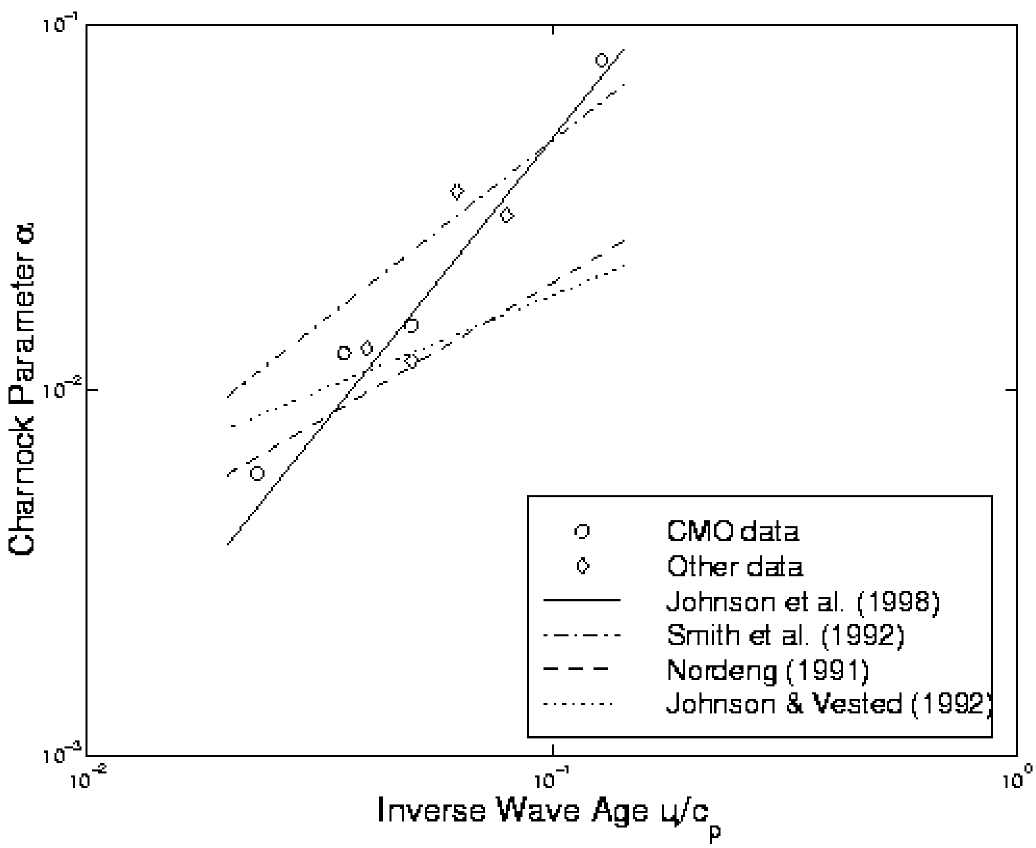

Figure 6. Formulations of the wave-age dependent Charnock parameter found in the literature.

The scaled roughness length z_r/σ_H expresses the ability of the waves to serve as roughness elements (Donelan 1990). The benefit of regressing the ratio of z_r/σ_H to inverse wave age is that the dimensionless ratios are formed from four independent parameters, and the regression avoids the problem of self-correlation by estimating the sea surface roughness from wave age parameters (σ_H and c_p) that can be measured in situ (Smith et al. 1992). Additionally, since the idea that the roughness length should be correlated with the height of the waves depends on the concept of rough aerodynamic flow, Donelan et al. (1992) and Martin (1998) limited their analysis to cases for which U_{10} > 7.5 m/s (e.g., Wu 1980; Donelan 1990). Therefore, their formulation does not apply to cases for which the surface layer appears to be aerodynamically smooth, U_{10} < 3 m/s, or to transitional flow.

In the Coastal Mixing and Optics (CMO) analysis provide by Martin (1998), the scaled roughness length exhibits a nearly cubic increase with wave age as expressed quantitatively by the regression line

$$\frac{z_r}{\sigma_H} = 9.6 \times 10^{-4}\left[\frac{U_{10N}}{c_p}\right]^{2.7} \qquad \textbf{(70)}$$

which displays good agreement to the regression line

$$\frac{z_r}{\sigma_H} = 5.5 \times 10^{-4}\left[\frac{U_{10N}}{c_p}\right]^{2.7} \qquad \textbf{(71)}$$

fitted to data obtained in 12 m of water on Lake Ontario (Donelan et al., 1993). These relationships also agrees well to the $(U_{10N}/c_p)^{3.5}$ power law obtained by Smith et al. (1992) from data obtained during the Humidity Exchange over the Sea (HEXOS) experiment in 18 m of water over the North Sea. In contrast, Dobson et al. (1994) found a weaker power law, $(U_{10N}/c_p)^{1.7}$, for data obtained during the Grand Banks ERS-1 SAR Wave Validation Experiment. However, the scatter in their data set did not allow them to resolve the slope (power law) well, and they indicate that a neutral or two way regression would give a steeper power law in better agreement with the power laws obtained using the CMO, Lake Ontario, and North Sea data sets. The close agreement in the power laws obtained in four independent experiments, which ranged in environmental conditions from lake to open ocean, suggests the this type of scaling provides a fairly universal relationship between sea-state, wave age, and aerodynamic roughness.

3. Roughness of Breaking Waves

Other studies by Banner and Melville (1976) and Melville (1977) have focused on the role of wave-breaking on momentum exchange. Recall that the Charnock relationship essentially parameterizes the rapid transfer of momentum from the gravity-capillary waves (i.e., the roughness elements) to the currents. This exchange takes place when the momentum sustained by these waves is dumped into the near-surface currents through small-scale wave breaking. Melville (1977) attempted to model this process by investigating the relationship between the phase speed of these breaking waves and friction velocity and found $c_o \approx u_*$, where c_o is the phase speed of the short waves. Melville went on to derive a form of the roughness length that is a function of wave age, long-wave slope, and surface drift velocity.

Melville's (1977) investigation found a weak relationship between wave-age and surface roughness. Instead, his result showed that the roughness was a strong function of the ratio of the wind drift u_o to the phase velocity of the short waves

$$\frac{u_o}{c_o} \approx \frac{u_o}{u_*} = \gamma \tag{72}$$

Melville reported values of γ as a function of u_* from Wu (1975) and Phillips and Banner (1974), which ranged from 0.67 for u_* = 0.23 m/s to 0.4 for u_* = 0.63 m/s. Interestingly, one can get a seemingly similar wave age dependence for α by fixing the phase speed of the dominate waves, varying u_* between 0.23 to 0.63 m/s, and allowing γ to linearly decrease from 0.67 to 0.4 over this same range. The curves using the indicated values of the peak phase speed are shown in Fig. 7.

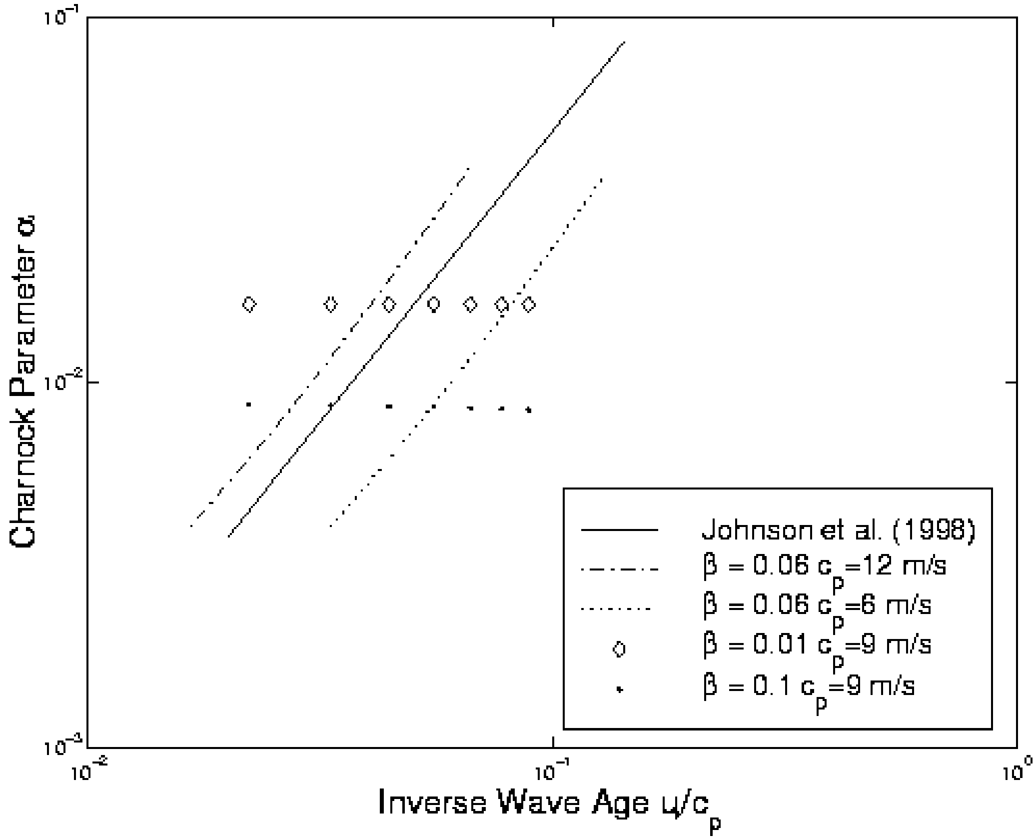

Figure 7. The equivalent of the Charnock parameter using the approach of Melville (1977). A simple dependence on phase speed is not predicted. Instead, the roughness is expected to be a function of wave-age, wave steepness (sea-state), and the ratio of the wind-drift to phase velocity of the short wave.

Since γ is closely related to the energy flux into the ocean currents due to small-scale breaking, one could ask the question: Is it the long waves or short waves that introduce the observed variability in the drag coefficient? For example, the modeling results presented by Crawford and Large (1996) show that the energy flux to the ocean currents E_{ao} "is a key air-sea interaction parameter because of its strong dependence on the time histories of wind forcing and surface currents ..." This suggests that we should be focusing less on E_{wo} and more on E_{ao}. However, Melville's (1977) model also contains a parameter that accounts for the effect of the steepness of the long waves

$$\beta = \frac{u_m}{c_p} \approx ak_p \qquad \textbf{(73)}$$

where u_m is the maximum orbital velocity, a is the amplitude at the spectral peak, and k_p is the peak wave number. Therefore, the model also suggests that the roughness of the sea is strongly affected by sea-state. This observation is in agreement with the scaling argument given by Donelan et al. (1993). This dependence is shown by the horizontal lines in Fig. 7 where we have fixed the phase speed and varied the steepness.

4. Modeling the Wave-induced Momentum Flux

A more straight forward approach to parameterized the wave-induced effects of the momentum flux is given by Janssen (1988; 1991). Janssen (1991) modifies **(38)** to include an additional scaling length

$$\tau_a = \tau_o + \tau_w = \rho C_D(z, z_{o_c}, L, z_\eta) U_r(z)^2 \tag{74}$$

where z_{o_c} is again given by a Charnock constant (i.e., it is only meant to account for the roughness of the gravity-capillary waves) and z_η is a length scale that accounts for the effect of the gravity waves (i.e., the form drag of the gravity waves). Janssen (1991) defined the length scale such that the wind profile over ocean waves is given by

$$U(z) = U(z_{o_c}) + \frac{u_*}{\kappa}\left[\ln\left(\frac{z + z_\eta}{z_{o_c} + z_\eta}\right) - \psi_m\left(\frac{z + z_\eta}{L}\right) + \psi_m\left(\frac{z_{o_c} + z_\eta}{L}\right)\right] \tag{75}$$

or

$$\frac{\partial U}{\partial z} = \frac{(\tau_a/\rho_a)^{1/2}}{\kappa(z + z_\eta)}\phi_m\left(\frac{z + z_\eta}{L}\right) \tag{76}$$

where surface velocity and the stability functions have been added for completeness. Janssen (1991) models the momentum flux going into the ocean as

$$\tau_a - \tau_w = \tau_o = \rho_a(\kappa z)^2\left|\frac{\partial U}{\partial z}\right|\frac{\partial U}{\partial z} + \rho_a \nu \frac{\partial U}{\partial z} \tag{77}$$

which is composed mainly of the momentum supported by the gravity capillary waves and viscous stress. Neglecting the viscous stress and the stability function, **(76)** and **(77)** can be combined and evaluated at $z = z_{o_c}$ to give

$$\tau_o = \tau_a \left(\frac{z_{o_c}}{z_{o_c} + z_\eta} \right)^2 \tag{78}$$

and

$$z_\eta = z_{o_c} \left(\frac{1}{\sqrt{1 - \chi}} - 1 \right) \tag{79}$$

where $\chi = \tau_w / \tau_a$. This expression implies that z_η is at most an order of magnitude larger than z_{o_c}, such that the wave-induced effects on the wind profile are negligible except very near the surface. Since measurements are made well above this height, Janssen (1991) provides a modified drag coefficient in neutral conditions given by

$$C_{DN}(z, z_2) = \left[\frac{k}{\ln\left(\frac{z}{z_2} \right)} \right]^2 \tag{80}$$

where

$$z_2 = z_{o_c} (1 - \chi)^{-1/2} \tag{81}$$

The drawback of this approach is that it requires an estimate of the momentum flux retained by the waves. However, as coupled atmosphere-wave and, ultimately, atmosphere-wave-ocean models become more commonplace, this type of parameterization will likely become the focus of coupled boundary layer research.

It is worth noting that Janssen (1988; 1991) actually associates τ_o in **(78)** with the turbulent component of the momentum flux. This is reasonable since it stems from the first term on the right-hand-side of **(77)**, which is based on turbulent mixing length theory. However, its surface value is closely related to the momentum flux supported by gravity capillary waves that is parameterized using Charnock's relationship.   Therefore, the notation given by **(78)** seems more appropriate.

Janssen (1988;1991) only considers the momentum retained by the gravity waves and not the momentum required to support the gravity-capillary waves (i.e., the roughness elements). Makin et al. (1995) consider the total momentum flux to the waves. They parameterize the roughness length as a modification to the roughness length for smooth flow

$$z_2 = z_{o_s}\left(1 - \frac{\tau_{aw}}{\tau_a}\right)^{-1/2} \qquad \textbf{(82)}$$

Note that this distinction is not made in Lionello et al. (1998), probably because there is some confusion as to the exact definition of τ_w in Janssen (1988; 1991). However, both parameterizations imply that the waves influence on the velocity profile is restricted to a very shallow layer, i.e., $z_\eta < 10 z_o$.

***Research Issues**: Determining the most appropriate parameterization of these processes is becoming increasingly important as investigators develop operational coupled atmosphere-ocean-wave models (e.g., Doyle 1995; Janssen et al. 1997; Lionello et al. 1998). Therefore, even if the momentum and energy exchange to the ocean is dominated by viscous stress and short wind waves, an accurate parameterization of the growth rate of the waves is critical to the success of wave prediction models. In coastal areas, ...*

*These model validation studies would clearly benefit from direct measurement of the wave-induced momentum flux over the open ocean. However, little is known about the structure and height of this wave-induced flow above the ocean surface, and there have been no direct measurements of the wave-induced momentum flux at sea. Equation **(15)** suggests that measurements of wave-induced air pressure perturbations and wave slope can be used to quantify wave-induced momentum flux (Snyder et al. 1981). However, it is presently impossible to measure pressure at the surface, and extrapolating from measurements at height is problematic because the vertical structure of the wave-induced pressure field is not well known. Hare et al. (1997) have shown that this is particularly true over developing waves, where the wave-induced pressure field associated with the form drag does not decay monotonically.*

B. Inertial-Dissipation Method

In a stationary, horizontally homogenous, constant stress layer, the vertical derivative of the energy flux takes the form of the familiar TKE budget equation

$$\epsilon = -\overline{u'w'}\frac{\partial U}{\partial z} - \overline{v'w'}\frac{\partial V}{\partial z} - \frac{\partial \overline{w'e'}}{\partial z} - \frac{1}{\rho}\frac{\partial \overline{w'p'}}{\partial z} + \frac{g}{T_v}\overline{w'T_v'} \qquad \textbf{(83)}$$

MO scaling provides us with a dimensionless form of the TKE budget given by

$$\frac{\epsilon \kappa z}{u_*^3} = \phi_\epsilon(\zeta) = \phi_m(\zeta) - \phi_e(\zeta) - \phi_p(\zeta) - \zeta \qquad \textbf{(84)}$$

where ζ is the stability parameter defined using the MO length given by **(10)**. This expression is often used to estimate the momentum flux over the ocean from estimates of the dissipation rates and a parameterization of ϕ_ϵ from

$$\rho u_*^2 = \rho \left[\frac{\epsilon \kappa z}{\phi_\epsilon(z/L)}\right]^{2/3} \qquad \textbf{(85)}$$

This type of parameterization should be valid as long as the measurements are made above the WBL but within the constant-flux layer. However, the results from the MBL experiments have given strong evidence that this expression is not valid in the WBL.

The general reasons for the breakdown of the MO similarity due to wave-induced forcing has been discussed above. Specifically, the effect of wave-induced forcing on the kinetic energy budget is easily demonstrated by decomposing the velocity components into mean, turbulent, and wave-induced components

$$u(t) = U + u'(t) + \tilde{u}(t) \qquad \textbf{(86)}$$

where the wave-induced component is defined using an extension of Reynolds averaging known as phase averaging (e.g., Finnegan et al., 1984). This type of averaging can then be used to rewrite the TKE energy budget to include the wave-induced components. For example, the shear production term includes terms representing the energy production due to the interaction between the wave-induced flux and the mean shear

$$P = -\rho_a[\overline{u'w'} + \overline{\tilde{u}\tilde{w}}]\frac{\partial U}{\partial z} = \tau_a \frac{\partial U}{\partial z} \tag{87}$$

where the two terms in the bracketed expressions represent the turbulent and wave-induced momentum flux. The wave-induced momentum flux cannot be expected to obey MO scaling, which is expected to lead to a breakdown of similarity relationships like **(85)** within the WBL. This implies that using traditional Monin-Obukhov (MO) similarity theory to define the boundary conditions in numerical models is suspect.

The other strong influence that the waves can have on the energy exchange has been discussed in section **5.C**. Recall that the energy transport between the atmosphere and ocean waves is given by

$$E_{aw} \approx \overline{p_\eta w_o} \approx \overline{p_\eta \frac{\partial \eta}{\partial t}} \tag{88}$$

where w_o is the piston velocity. This term couples the KE budget to the ocean surface since it represents the boundary conditions for the pressure transport term

$$-\frac{1}{\rho_a}\frac{\partial \overline{wp}}{\partial z} \tag{89}$$

A simple model for the pressure transport that arises due to the energy flux into the waves can be derived following the approach of Janssen (1999) using the energy input given by Terray et al. (1996)

$$E_{aw} = 0.5 c_p \tau_a \qquad \frac{u_*}{c_p} > 0.08 \tag{90}$$

and a parameterization for the older waves that provides a good fit to the data given by the quadratic or linear relationships

$$E_{aw} = 65\frac{u_*^2}{c_p}\tau_a \qquad \frac{u_*}{c_p} < 0.08 \qquad \textbf{(91)}$$

and

$$E_{aw} = [6u_* - 0.13c_p]\tau_a \qquad \frac{u_*}{c_p} < 0.08 \qquad \textbf{(92)}$$

The function given by **(92)** is perhaps more appropriate because it allows for the transfer of energy from waves to wind over very old seas. The functions represented by **(90)** to **(92)** are shown in Fig. 8.

For simplicity, we assume that the surface energy flux decays exponentially as e^{-2kz}. By taking the derivative and normalizing the result by $u_*^3/\kappa z$ we obtain a parameterization for the wave-induced pressure transport given by

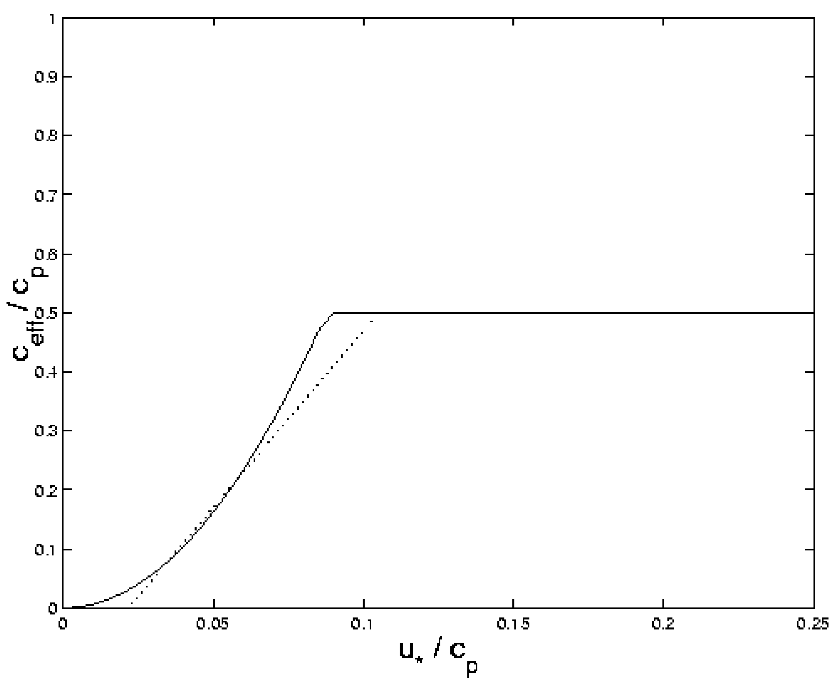

Figure 8 Graphical representation of (90) through (92).

$$\frac{\kappa z}{\rho_a u_*^3}\frac{\partial\overline{\tilde{w}\tilde{p}}}{\partial z} = \kappa kz\frac{c_p}{u_*}e^{-2kz} \qquad \frac{u_*}{c_p} > 0.08 \tag{93}$$

$$\frac{\kappa z}{\rho_a u_*^3}\frac{\partial\overline{\tilde{w}\tilde{p}}}{\partial z} = 130\kappa kz\frac{u_*}{c_p}e^{-2kz} \qquad \frac{u_*}{c_p} < 0.08 \tag{94}$$

or

$$\frac{\kappa z}{\rho_a u_*^3}\frac{\partial\overline{\tilde{w}\tilde{p}}}{\partial z} = 2\kappa kz[6 - 0.13\frac{c_p}{u_*}]e^{-2kz} \qquad \frac{u_*}{c_p} < 0.08 \tag{95}$$

This result is rather interesting as it suggests two distinct regimes with a maximum in the wave induced pressure transport at the transition. The transport decreases for both older seas and younger seas on either side of $c_p/u_* \approx 9$ as shown in Fig. 9. Although, there are a number of assumptions that went into this result, it is based on reasonable physical arguments and underlying observations. The observation that the energy input varies linearly with phase speed over young seas may explain why the inertial-dissipation appears to work reasonably well in coastal areas, particularly when one considers that the height of these measurements often places them at relatively higher values of kz than over the open ocean.

Research Issues*: This result has a number of implications for both estimating the momentum flux over the ocean (e.g., the inertial-dissipation method) and in the closure schemes used in numerical models (e.g.,* $TKE-\epsilon$ *closure and subgridscale parameterizations in LES). The challenge is how to determine parameterizations that account for the flux of kinetic energy into the ocean as a function of sea state. In this example, this might involve determining a function that accounts for the "dissipation deficit" as a function of* kz *(or alternatively* $k(z+H_s)$*, where* H_s *is the significant wave height) and* u_*/c *(or alternatively* $(U-c)/c$*, if we can avoid scaling difficulties when the two speeds are equal). This result must be combined with the effect of the waves on the production terms, since we know (at least indirectly) that young sea enhance* *the drag on the ocean surface. This should result in enhanced shear production, which could offset the dissipation deficit measured under these conditions.*

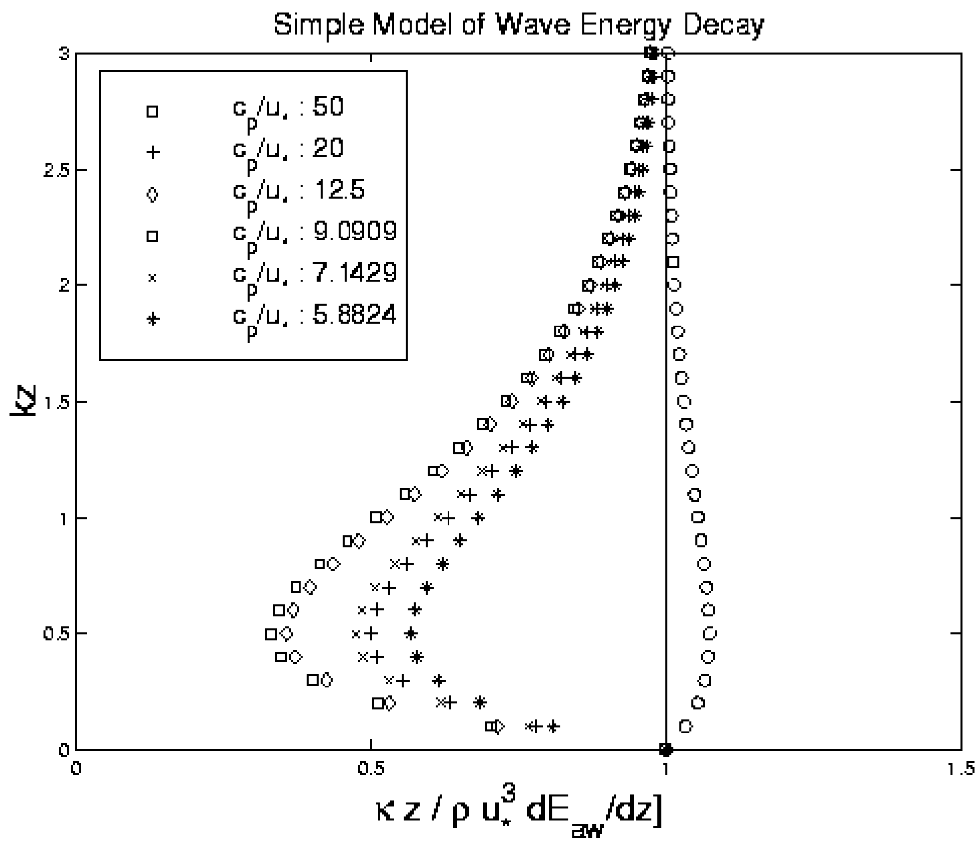

Figure 9 A simple model of the energy transfer from the atmosphere to the ocean. The curves represent different wave ages as labeled in the panel.

9. Coastal Processes

Recent experiments and theoretical modeling studies have addressed numerous issues involving strong spatial and temporal variability within the coastal marine atmospheric boundary layer (MABL). For example, when the flow is offshore, wave growth and advection of turbulence from land seriously complicate the spatial distribution of the stress downstream from the coast. In addition, flow against incoming swell is thought to augment the stress. Close to the shore where the depth becomes less than one wave amplitude of the swell, dramatic wave steepening and breaking occur (Thornton and Guza 1982, 1983; Holman and Sallenger 1985; Holland et al. 1995). Irregularities of the bottom topography along the coast and wave refraction lead to irregularities in the surface wave field along the coast (Munk and Traylor 1947).

Therefore, information on wave state is normally essential for predicting surface stress in the coastal zone. Vickers and Mahrt (1997) find that the width of the wave spectra explains more variance of the drag coefficient than wave age, in spite of artificial correlation associated with application of wave age. Broad spectra represent confused seas, multiple peaked spectra and nonequilibrium wave state. Coastal zone atmospheric flows are often nonstationary, sometimes forced by diurnal variation of the differential heating across the coast. Such nonstationarity of atmospheric flows prevent equilibrium wave states. In models where information on wave state is unavailable, fetch-dependent parameterizations of the drag coefficient (Perrie and Toulany 1990; Geernaert and Smith 1996) represent some of the influences on the stress in offshore flow.

Offshore flow is traditionally viewed in terms of development of internal boundary layers. With offshore flow of warm air over cooler water, the turbulence near the surface may nearly collapse and definition of an internal boundary layer becomes obscure (Smedman et al. 1995). With offshore flow of cooler air over warmer water, the convective internal boundary layer is better defined (Källstrand and Smedman 1997). The thin depth of the convective internal boundary layer suppresses the large convective eddies and the surface fluxes are substantially less than predicted by Monin-Obukhov similarity theory (Mahrt et al. 1998). That is, the depth of the internal boundary layer becomes an additional length scale influencing he fluxes even close to the surface. Vickers and Mahrt (1999) combine the influence of the Obukhov length, boundary layer depth and wave state into one similarity theory.

All of the above effects can be enhanced by coastal topography (e.g., Thompson et al. 1997). In previous investigation, particular emphasis has been placed upon shallow, inversion-capped marine ABL interaction with coastal orography, such as is the norm along the U.S. West Coast during the summertime. The dominant cross-shore scale of variability is the Rossby radius of deformation, which is a measure of the offshore distance over which the coastal mountains affect geostrophic adjustment. Along the California coast, the Rossby radius is often greater than 100 km, while the horizontal width of the coastal range is frequently less than this. Overland (1984) demonstrates by scale analysis that with such "knife edge" mountains pronounced ageostrophic flow is to be anticipated in the along-coast direction and that high-resolution mesoscale models are needed to properly capture the coastal dynamics.

Numerous additional mesoscale complexities arise in this coastal zone. The large scale thermal contrast and synoptic pressure gradient between warm continent and cool, sloping Marine ABL commonly create a northerly coastal low level jet (LLJ) along California during the summer. This LLJ recently has been investigated experimentally (Zemba and Friehe 1987; Beardsley et al. 1987; Bridger et al. 1993; Rogers et al. 1998) as well as theoretically and by modeling (Samelson 1992; Burk and Thompson 1996; Holt 1996). The surface stress and curl of stress produced by this LLJ drive significant upwelling in coastal waters (Enriquez and Friehe 1995). The LLJ contains considerable along coast variability arising from flow interaction with the varying coastline shape. Some of the patchiness in the LLJ structure occurs due to topographic blocking, mountain-valley and sea-land breeze circulations, and orographically induced mesoscale pressure gradients.

Additionally, the shallow, strongly capped marine ABL with high wind speed frequently produces supercritical flow, which has several characteristic features that add yet more complexity to the coastal mesoscale picture. Among these are expansion fans, wherein the flow accelerates and the marine ABL rapidly lowers when traversing a convex bend having coastal topography greater than the marine ABL depth. Also, sharp jumps in marine ABL depth occasionally occur associated with a flow transition from a super- to sub-critical state (Samelson, 1992; Burk et al., 1999, Dorman et al., 1999). Thus, the interaction of marine flow with thermally varying coastal orography within a narrow baroclinic zone produces distinct characteristics to the atmospheric forcing impressed upon the ocean.

The ocean responds with its own distinct pattern of circulations and SST distributions which feedback to the atmosphere. Recent independent observations of the sea surface temperature (SST) and the wind stress obtained during Coastal Waves 96 (Rogers et al., 1998) indicate a spatial correlation on a scale of about 20 km. It is difficult to be certain, however, whether this variability is due entirely to atmospheric forcing, or in water processes, or a combination of both. Simultaneous observations of the spatially varying ocean and atmospheric boundary layers could resolve this uncertainty and provide insight into the processes controlling the SST distribution.

The depth of the marine boundary layer is very sensitive to various processes that are often poorly observed and not well resolved by many numerical models. This often leads to an underestimate of the depth of the boundary layer and consequent poor prediction of boundary layer cloud fraction and cloud depth. In turn, this increases the uncertainty in boundary layer simulations because of the effect of the cloud field on radiative transfer and the heat exchange between the ocean and the atmosphere.

Atmospheric observations during Coastal Waves 96 also revealed the present uncertainties in the estimates of the surface fluxes of heat, moisture and momentum in stable conditions. Comparison of direct flux measurements with bulk flux estimates of the sensible and latent heat revealed errors in excess of 50 W m^{-2}. The cause of these variations is unclear, but likely related to the form of the non-dimensional heat, moisture and momentum profiles, which have been derived largely form over land observations (Rogers et al. 1998).

10. Ocean General Circulation Models

Existing general circulation models (GCMs) have notable deficiencies including, among others, the limited treatment of interactions among the atmosphere, ocean, cryrosphere and land surface, and inadequate representation of processes within each of these systems. These processes become especially important in a model that couples the ocean and atmosphere. Because the atmosphere feels the ocean mainly through sea surface temperature (SST), the ocean general circulation models (OGCMs) must accurately simulate an upper ocean. OGCMs used for climate simulations use coarse resolution and integrate over long time scales; consequently, more of the physics fall into the sub-grid scale and therefore must be parameterized. The mixing and transport processes that govern the exchange of heat and water between the ocean and atmosphere occur through these unresolved, small-scale processes. Ultimately, the parameterization of these processes determine the distribution of heat throughout the global ocean.

A. Vertical Mixing

Vertical mixing processes in the ocean may be the key to modeling and understanding many crucial aspects of climate change. The two most direct influences of the atmosphere on the oceans are the forcing of vertical fluxes of mass from the mixed layers on the space scales of the atmospheric wind patterns, and the forcing of deep convection by the combined effects of intensive buoyancy flux and wind mixing. In a model of the closed loop between the atmosphere and ocean, the representation of heat exchange to the atmosphere needs to be accurate. In essence, this means producing adequate simulations of the ocean mixed layer and SST. Deep mixed layers, driven by a combination of wind and buoyancy, are an important factor and a high priority for modeling because they are important agents in ventilating the thermocline (Gregg, 1987). The layers of the ocean that are vertically adjacent to the mixed layer are dominated by Ekman pumping or suction and subduction (Cushman-Roisin, 1987). These zones interact through diapycnal mixing; in contrast, within the deep interior of the ocean, mixing is predominately along isopycnals (Gargett, 1984; 1988). On a decadal time scale, mixing along isopycnals, associated with surface-wind-driven Ekman pumping and buoyancy flux, is responsible for the basin-scale ventilation of subarctic gyres (Luyten, et. al., 1983; Luyten and Stommel, 1986; Ledwell, et. al., 1993).

At high latitudes, intermediate and deep waters are formed by deep penetrative convection and the movement of cold, dense waters off the ice-covered continental shelves. Buoyancy-driven penetrative convection occurs in localized areas in these regions, and is a violent, relatively short-lived event with vertical scales ultimately limited by the ocean depth. This process transports and mixes water over many hundreds of meters during a time period of hours (Aagaard and Carmack, 1989). Where this process occurs, the across-isopycnal advection gives rise to bottom water formation and controls the vertical structure of deep water masses. These deep and intermediate waters reach the rest of the ocean through constricted straits, sills and passages, influencing the deep circulation patterns that in turn affect the heat transport within the ocean.

B. Mixed Layer Models

The air-sea fluxes of heat, fresh water, and momentum are known to be of primary importance in forcing the oceanic mixed-layer. In the mid to late seventies a number of fields studies were conducted from the R/P FLIP to investigate mixed-layer response to atmospheric forcing. Using new current meters developed with ONR funding, these studies showed a near-surface velocity field that was coherent with and to the right of the local wind. Later work showed that the departure from Ekman-like behavior could be explained by the effects of buoyancy (Price et al. ,1986). Price et al. (1986) showed that the diurnal cycling of the heat flux created a shallow diurnal mixed layer that trapped the wind-driven flow near the surface in weak to moderate winds. These and other observational studies have lead to the development of mixed-layer models that attempt to simulate mixed-layer evolution.

Mixed-layer modeling provides an important connection between the atmospheric and oceanic boundary layer, but has not been universally incorporated into OGCMs. Many OGCMs use simple constant eddy viscosity mixing parameterizations that approximate the mixing in the ocean interior. In the surface layers, a complex energy budget, turbulent mixing, convection and advection are needed to adequately parameterize the exchange processes with the atmosphere. Cane (1993) reports that when the constant eddy viscosity is tuned to give a good surface mixed layer, it creates too much mixing in the deeper ocean. Investigators who use coupled atmospheric and ocean models have assumed mixed layers of constant depth (Hansen et. al., 1984; 1988; Manabe and Stouffer, 1980; Washington and Meehl, 1984; Wilson and Mitchell, 1987). However, limitations in using a mixed-layer of constant depth leads to errors in determination of seasonal ocean temperatures. Gallimore and Houghton (1987) and Meehl and Washington (1985) characterized the spatial and zonal mean errors in ocean heat transport, seasonal variations in mixed-layer depth, and upwelling. They found that although a 50-m deep, fixed mixed layer simulates a reasonable amplitude for the annual cycle of ocean temperature, the seasonal cycle was incorrect. The use of Meehl's (1984) variable depth mixed layer improved some aspects of the simulation but underestimated the zonal mean heat storage and the annual variation of extremes of temperature (Gallimore and Houghton, 1990).

Bulk models address the limitations of assuming a constant mixed-layer depth; however, they assume homogeneous temperature, salinity and velocity in a surface layer and assume no penetrating convection (Garwood 1977; Kraus and Turner 1967; Niiler 1975). The turbulent erosion (TEM, e.g., Kraus and Turner 1967), dynamic instability (DIM, e.g., Pollard et al. 1993 and Price et al. 1986), and hybrid (Chen et al. 1994) models are variations of mixed-layer slab models. These models are popular because they have few tunable parameters, have relatively good success at simulating temperature and salinity evolution over diurnal and seasonal cycles given accurate forcing fields, and are computationally efficient.

However, confidence in such models is restricted due to their ability to reproduce only the bulk responses of the upper ocean (such as rate of deepening and budgets of heat and salt). As such, they are unable to predict vertical structure within the turbulent surface layer because of the homogeneous assumption and are not appropriate for parameterizing turbulence within the ocean interior. This may cause a problem in deep wintertime mixed layers (150-200 m) where the vertical current structure is dominated by an Ekman-like spiral in the current direction. Bulk models also fail to adequately simulate equatorial regions because of the strong vertical current shear associated with the equatorial undercurrent. Additionally, as tunable parameters are adjusted or added in an attempt to parameterize processes such as penetrative convection and wave-current interactions, these models become unwieldy and undependable parameterization choices for global models.

An alternative approach, such as that of Pacanowski and Philander (1981), assumes that mixing is a function of the gradient Richardson number (Ri_g). However, this scheme gives too little mixing at low Ri and too much mixing at high Ri_g (Peters et al., 1988). Cane (1993) notes that a more serious problem is that the data seem to indicate that mixing does not depend on Ri_g alone. Reason et al. (1993) compared three different vertical mixing schemes (Kraus and Turner, 1967; Pacanowski and Philander, 1981; and an eddy diffusion scheme by Henderson-Sellers, 1988). These were imbedded in a coarse resolution OGCM and examined under annual and monthly mean forcing. They conclude that the Kraus-Turner mixing scheme is more robust and applicable to global ocean studies as judged by the ability to reproduce the seasonal growth and decay of the mixed layer and to reproduce the major circulation features. They used the Krauss-Turner scheme together with an implicit vertical-diffusion method for convection described by Bryan and Lewis (1979).

A critical aspect of mixed-layer modeling is determining the correct behavior at the base of the mixed layer, the region where the mixing and the dynamical processes must be coupled. This coupling issue was investigated by Adamec et al. (1981) in a study in which they embedded a mixed-layer model similar to Garwood's (1977) model in a two-dimensional model. They also changed the convective adjustment to be governed by a dynamic stability condition that considers both the vertical current shear and vertical temperature gradient. This work demonstrates how important the dynamic (and static) stability are to the evolution of the mixed layer.

Rosati and Miyakoda (1988) included the Mellor-Yamada 2.5 turbulence closure scheme in their global simulation at 1 resolution. The simulated ocean was not more accurate for SST, but produced a more realistic mixed-layer structure than with constant eddy coefficients (Cane, 1993; Rosati and Miyakoda, 1988). Turbulent closure models such as Mellor and Yamada (1982) assume isotropy (which breaks down during convection) with parameters fixed to laboratory experiments and historically underestimate ocean mixing. As a result, the Mellor-Yamada scheme generally tends to underestimate the growth of the mixed layer because of a weak representation of wind-driven mixing and penetrative convection at the mixed layer base (Martin, 1985).

This is probably the major deficiency of the model, which results in a systematic overestimation of the sea surface temperature (Kantra and Clayson 1994). Smith and Hess (1993) compared the Pacanowski and Philander model with a second-moment closure model (such as Mellor-Yamada) for an equatorial Pacific Ocean simulation. They found that the Pacanowski and Philander scheme ensures that viscosity is greater than diffusion, whereas the closure scheme has a tendency towards greater diffusive rates.   Kantra and Clayson (1994) have included a shear instability-induced mixing mechanism to the amended Mellor-Yamada expansion given by Galperin et al. (1988) to improve the model simulations. Kantra and Clayson (1994) state that the inclusion of this mechanisms leads to a more realistic and reliable mixed layer model.

While the improvement of discrete models such as that of Mellor-Yamada is expected to continue, the models remain computationally expensive compared to bulk models. For example, Haidvogel and Bryan, (1992) have shown that the discrete models can take up to 10 times more computer time to apply than the bulk models.   The question of cost versus performance has led researchers to develop alternative approaches that attempt to resolve some of the structure in the mixed layer using much simpler closure schemes. The most recent of these schemes is the K-profile parameterization (KPP) models described by Large et al. (1994).

The KPP models allow for a finite diffusivity in the mixed layer and are motivated by MO similarity theory, which assumes a constant flux of momentum and buoyancy through a boundary layer. The models have complex thermocline mixing schemes with penetrating convection to account for mixed layer processes that cannot be accounted for by K-theory. Large et al. (1994), Large and Crawford (1995), and Crawford and Large (1996) have shown that this model provides accurate simulation of mixed layer deepening and diurnal modulation of the sea surface temperature.

These models have been found to break down under solar penetrative heating. The primary reason for this breakdown is due to the KPP schemes reliance on the constant turbulent flux assumption of MO similarity theory, which is not valid for the ocean mixed layer for two reasons. First, penetrating shortwave radiation provides a buoyancy flux profile independent of turbulent mixing. Secondly, as in the atmosphere, coherent structures in the mixed layer such as Langmuir circulations may transport buoyancy and momentum independently of turbulent motions. Finally, as with all of the models described above, the model does not attempt to include the effect of surface waves on the energy transfer between the ocean and atmosphere. As discussed above, the effect of the waves may be negligible in simulating many open ocean processes.

C. Wave-Current Interaction

The importance of surface wave forcing and wave-current interactions are less well understood. One-dimensional mixed-layer models have been somewhat successful in predicting variability in the upper ocean, such as diurnal cycling. Most modeling efforts and observational efforts have ignored surface gravity wave effects. However, recent observational work and multidimensional modeling efforts are starting to shed some insight on the dynamics of wave-forced mixing and Langmuir circulations.

A number of investigators (e.g., refs??) have postulated that the organized motions associated with Langmuir circulations should provide an effective means to transport momentum through the mixed layer. ONR sponsored the 1983 Mixed Layer Dynamics Experiment (MILDEX) to test this hypothesis. The MILDEX observations reported by Weller and Price (1986) and Smith et al. (1987) clearly show variability and large vertical velocity and shear in the surface mixed layer. During a period of moderate wind and wave forcing, they observed downward flowing jets beneath and a weak return flow between surface convergence as shown in Fig. 10. The observations clearly demonstrate the vertical circulations but shed little information on their role in the vertical transport of momentum and buoyancy through, and entrainment at the base, of the mixed layer.

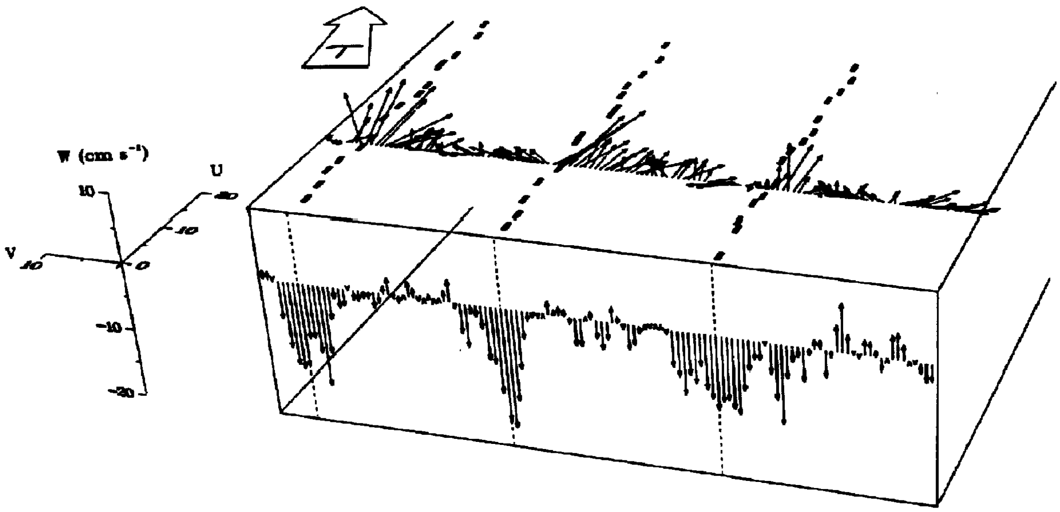

Figure 10: Observations of vertical circulations in the ocean mixed layer taken from FLIP (Weller et al. 1985).

D. Beyond the Mixed Layer

There are three basic observations which indicate that the mixed layer is not a rigid base to mixing of momentum and heat. The first comes from drifting thermistor chain buoys and other type of temperature profile data near Ocean Weather Stantion Papa, OSW-P (50°N, 145°W). Large et al. (1986) reported that during strong storms, the water beneath the mixed layer heats up, while the surface temperature cools down. The mixed layer heat budget shows that the mixed layer loses much more heat than the atmosphere can take up. As a result, some of it goes under the mixed layer, as if the small scale mixing increased during the storm. The results also indicated that portions of these high mixing regions remain distinct from the mixed layer, i.e., they did not regions did not total entrain to become a single, deeper mixed layer.

The second observation comes from the velocity data collected at both the Atlantic and Pacific 10°N. hydrographic sections where an ACDP was used to measure the currents directly. The velocity profiles and temperature profiles taken during these transects reveal that a substantial amount of wind-driven momentum can be found below the mixed layer (Chereskin and Roemmich, JPO 1991, 869-979).

Thirdly, it is evident from observations of inertial motions (possibly due to a specific storm) and microsturcture in warm rings at the thermocline depth that much more vigorous shear and turbulent activity occurs there than the "usual" thermocline found at that latitude (Kunze, Schmnitt and Tooles, JOP 1995, 942-957). A numerical modeling study of ... by Lee and Niiler, JGR, 1998, 7579-7571) shows ...

I think that an experiment that has a fresh look at the relationship to wind-driven currents (and heat and salt mixing) in the upper ocean would be exciting and germane. This would be a mid-ocean mesoscale (the 200 mile air-craft position more than the dashing seal position) and would be of great interest to modeling of wind-driven currents on time scales of several days to several centuries. It would have to be fully three-dimensional!

E. Mixed Layer Parameterizations

The models we review include the bulk mixed-layer models of the form discussed in Kraus and Turner (1967), Thompson (1976), Garwood (1977), and Niiler (1975), the modified bulk layer model of Price et al. (1986) hereafter denoted by PWP, the Mellor and Yamada (1982) level 2 discrete grid model (hereafter MY2), and the nonlocal K profile parameterization (hereafter KPP) described by Large et al. (1994) . The limitations of bulk layer models and discrete grid models were discussed above. In the following sections, we discuss the structure and pertinent equations that define the models.

1. Bulk Mixed Layer Models

The standard bulk layer model solves the set of equations

$$\frac{d}{dt}(hU_x) = fhU_y + \frac{\tau_{ox}}{\rho_o} \qquad \textbf{(96)}$$

$$\frac{d}{dt}(hU_y) = -fhU_x + \frac{\tau_{oy}}{\rho_o} \quad \textbf{(97)}$$

where h is the mixed layer depth, U_x and U_y are the mixed-layer mean horizontal components of velocity in the zonal and meridional directions, x and y, f is the Coriolis parameter, τ_{ox} and τ_{oy} are the shear stress components, and ρ_o is the mean mixed-layer density. The standard model almost always ignores the influence of waves on the shear stress and sets $\tau_o = \tau_a$. The pressure gradient terms in **(1)** and **(2)** is represented by the spatial variations in h, however, this spatial variability is often ignored in bulk models or the geostrophic component is removed using a reference velocity.

This set of equations can be coupled by determining h through a diagnostic equation such as a bulk Richardson number criterion,

$$Ri_B(h) = \frac{gh\Delta\rho_o}{\rho_o(\Delta U)^2} = Ri_{Bc} \quad \textbf{(98)}$$

where $\Delta\rho_o$ is the density difference across the bottom of the mixed layer, g is the acceleration of gravity, ΔU is the velocity difference between the mixed layer and the underlying water, and Ri_{Bc} is the critical value of the bulk Richardson number (Thompson 1976). Pollard et al. (1973) use a critical value of 1 while Price et al. (1986) use 0.65. Alternatively, the mixed-layer depth can be calculated using a prognostic approach based on an entrainment equation

$$-\Delta\rho_o \frac{h}{\rho_o}\frac{\partial h}{\partial t} = 2m\overline{E}\,\overline{\sigma}_w \quad \textbf{(99)}$$

where m is an entrainment scaling constant, $\overline{E}$ is the mean turbulent kinetic energy (TKE) of the mixed layer, and $\overline{\sigma}_w^2/2$ is the mean vertical component of TKE in the mixed layer. The parameters on the right side of **(99)** are diagnosed using assumed budgets for the mixed layer TKE and involve considerably more computational effort than the Ri_B criteria in **(98)**. The cost of predicting the mixed-layer depth, which depends on the complexity of the entrainment estimation, can limit the usefulness of this approach.

2. PWP Mixed Layer Model

One problem with the bulk layer model technique is the formation of a sharp discontinuity at the base of the modeled mixed layer. Price et al. (1986) modified the bulk-layer approach by applying a second Richardson number criteria based on the gradient Richardson number,

$$Ri_g = -\frac{g}{\rho_o}\frac{\partial \rho_o}{\partial z}\left(\frac{\partial U}{\partial z}\right)^{-2} = N^2\left(\frac{\partial U}{\partial z}\right)^{-2} \qquad \textbf{(100)}$$

where N is the buoyancy frequency. In stratified regions, such as at the base of the mixed layer, Ri_g is limited to values greater than 0.25 by mixing temperature, salinity, and momentum at two levels, j and $j+1$, according to

$$\phi_j' = \phi_j - \left[1 - \frac{Ri_g}{\overline{Ri}_g}\right]\frac{(\phi_j - \phi_{j+1})}{2} \qquad \textbf{(101)}$$

$$\phi_{j+1}' = \phi_{j+1} - \left[1 - \frac{Ri_g}{\overline{Ri}_g}\right]\frac{(\phi_j - \phi_{j+1})}{2} \qquad \textbf{(102)}$$

where ϕ is temperature, salinity, and momentum, Ri_g is a constant set to 0.3 to ensure stability, and primed variables denote the mixed values. These two equations are iterated until Ri_g is above the critical value of 0.25 over the stratified portion of the profile. As shown by Price et al. (1986), this technique ensures a smooth transition between the mixed-layer profile and the underlying thermocline. The adjustment also compensates for shear flow instability that may be active in the interior ocean where large scale dynamics force regions of strong vertical shear.

3. MY2 Mixed Layer Model

Unlike the bulk mixed layer models, the Mellor and Yamada (1974) level 2 turbulence closure scheme maintains discrete values of temperature, salinity, and momentum throughout the vertical profile and performs mixing via changes in the eddy diffusivity coefficients. This is an attractive characteristic with regard to OGCMs that already have a eddy diffusivity term in the equations. The scheme calculates eddy diffusivities using,

$$K_m = lqS_M \quad K_h = lqS_H \tag{96}$$

where the subscripts m and h denote momentum and heat diffusivity coefficients, l is an estimated turbulent length scale, S_M and S_H are stability functions that depend on the R_g, and q is the turbulent velocity scale equal to $\sqrt{2E}$, which is similar in magnitude to u_*. The TKE is determined from

$$\epsilon = \frac{q^3}{cl} = K_M\left[\left(\frac{\partial U_x}{\partial z}\right)^2 + \left(\frac{\partial U_y}{\partial z}\right)^2\right] + K_H\frac{g\partial\rho_o}{\rho_o\partial z} \tag{104}$$

where c is a constant setting the dissipation length scale. This equation represents a balance between the production of turbulence by shear and buoyancy with the dissipation of turbulence through molecular viscosity. Shear instability with this model is suppressed when the Richardson number exceeds a critical value near 0.25. As shown by **(104)**, this model is unable to simulate penetrative convection because shear production is the only source of TKE in stratified regions.

Craig and Banner (1994) have attempted to include the influence of the energy flux from the waves to the ocean, E_{wo}, by including the total energy transport term in **(104)**. This is accomplish by parameterizing the combined energy flux (pressure plus energy) divergence in the TKE equation such that **(104)** becomes

$$\frac{q^3}{cl} = K_M\left[\left(\frac{\partial U_x}{\partial z}\right)^2 + \left(\frac{\partial U_y}{\partial z}\right)^2\right] + K_H\frac{g\partial\rho_o}{\rho_o\partial z} + \frac{\partial}{\partial z}\left[K_q\frac{\partial E}{\partial z}\right] \tag{105}$$

where $K_q = lqS_q$ and S_q is another stability function. At the interface, the boundary condition for this additional term can be parameterized using the notation given by Terray et al. (1996) as

$$\frac{E_{wo}}{\rho_w} = \frac{\partial}{\partial z}\left[K_q\frac{\partial E}{\partial z}\right]_s \approx \bar{c}\,\frac{\tau_a}{\rho_w} \tag{106}$$

where the subscript s indicates evaluation at the surface. As state in section **5.C.4**, Craig (1996) used this form of the mixed layer model, with the buoyant production term set to zero and the constants fixed to commonly used neutral values, to obtain good agreement with the laboratory results of Cheung and Street (1988).

4. KPP Mixed Layer Model

The K-profile parameterization (KPP) represents an efficient implementation of a K dependent mixing scheme, as used in Mellor and Yamada, with a simplified boundary layer model (Large et al. 1994). The method relies on the observation that most turbulent mixing in the ocean can be separated into boundary-based and interior generated turbulence. Near the upper boundary, the scheme assumes a profile for the eddy viscosity following ideas put forth by Troen and Mahrt (1986) and O'Brien (1970). Vertical turbulent fluxes in the boundary layer are modeled using

$$\overline{wx}(z) = -K_x(z)\left(\frac{\partial X}{\partial z} - \gamma_x(z)\right) \qquad \mathbf{(107)}$$

where x represents momentum or a scalar quantity, K_x is the eddy diffusivity for quantity x and γ_x is a counter-gradient flux for nonlocal transport. The nonlocal transport term is nonzero only for scalars in convective conditions. Values of K_x are directly proportional to h and are assumed to follow an arbitrary cubic polynomial shape (see O'Brien 1970) normalized by a turbulent velocity scale. The turbulent velocity scale is consistent with Monin-Obukhov similarity theory near the surface , i.e., the amplitude depends upon the surface momentum and buoyancy fluxes. Its value is continuous with interior mixing rates at the base of the mixed layer, below which the fluxes are modeled using a eddy viscosity that is a function of the local gradient Richardson number defined by **(100)**. The eddy viscosity decreases as the Richardson number approaches ~0.6 to a uniform background value of 1.0 x 10^{-4} m^2 s^{-1} for momentum and 0.1 x 10^{-4} m^2 s^{-1} for scalars.

A critical parameter in the KPP model is the boundary layer depth, h. The boundary-layer depth is determined using the bulk Richardson number approach

$$Ri_B(h) = \frac{g\Delta\rho_o}{\rho_o}\frac{h}{(\Delta U)^2 + V_t(h)^2} \geq Ri_{BC} \qquad \mathbf{(108)}$$

where Δ denotes a difference between a near surface reference value and the value at h (as opposed to the difference across the base of the mixed layer as in bulk models), and $V_t(z)$ represent the turbulent contribution to the velocity shear. This latter term is most important in strong convection and in cases with little or no mean shear (Large et al. 1996) and is proportional to the turbulent velocity scale describe above.

The critical value of the bulk Richardson as defined by **(109)** is usually chosen between 0.3 and 0.4 using KPP. Because h depends on the surface values of buoyancy and velocity, as well as the interior ocean values, it defines a non local measure of the turbulence. In other words, the value of K at some depth is determined by the overall shear and buoyant stability of the boundary layer, and not the local Richardson number or shear as is the case in local schemes (e.g. Pacanowski and Philander 1981).

KPP has several advantages in principle over other types of boundary layer parameterizations: it specifies mixing rates, not outcomes (unlike mixed-layer or instantaneous adjustment schemes), and it represents non-local transport over the whole boundary layer (unlike single-point closure schemes). Its criteria encompass a wide range of stratification and surface stress and buoyancy-flux conditions, and it has been extensively tested against observations in a one-dimensional mode (Large et al. 1994). It has also been tested, though somewhat less extensively, against LES solutions and used in several 3D oceanic and atmospheric circulation models.

Probably the biggest drawback of the KPP approach is the dependence on a presumed vertical turbulence structure having a well-defined boundary layer near the surface and a relatively non-turbulent interior (more recent implementations have included a bottom boundary layer). For much of the ocean, this does not pose a significant problem, particularly when considering flow problems on climatic time scales. However, for short-term forecasts in regions with signification bottom topography, local mid-depth mixing processes may dominate over boundary layer turbulence. For example, strong shear generated by internal tides or internal waves generated by flow over bottom topography can completely mix the coastal ocean (J. Moum personal communication).

Shear associated with these processes can be resolved in today’s coastal models, and should be considered in mixing parameterizations. The mathematical framework of KPP may be adaptable to include some of these additional effects once they are well enough known.

Additional important frontier issues of this type are surface gravity waves, mesoscale non-stationarity and heterogeneity, strong forcing at the entrainment interface (e.g., by inertial shear instability or cloud processes), and bottom-layer turbulence over irregular topography.

5. Wave-Current Interaction

There is still little direct evidence that the coherent structures associated with Langmuir circulations vertically transport heat and momentum in the mixed layer. Recently, however, two and three-dimensional mixed-layer models have been used to examine more closely the role of Langmuir circulations. The 3-D model presented by Thorpe (1997) and the 2-D model presented by Li and Garrett (1997) both suggest that there would be enhanced shear instability and entrainment beneath the downwelling jets associated with Langmuir circulations. Li and Garrett (1997) used a 2-D model to explore the strength of Langmuir cell activity in parameter space. Their study suggests a critical Froude number of 0.6 exists for the cells and that enhanced downwelling in convergence zones would be limited to a depth of $10 u_* N^{-1}$. They also suggest a Langmuir cell parameterization for DIM models where the mixed layer would deepen due to Langmuir cell activity unless

$$\Delta b = \frac{g \Delta \rho_o}{\rho_o} \geq c \frac{u_*^2}{h} = 1.44 \frac{U_S u_*^2}{K_m} \frac{\lambda_{LC}}{2\pi h} \qquad \textbf{(109)}$$

where Δb is the buoyancy jump, U_S is the Stokes drift velocity, and $\lambda_{LC}/2\pi$ is the e-folding depth of the Stokes drift velocity, where λ_{LC} is approximately equal to the wavelength of the dominant waves. This constraint can be used, e.g., as a third Richardson number criteria in the PWP model as

$$Ri_{LC} = \frac{g h \Delta \rho_o}{\rho_o u_*^2} \geq c \qquad \textbf{(110)}$$

where c is approximately equal to 50 for fully developed waves (Li and Garrett 1997). In this form of the Richardson number the velocity jump has been replace by the friction velocity, which Li and Garret (1997) argue is more appropriate for scaling the Langmuir circulations.

According to these models, this mechanisms can sustain mixing even after the wind-driven Ekman transport becomes negligible. This situation is most like to occur under decaying seas where the Stokes drift generated by the slowly decaying waves remains strong long after the shear stress diminishes. Observational evidence for this is given by Pluddemann et al. (1996), who used acoustic remote sensing techniques to quantify the circulation strength of the Langmuir cells. Pluddemann et al (1996) found that the Langmuir circulation was detectable for up to a day after abrupt reductions in the shear stress. These observations found that the circulation strength is more closely related to Craik-Leibovich velocity scaling (Craik 1977, Leibovich 1977)

$$V_{CL} \approx (u_* U_S)^{1/2} \qquad \textbf{(111)}$$

than the friction velocity alone. This is obviously consistent with the idea that the Langmuir cell strength depends on both the wind and wave field. The findings of Pluddemann et al. (1996) suggest that a more appropriate Richardson number criterion may be given by

$$Ri_{LC} = \frac{g h \Delta \rho_o}{\rho_o V_{CL}^2} \geq 1.44 \frac{u_*}{K_m} \frac{\lambda_{LC}}{2\pi} \approx 0.6 \frac{\lambda_{LC}}{z} \qquad \textbf{(112)}$$

where we have used the neutral value of **(13)** for K_m. This implies that the depth of the mixed layer driven solely by the Langmuir circulations is approximately equal to the depth where the wavelength matches the value of the Richardson number.

Research Issues*: The studies reviewed here indicate that as of yet there is no obvious or "best" choice for surface mixing parameterizations. In addition, the parameterizations must be combined with convective adjustment schemes within the OGCM, or new convective adjustment conditions must be developed in a consistent way to compliment the operations of the mixed-layer model. Improvements in our understanding of the strengths and weaknesses of these parameterizations facilitate the development of an integrated mixed-layer model for use within an OGCM. We use the term "integration" to mean combining a penetrative convective adjustment scheme, e.g., the Ocean Parameterized Plume Scheme (OPPS) described in Paluszkiewicz and Romea (1997), with the most appropriate mixed-layer modeling approaches in a hybrid scheme. Many of the mixed layer models discussed above have beneficial aspects;*

Price et al.'s (1986) model combines aspects of Kraus-Turner and Pacanowski and Philander and has particular promise. A more integrated vertical mixing parameterization should lead to improved surface mixed-layer modeling within the OGCM and should prove to be computationally affordable and desirable.

Aside from the successful observations of Langmuir circulations in the mixed layer made during MILDEX, there has been little observational work on Langmuir circulations to direct and validate modeling efforts. This is due to the difficulty of measuring the strength, variability and mixing from Langmuir cells in the presence of orbital velocity fluctuations associated with surface gravity waves. However, the recent modeling work of Skyllingstad and Denbo (1995), Thorpe (1997), and Li and Garrett (1997) suggest testable hypotheses about the role of Langmuir cells in mixed-layer dynamics and thermocline entrainment. Their work describes the theoretical vertical distribution and strength of the circulations and specifically quantifies the strength of the Langmuir circulations in terms of wind/wave forcing and vertical density structure (see section 9.D.5). Thus, in addition to the mixed-layer observations, accurate surface wave and air-sea flux measurements are required to determine the forcing conditions and to interpret observations.

In summary, it has become quite clear that the ocean is not just an upside-down atmospheric boundary layer, but has differences due mostly to the large role of surface waves. To improve our understanding of wave-induced and turbulent processes in the mixed layer requires more than just measurement of the dissipation rate. We must measure the basic turbulence properties to figure out how this makes the ocean boundary layer different from other boundary layers. Basic properties include the distribution of turbulent kinetic energy, velocity, temperature, salinity, and density variance. Measurements in the form of variance spectra would be especially useful to provide the temporal/spatial distribution of these fluctuating quantities. Even more valuable, would be direct measurements of the fluxes of heat, salt, density, and momentum.

Modern instrumentation is beginning to allow us to measure most of these quantities (e.g., D'Asaro et al. 1996; Trowbridge 1998; Sanford and Lien 1999). As these measurements become available, we can begin to identify the physical processes that produce the distributions of these turbulent quantities that have been inferred from previous experiments. We would then be able to investigate how are these quantities related to the various surface fluxes, the mean *shear, thermal stratification, and buoyancy. In particular, we need to identify the energy flux from the surface waves to turbulence due to wave breaking versus the energy flux from the surface waves to turbulence due to wave/vortex interactions.*

The various mixed layer models differ in that they assume different things about these quantities. For example, the KPP model assumes MO similarity , certain profiles of the fluxes, and a "boundary layer depth." These measurements are necessary to investigate these assumptions, i.e., the applicability of MO similarity to the OBL, the vertical distribution of the fluxes, and scaling arguments for the OBL depth. Therefore, the way to build better models of upper ocean turbulence is to measure upper ocean turbulence in detail and compare the data to models. This is a huge challenge for the observational community, but one that is becoming more tractable with current technology.

11. Numerical Simulations

Meteorologists and oceanographers commonly distinguish numerical simulations from numerical models. As describe in the above sections, parameterizations of turbulent mixing in atmosphere and ocean models typically rely on empirical relationships between mixing strength and average vertical properties, such as shear and buoyant stability. Turbulent processes are not directly simulated in these parameterizations, but are estimated using theory and observations that correlate with vertical mixing. In contrast, direct numerical simulations (DNS) resolves all scales down to the viscous limit and does not depend on any empirical constants. However, DNS is limited to studying low Reynolds number flows.

Large-eddy simulation (LES) models directly simulate a portion of the turbulent eddy fields and rely on relatively simple parameterizations to account for the unresolved fraction of the turbulent energy. Therefore, LES distances itself from mesoscale modeling in that LES seeks to explicitly resolve the large scale turbulent motions and parameterize only the very small scale turbulence fields, i.e., the subgrid scale (SGS) motions. The SGS parameterization in LES is based on inertial subrange theory and assumes that the grid spacing is more or less isotropic. The premise behind LES is that large scales in a turbulent flow contain most of the energy and are therefore of prime importance. Moreover the resolved field is more dependent on boundary conditions and thus varies markedly depending on the physical situation modeled. On the other hand, the small scale motions contain appreciably less energy (as compared to the resolved scales) and are more isotropic and universal in their behavior acting mainly to dissipate energy. Thus a model like LES which explicitly resolves the large scale turbulent motions subject to a parameterization of the small scales can be expected to exhibit a large degree of generality and possess reasonable predictive capabilities. The turbulence resolving power, SGS modeling practices, and isotropic grid spacings used in LES are in sharp contrast to traditional mesoscale modeling that parameterizes *all* turbulent motions and uses very anisotropic grid spacing.

Numerical simulations of turbulent flows using DNS and LES have become an important tool for studying the basic physics of turbulent flows (for reviews see Wyngaard 1984; Rogallo and Moin 1984; Lesieur and Métais 1996; and Moin and Mahesh 1998). LES originated with Deardorff (1970) and now finds extensive use in both geophysical and engineering studies. Advantages of LES are that it accurately predicts time dependent 3-D turbulence fields. In geophysical applications, LES is most often used to study turbulent dynamics in the planetary boundary layers (PBLs). With LES it is possible to simulate realistic flow conditions in a controlled fashion; e.g. buoyancy, geostrophic winds, boundary layer capping inversion, surface boundary conditions and surface roughness are parameters which can be readily modified in LES. Thus, with LES it is possible to perform canonical studies whereby physical forcings are systematically varied to isolate a certain process. LES can also be used to simulate flow at an observational site with measured forcings as initial conditions. Each LES run serves as an ``experiment'' in its own right, and provides a complement to direct measurements.

The technology behind LES is maturing to a stage where for some flows LES results are nearly equal to their observational counterparts. For instance, a comparison of several planetary boundary layer LES codes revealed that despite the differences in numerical methods, SGS parameterization, and other factors, the code-to-code variation was less than the scatter in the available experimental data (Nieuwstadt et al. 1993).

A good example of a widely used code for investigating PBL flows is the LES developed at the National Center for Atmospheric Research (NCAR). The spatial discretization in this LES code is pseudospectral in horizontal directions and finite difference in the vertical, with third order Runge-Kutta time stepping. Periodic boundary conditions are used in horizontal directions and Monin-Obukhov similarity theory is used at the surface (Moeng 1984) while a radiation condition is employed at the upper boundary (Klemp and Durran 1983).

In addition to the usual dynamical variables, an arbitrary number of passive scalars can be included. For example, Feingold et al. (1994) coupled an LES model with a size-resolving aerosol and/or droplet distribution model to the study of fog, marine stratocumulus, and aerosol processing. In their study, the aerosol and cloud droplet spectra are broken down into a series of size range bins, and dynamic equations are integrated in time for each bin size. Feingold et al. (1994) also included interactions between various bins due to processes such as coalescence and scavenging of aerosol by cloud drops. Parameters passed from the droplet model can be used to investigate radiative cooling effects on cloud formation and PBL structure.

Further, recent SGS developments reproduce MO similarity theory in the surface layer (Sullivan et al. 1994), which overcomes a long standing shortcoming of previous LES for PBL flows that were not able to reproduce MO similarity theory in the surface layer. This is largely a consequence of previous SGS models being overly dissipative near boundaries and the new code having a novel nesting procedure that allows for fine nested meshes to be embedded within an outer coarse grid (Sullivan et al. 1996).

LES codes have been successfully used for numerous studies of atmospheric and oceanic PBL turbulence for a variety of thermal and shear conditions. For example, Moeng and Wyngaard (1989) studied turbulent transport and evaluated second-order closure schemes, Moeng et al. (1999) investigated the effects of radiation and stratocumulus on PBL turbulence, Moeng and Sullivan (1994) compared PBLs driven by buoyancy and shear, McWilliams et al. (1999) examined coherent structures in the marine boundary layer, Sullivan et al. (1998) identified entrainment mechanisms at the PBL inversion, and Lin et al. (1996) studied coherent structures in a neutrally stratified PBL.

One of the recent developments has concentrated on examining the coupling mechanisms among atmospheric and oceanic turbulence and surface gravity wave fields. We should note that there have only been a few studies using DNS and LES to examine turbulent flows over complex geometry, like wavy surfaces. Cherukat et al. (1998) and Maass and Schumann (1994) consider turbulent flow over sinusoidal surfaces driven by a pressure gradient (i.e., channel flow). Gong et al. (1996) use LES to simulate turbulent flow developing over sinusoidal waves in a wind tunnel, and Choi et al. (1992) employ DNS to study turbulent flow over streamwise oriented riblets. Also, Krettenauer and Schumann (1992) consider turbulent convection over wavy terrain utilizing DNS. It is important to mention that in all of these studies, the wavy boundary is *stationary* and thus not applicable to flow over water waves.

An idealization of turbulent air flow over a moving wavy surface is depicted in Figure 1. Here the water wave is assumed to be a two-dimensional, periodic, non-evolving, deep-water gravity wave with orbital velocities at the water surface given by first order wave theory. The turbulent air flow above the water wave is assumed to be periodic in the horizontal directions (x,y) and is sustained by an imposed large scale constant velocity.

Despite the relative simplicity of this model flow, the presence of a moving wavy lower boundary is sufficiently complicating that a new numerical method had to be developed to simulate turbulent flow in this geometry. The numerical scheme borrows elements from the NCAR LES (Moeng 1984; Sullivan et al. 1994; and Sullivan et al. 1996) and the recent developments described by Zang et al. (1994). The algorithm is a mixed pseudospectral finite-difference scheme that utilizes a surface fitted grid, a conformal mapping between physical and computational space, and a collocated grid architecture for all variables. A complete description of the numerical method is given by Sullivan et al. (1999).

As with atmospheric LES, ocean LES provides an accurate three-dimensional data set for analysis of turbulent processes, such as turbulent fluxes of salinity, heat, and momentum, and can be used to better understand the response of the ocean surface boundary layer to surface fluxes and large-scale dynamical forcing - as long as the model resolution is sufficient. The accuracy of LES models is greatly influenced by the strength of flow stratification and vertical current shear. Strong stratification acts to reduce the size of the largest turbulent eddies, requiring increased resolution for credible prediction with LES (Skyllingstad et al. 1999). A simple measure for determining resolution requirements is the Ozmidov length scale defined as,

$$L_o = \left(\frac{\epsilon}{N^3} \right)^{1/2} \qquad \textbf{(113)}$$

which estimates the length scale of the largest turbulent eddies based on the strength of the stratification. The Ozmidov length scale determines when the turbulent vertical velocity, as diagnosed by the turbulence dissipation rate, is suppressed by stratification. When LES resolution is near the Ozmidov length scale, then the strength of turbulence is generally suppressed, although eddy fluxes may still be accurately simulated if the source of the turbulence is from a region away from the stratification (Skyllingstad et al. 1999; Wang et al. 1996). Strong vertical current shear can have a similar effect on the scales of turbulence. Strong shear tends to tilt and stretch large eddies, destroying boundary layer scale coherent structures. A length scale comparable to the Ozmidov scale but for shear can be defined as

$$L_{shear} = \left[\frac{\epsilon}{\left(\frac{\partial U}{\partial z}\right)^3}\right]^{1/2} \tag{114}$$

This length scale provides a resolution limit for shear dominated flow, assuming an estimate of ϵ is known.

Ocean applications of LES have focused mostly on turbulence associated with the surface boundary layer. McWilliams et al. (1993) used a modified version of the NCAR LES code to study the oceanic PBL. Skyllingstad and Denbo (1995) used a LES model to investigate wave-current interactions. Their results suggest vertical velocity variance in the mixed layer that is enhanced when a parameterization of wave-induced forcing (Stokes force) is included in the simulations (Fig. 11). They find that the distribution of velocity fluctuations is skewed in these cases and that the skewness scales with Craik-Leibovich velocity scaling (Craik 1977, Leibovich 1977)

$$V_{CL} \approx (u_* U_s)^{1/2} \tag{115}$$

where U_s is the Stokes drift velocity. These results are corroborated by McWilliams et al. (1997) using the modifed NCAR LES code to investigate Langmuir circulations. They also find a strong relationship between the CL scaling and Langmuir circulation strength. McWilliams et al. also point out the importance of including the effects of the Coriolis Stokes drift term in modifying the surface Ekman transport. Because of surface wave Stokes drift, the Ekman transport is strengthened and rotated more significantly in the clockwise direction.

Application of LES has also lead to a better understanding of diurnal surface forcing and current shear in defining the ocean boundary layer. Wang et al. (1998) and Wang et al. (1996) used LES to show how nightime cooling generates convection and unstable internal waves and a cycle in the strength of mixing in the equatorial Pacific boundary layer. Skyllingstad et al. (1999) examine the effects of resonant wind forcing in mid latitudes and the role of shear-generated entrainment. They find that Langmuir circulations act as a catalyst, strengthening entrainment in downwelling regions where the inertial current shear is maximized. Results from LES have also helped improve vertical mixing parameterizations. For example, the OPPS model developed by Paluszkiewicz and Romea (1997) is based in part from LES simulations presented in Denbo and Skyllingstad (1995) and Skyllingstad et al. (1996). More recently, Large and Gent (1999) applied LES results from the equatorial pacific as an independent test of the KPP model, finding good agreement between the LES and KPP results.

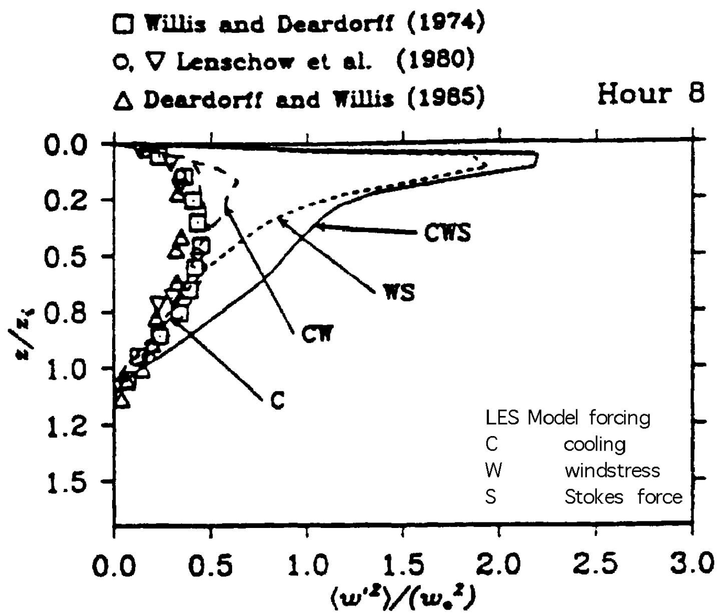

vertical velocity variance

Figure 11: Vertical distribution of vertical velocity variance for LES model. (Skyllingstad and Denbo 1995).

***Summary**:* *Ocean modelers have begun to make use of LES to study wave-driven and convective processes in the ocean. Skyllingstad and Denbo (1995) used an LES model to investigate wave-current interactions. Their results suggest vertical velocity variance in the mixed layer that is enhanced when wave forcing is included in simulations. They find that the distribution of velocity fluctuations is skewed in these cases and that the skewness scales with Craik-Leibovich velocity scaling.*

Research Issues: *A key problem in understanding air-sea coupling is explaining the effects of* *surface waves on the upper ocean. In LES applications, surface waves have been parameterized using the Stokes vortex approach derived by Craik and Liebovich for irrotational steady waves. However, we know that surface waves have a much broader influence on the upper ocean momentum and turbulence fields, for example through wave breaking and wave orbital velocity shear strain. These effects have not been addressed using LES models and have at best been modeled only through empirical methods (e.g. Craig and Banner 1994). Because much of the atmospheric momentum entering the ocean passes through surface waves, it is imperative that a solid understanding of wave-induced mixing be obtained.*

*Combining observations of ocean turbulence with LES can provide a powerful tool for understanding turbulent processes. In the ocean, very few LES experiments have been performed comparing model results with measured turbulence fields. For example, Pluedemann et al. (1996) present a thorough investigation on the structure and variability of Langmuir circulations during the Surface Waves Processes Program. Application of LES for this field experiment could provide explanations for the behavior noted by Plueddeman et al., namely the continuation of Langmuir circulations well after decreased winds. Observed velocities associated with Langmuir circulations could also be used to validate the accuracy of the Stokes drift parameterization and Craik and Liebovich scaling. ***** Lagrangian float measurements reported in D'asaro and Diariki (1997).*

12. Wind-Wave Interaction Models

There have been numerous approaches to modeling the effect of the waves on the wind field and momentum flux reported in the literature (e.g., Townsend 1972; Gent and Taylor 1976; Janssen 1989; Chalikov and Makin 1991; Belcher and Hunt 1993; Chalikov and Belevich 1993). Some of the approaches used to define the boundary conditions in these various models are in sections **6** through **8**.

13. Navy Atmospheric Models

Atmospheric forecasts are based on a prognostic set of equations that are numerically marched forward in time in model simulations. In general, the prognostic equations include the equation of motion, continuity equation, and equations that predict the evolution of the temperature and humidity fields. What sets various models apart are the way the equations are represented in the numerical model, which we often call the model numerics. The representation can involve spectral decomposition and a whole stable of finite-differencing and grid schemes (e.g., finite volume and finite element). As part of these numerics, the treatment of how the boundaries are handled also sets the models apart. Lateral boundaries can be periodic, fixed or act as sponges. Lower boundaries generally require parameterizations for the surface fluxes that account for changes in surface characteristics (i.e., topography, soil type, and surface roughness). Additionally, the models are set apart by the way they handle clouds, radiation, and precipitation.

A. NOGAPS

The Navy Operation Global Atmospheric Prediction Model (NOGAPS) represents ...

B. COAMPS

One of the primary objectives of the Coupled Boundary Layers Initiative is to develop truly coupled operational models, i.e., to put the CO in COAMPS. The Naval Research Laboratory's Coupled Ocean/Atmospheric Mesoscale Prediction System (COAMPS) (Hodur 1997; Hodur and Doyle 1999) is a finite-difference approximation to the fully compressible, nonhydrostatic equations that govern atmospheric motions. COAMPS can be applied as an analysis-nowcast and short-term (up to 48 hours) forecast tool applicable for any given region of the earth. COAMPS includes an atmospheric data assimilation system comprised of data quality control, analysis, initialization, and non-hydrostatic atmospheric model components and a choice of two hydrostatic ocean circulation models and an ocean wave model.

The equations used in the COAMPS atmospheric model are based on the nonhydrostatic formulation of the primitive equations. Nonhydrostatic effects must be included when modeling phenomena in which the horizontal scale is approximately the same or less than the vertical scale of motion. This is often the case for convection and flow over and around steep terrain. In these cases, the vertical acceleration can be quite significant. For larger scales of motion, a scale analysis shows that the balance between the vertical pressure gradient and the force of gravity are the only terms that need to be retained in the vertical velocity equation.

The atmospheric equations are solved in three dimensions with a terrain-following vertical coordinate, $_z$ (Gal-Chen and Somerville 1975). The model equations are solved on a system of nested grids that enable highest resolution to be focused over a specific region of interest. The finite difference schemes are of second-order accuracy in time and space. An option exists for fourth-order accurate horizontal advection. A time splitting technique that features a semi-implicit treatment for the vertical acoustic modes enables efficient integration of the compressible equations (Klemp and Wilhelmson 1978; Durran and Klemp 1983). Reflection of waves at the upper boundary is suppressed by a gravity wave absorbing layer using a Rayleigh damping technique based on the work of Durran and Klemp (1983) or a top-boundary radiation condition following Klemp and Durran (1983).

The planetary boundary-layer and free-atmospheric turbulent mixing and diffusion are modeled using a prognostic equation for the turbulent kinetic energy (TKE) budget based on the level 2.5 formulations of either Therry and LaCarrére (1983) or Mellor and Yamada (1974). Additionally, an option exists for the computation of the turbulent mixing through a large-eddy simulation parameterization (Hodur 1997). The surface fluxes are computed following the Louis (1979) formulation, which makes use of a surface energy budget based on the force-restore method. The subgrid-scale moist convective processes are parameterized using an approach following Kain and Fritsch (1993). The explicit grid-scale evolution of the moist processes are explicitly predicted from budget equations for cloud water, cloud ice, rain drops, snow flakes, and water vapor (Rutledge and Hobbs 1983). The short- and long-wave radiation processes are parameterized following Harshvardhan et al. (1987).

An incremental update data assimilation procedure enables mesoscale circulations to be retained in the analysis by using the previous COAMPS forecast fields for the first-guess. The initial fields for the nonhydrostatic model are created from a multivariate optimum interpolation analysis of upper-air sounding, surface, aircraft and satellite data that are quality controlled (Baker 1992) and blended with 6-h or 12-h COAMPS forecast fields based on the work of Barker (1992). The analysis increments, which are produced on fixed pressure levels, are interpolated to the model sigma-levels and added to the COAMPS forecast fields on the model sigma-levels. Such a use of an incremental update cycle has been found to be more effective than an interpolation of the analysis fields to the model sigma levels. Real-data lateral boundary conditions make use of Navy Operational Global Analysis and Prediction System (NOGAPS, Hogan et al. 1991) forecast fields following Davies (1976). For idealized experiments, the initial fields are specified using an analytic function and/or empirical data (such as a single sounding) to study the atmosphere in a more controlled and simplified setting (e.g., see Doyle 1995; Hodur 1997). A digital filter (Lynch and Huang 1992) may be used for initialization in order to minimize spurious modes forced at the start of a forecast.

COAMPS can be coupled with either of two ocean models. These include the navy Coastal Ocean Model (NCOM) and the Princeton Ocean Model (POM). In a fully-coupled mode, the atmospheric and ocean models can be integrated simultaneously so that the precipitation and the surface fluxes of heat, moisture, and momentum are exchanged across the air-ocean interface every time step. Additionally, a coupled COAMPS/Wave Model (WAM) is under development and will provide a means for exchange of the momentum flux at the air-sea interface. Optionally, the atmospheric model or the ocean models can be used as a stand-alone system. At this time, the option to utilize an ocean model within COAMPS is limited to our in-house R&D effort. Our plans call for exhaustive testing of the capabilities of a fully-coupled system before this system is transitioned for use to operations.

Typical mesoscale phenomena that COAMPS has been applied to includes mountain waves, land-sea breezes, terrain-induced circulations, tropical and extratropical cyclones, mesoscale convective system, coastal rainbands, and frontal systems. The model grid size can range from a few hundred kilometers (synoptic scale) down to approximately one meter when using the LES mode. In practice, real data simulations are typically made with resolutions of a few kilometers or larger, with LES simulations limited to simulations of idealized data in which the horizontal and vertical grid spacings are O(10) meters, or less.

One current limitation to our ability to accurately model mesoscale coastal phenomena is the lack of observations at the air-sea interface on the proper time and space scale. Uncertainties in the surface flux and boundary-layer parameterizations are especially large for high wind speed and heavy weather cases, which are conditions that adversely impact Navy operations. Measurements of fluxes and state variables near the air-sea interface are needed to validate coupled modeling systems and aid in the assessment of optimal coupling methods and parameterization improvements for the mesoscale.

C. Hurricane Models

Use Kurihara et al. 1998 for GFDL now in use by Navy. Numerous studies (Emanuel 1995; Wang et al. 1999) have shown that intensity predictions by hurricane models are very sensitive to how the surface processes are parameterized. For example, the numerical simulation conducted by Emanuel (1995) suggest that drag coefficient must become smaller than the scalar exchange coefficients at high wind speeds. This finding is at odds with the any extrapolation of our current parameterizations to hurricane strength winds. [Check out Wu 1982 for drag coefficients (breeze to hurricane)].

Research Issues: The process studies conducted with funding from ONR and other agencies have resulted in several published parameterizations of air-sea processes that attempt to include the effects of, e.g., stability, sea-state, wave age, and sea spray. However, aside from perhaps the simplest models of surface drag over the open ocean that include stability corrections, few of these parameterizations have found there way into operational Navy models. This is due to the uncertainty in these parameterizations and questions about the importance of including them in forecast models. MUCH MORE WILL BE WRITTEN HERE ONCE THE SECTIONS HAVE BEEN FILLED IN.

14. Navy Ocean Models

The variety of surface characteristics around the globe requires atmospheric models to include the effects of changing surface roughness and topography. This variety provides ocean modelers with even more challenges since the ever changing topography of the ocean floor must be combined by the lateral boundaries formed by the land-sea interface. This prevents the use of spectral models to simulate global ocean circulation. The dominate features of the global circulation such as western boundary currents require higher resolution models that typically run in global atmospheric models. The need for lateral boundary conditions and higher resolution greatly increases the number of CPUs needed to model ocean circulation. As a result, most previous ocean modeling has focused on regional circulations.

A. POM

The Princeton Ocean Model (POM) is the most widely used of the baroclinic coastal ocean models. The Princeton Ocean Model is based on a formulation by Alan Blumberg and George Mellor (Blumberg and Mellor, 1987). POM has a free surface and uses the sigma coordinate in the vertical and curvilinear, orthogonal coordinates in the horizontal. The sigma coordinate systme is a bottom following vertical coordinate system given by

$$\sigma_I = \eta - \frac{\eta - h_B}{N} I \qquad ; \qquad I = 0 \ldots N$$

where η represents the free surface and h_B is the bottom depth. This coordinate system allows the model to resolve the ocean circulation over varying bathymetry such as the transition from the deep ocean to the continental shelf.

This model is a 3-D, primitive equation model with complete thermohaline dynamics. It uses a non-linear equation of state for sea water to determine the in situ density. In most applications, the POM uses the second order close scheme of Mellor and Yamada (1982) for the mixed and bottom boundary layers. However, variations of the POM abound where the differences generally involve different configurations of the coordinate system and/or mixed layer parameterization. Horizontal mixing is parameterized using the Smagorinsky (1963) scheme, which is a Laplacian formulation with mixing coefficients proportional to the local grid spacing and velocity shears.

The model equations are discretized on the Arakawa C-grid, a commonly used staggered grid. Second-order accurate spatial differencing is used throughout. The temporal differencing uses a split- explicit numerical scheme in which the terms responsible for the fast surface gravity waves (otherwise known as the external or free surface mode) are treated using a much smaller time step than that for the internal mode. Leap-frog time differencing is used throughout with the exception of the horizontal diffusion terms which are lagged in time and the vertical diffusion terms which are treated implicitly. The Asselin (1972) time filter is applied at each time step to reduce time splitting.

The model is readily available and may be downloaded from the ftp site **ftp.gfdl.gov**. The model website at **www.aos.princeton.edu/WWWPUBLIC/htdocs.pom/** is well maintained and offers, among other items, a list of publications that have used the POM formulation, a list of upcoming meetings pertinent to POM users. Other terrain-following models include the Rutgers/UCLA Regional Ocean Modeling System (ROMS; e.g., see Song and Haidvogel, 1994) and the Dartmouth finite element model QUODDY (Lynch et al., 1996). Separate users group meetings have been convened for each of these model classes in the past. For the first time in 1999, a simultaneous meeting will be held for users of both the POM and SCRUM/ROMS sigma-coordinate models.

B. NCOM

Talk's about combination of sigma and z.

C. NLOM

Talk about NLOM's usefulness in data assimilation.

D. POP

Vertical mixing parameterizations options implemented in the Parallel Ocean Program (POP) model are the Pacanowski and Philander (1981) scheme and KPP (Large et al. 1994). The latter provides non-constant vertical viscosities and diffusivities based on gradient Richardson numbers. KPP was parallelized and implemented in POP in 1998. It calculates a boundary layer depth, and expressions for the diffusivity and non-local transport throughout the boundary layer. The diffusivity and its gradient match interior values at the bottom of the boundary layer. The interior values are a sum of the parameterized effects of internal wave breaking, convection, and vertical shear instability. Diagnostics from KPP (mixed layer and boundary layer depths) have been compared with NCOM as POP will be used as the ocean component of the Climate System Model (CSM) in the near future. Differences have been reconciled in terms of different code implementations i.e. use of a look-up table in NCOM for the flux profiles, while the analytic form is used in the POP KPP. An implicit vertical mixing scheme is used with KPP. This is needed since KPP uses very high diffusion coefficients to perform convection in convectively unstable columns. Implicit vertical mixing must be used to avoid unnecessarily small time steps (pers. comm. P. Jones).

15. Wave Models

A. WAM

The most widely used and best tested ocean wave model in the world is the WAM model developed by the WAMDI-Group (1988). The code is well documented and highly optimized to run on many different computational platforms. The WAM model has been extensively used for forecasting on global and regional scales at many weather prediction centers around the world (ECMWF, KNMI, FNMOC, NMC, NAVOCEANO, etc.), for special experimental programs and case studies such as SWADE, LEWEX, ERS-1 calibration/validation, hurricanes. The most frequently implemented version of the model is the so-called Cycle-4 version of WAM, or WAM-4 which includes a shallow water extension (shoaling, refraction and bottom dissipation) and wave-current interaction effects as well as a simple coupling of the atmospheric boundary-layer to the wave model following Janssen (1991). The new WAM-5 model is also available.

In WAM, the evolution of the directional wave spectrum $F(f,\theta;\phi,\lambda,t)$ as a function of frequency, f, and direction, f, in spherical coordinates defined by latitude, ϕ, and longitude, λ, is determined from the integration of a slightly modified form of the energy balance equation given by **(26)**

$$\frac{\partial F}{\partial t} + (\cos\phi)^{-1}\frac{\partial}{\partial\phi}(c_\phi\cos\phi F) + \frac{\partial}{\partial\lambda}(c_\lambda F) + \frac{\partial}{\partial\theta}(c_\theta F) = S_{in} + S_{nl} + S_{ds} + S_{bot} \qquad \textbf{(117)}$$

where c_ϕ, c_λ, and c_θ are the appropriate group velocities along a great circle path. The four source terms consist of S_{in}, an empirical wind input function based on the results of Snyder *et al*. (1981), S_{nl}, the nonlinear energy transfer integral following Hasselmann et al. (1985), and S_{ds}, the dissipation due to white-capping waves from Komen et al. (1984) and S_{bot}, the dissipation term due to bottom friction (Weber 1991). WAM-4 incorporates the source terms described by Janssen (1991). Namely, the input is quadratic in the ratio of friction velocity to phase speed,

$u_*/c(f)$, and the dissipation is proportional to the fourth power of the frequency. The wind input is given at standard height, usually 10 meters, and the surface stress is calculated internally within the wave model as a function of both wind speed at height and stage of wave development. The present implementation has 25 frequency bins logarithmically spaced from 0.042 Hz to 0.41 Hz at intervals of $\Delta f/f$ = 0.1 and 24 directional bins 15 degrees apart. In principle it is possible to modify the frequency and directional resolution which has been done for special occasions.

WAM in itself has been successful, opening the doors to studies that were not possible with older generation wave models. Using SEASAT scatterometer and radar altimeter data, WAM was employed to validate scatterometer-assimilated wind fields with altimeter wave heights (Bauer et al. 1992). Romeiser (1993) compared global WAM-2 wave height predictions with GEOSAT altimeter data. Janssen et al. (1997) compared WAM-4 wave height predictions with buoy and altimeter data and found significant improvement over earlier verification results. In SWADE WAM-4 was successfully implemented on a three-nest grid system to represent correctly the influx of wave energy from distant storms, especially swell propagation over a basin scale like the Atlantic. Graber et al. (1991) and Cardone et al. (1995) used this nesting scheme to test several wind field descriptions for an intense storm in SWADE to quantify the errors in the wind forcing. Other studies by Cavaleri et al. (1991) examined the effect of coastal orography on wave prediction in an enclosed basin in the Mediterranean Sea. The fact that the wind is hardly constant for long periods as assumed for most ocean models also provides a source of error when modeling ocean waves. Observations have shown that the wind oscillates around its mean value and that the normalized standard deviation of these oscillations varies with air-sea stability conditions and can reach turbulence levels as high as 30%. Cavaleri and Burgers (1992) examined this effect with WAM and found that with increasing turbulence levels the local predicted wave height also increased considerably.

Clearly waves play a critical part in a coupled atmosphere-ocean system. To this end several initial studies were undertaken to test the impact of waves in various components of a complete coupled atmosphere-ocean system. It is generally accepted that a coupling of the atmospheric boundary layer and the wind waves yields increased surface drag coefficients, especially during the early stages of storms or ahead of fronts. It is obvious that in a simple feedback mechanism the stress, which generates the waves, is enhanced and hence increases the momentum flux into the waves. This increase in momentum also affects the current distribution and the surge, which in turn may also influence the evolution of the wave field in coastal regions.

A coupled wave-surge model using WAM was first applied by Wu and Flather (1992) to the hindcast of a severe storm in the Irish Sea. Their study confirmed that the impact of waves on surge are significant producing not only changes in the local wave height up to ±1 m representing a 10-20% of the local SIGNIF Hs values, but also in surge elevation, especially in shallow areas. Several studies considered the influence of waves on the atmospheric circulation in climate models. Weber et al. (1993) speculated that one of the consequences could be a variation of the storm intensity and latitudinal shift. The coarse ECHAM model coupled to WAM did not produce these anticipated results. Janssen (1994) repeated these simulation with a higher resolution version of this model and found a small but positive impact on the atmospheric forecast. Doyle (1995) performed similar studies with the Navy's COAMPS model during cyclogenesis and found that the roughness effects associated with the young waves modulated the deepening rate during rapid cyclogenesis and enhanced the cyclone filling process. Until now, most of the coupling was performed with simple parameterizations. In a recent study by Powers and Stoelinga (1999) it was concluded that the mesoscale atmospheric simulations were quite sensitive to the form of the marine roughness parameterizations. These initial results strongly suggest that further studies are needed with better physics describing the interactions and transfer processes at the air-water interface.

Although the WAM model is greatly improved over the past decade since its conception and development, uncertainties remain in how the underlying physical processes are modeled. This is especially true for those processes which transfer energy from the atmosphere to surface waves and dissipate energy within the wave field. It is well established that uncertainties in the wind forcing are the largest source of errors in model generated wave fields in operational implementations of contemporary wave models (e.g. Janssen et al. 1984; Cardone and Szabo 1985; Bauer et al. 1992; Cardone et al. 1995), and are usually so large as to mask errors associated solely with deficiencies in the wave models physics or numerics.

With the implementation of WAM in the Navy’s operational wave forecasting centers long-term comparisons between model and measurements in the world’s oceans have been made over the past four years. The statistics elucidate identifiable shortcomings attributed solely to the wave model. In general these deficiencies only affect approximately 10-15% of the overall results, but occur during critical weather conditions. Some of the key deficiencies in the WAM model are associated with:

1. Consistent underestimation of peak wave periods.
2. Poor modeling of swell (which is connected to 1.)
3. Poor performance in hurricanes and typhoons related to reduced wave growth and improper radiation of swell.

The first deficiency marks a general trend for WAM and has been documented, for example, on a global scale (Wittmann and Clancy 1995), and on a regional scale (Jensen 1996). The second shortcoming is much related to the simple upwind propagation scheme employed in WAM. The first order explict scheme used in WAM for propagation has been shown to be very dispersive (Lin and Huang 1996a, Tolman 1992) which explains the often notable streaking and poor swell prediction (especially time of arrival of swell). While higher-order advection schemes can improve the propagation of swell as shown by Bender (1996) with a third order propagation scheme, run times often double and render such schemes not practical in operational centers. Tolman (1992) demonstrated that first order schemes used in third generation wave models misrepresent the physics under ideal situations, whereas the sharp and smooth transport algorithm (SHASTA, or termed by Lin and Huang 1996 as the iterative approximation of the Crank-Nicholson scheme-center-space scheme) showed to be a better numerical approach.

Finally a severe shortcoming of WAM is its representation of the nonlinear wave-wave interactions. This highly nonlinear and computationally very expensive mechanism is at the heart of WAM and is implemented by the Discrete Interaction Approximation (DIA). The DIA is the technological advancement that makes WAM work but now perhaps outdated. Several researchers recently noted that the DIA produces unrealistic interaction patterns (Banner ????). Recent advances in research models (e.g. Lin et al. 1997 and Resio 1993) have computed the nonlinear wave-wave interaction source term directly. Computationally these methods have been restrictive in an operational wave model. However with recent advances in computer hardware as well as improvements to the speed via parallelization, the implementation of these methods may become realistic, or alternate approximations could be implemented.

Extensive details on the WAM model, its underlying physics and on wave modeling in general can be found in excellent book by Komen *et al*. (1994) which is the result of a decade long international collaboration of many scientists and researchers.

B. SWAN

The SWAN model is a third generation spectral wave model. A detailed description of the model is given by ( ). The model is similar in many aspects to WAM, but optimized for use in coastal applications. Although the WAM model contains some aspects of shallow water wave physics both in the source terms and propagation, experience has shown that it can have significant computational instabilities in shallow water. In particular, the bathymetry must often be significantly smoothed in order to obtain a stable simulation. This however defeats the purpose of using shallow water physics if you must represent the gradients in the depth field to maintain numerical stability. Also in very shallow water, depth induced wave breaking is not included nor is the effect of nearly resonant triad wave interactions that build sub- and super-harmonics in the wave spectrum as wave pass over a bar.

The SWAN model has several options for source terms (which may be included or excluded by "switches": WAM Cycle 3, WAM Cycle 4, and a version of second generation source terms. Additionally the model contains a depth induced breaking source function proposed by Battjes and Janssen( ), and a three wave source term due to Eldeberkey ( ). The propagation scheme is an implicit scheme that is more accurate than WAM's and can be used on rid meshes 100 m or shorter. Typical model domain sizes are 25 km on a side. The model can be nested with WAM and was intended to be driven by WAM on an outer boundary. Research is being sponsored by ONR (see web site :) with the following objectives: improve the discrete interaction approximation (DIA) from WAM so that it is more accurate, improve the propagation routine so that larger domains can be accurately simulated, improve the three wave interaciton source term, and add diffraction to the propagation code. In addition, data assimilation modules are being developed as is an adjoint model.

16. Coupled Models

We reserve the description "coupled models" for those models that allow the boundary layers to interact, thereby affecting the dynamic response on both sides of the interface. Therefore, in a fully coupled model we do not have the option to treat the atmospheric as a given as shown in your Figs. 1 and 2. The forcing is very closely linked and fully interactive with the rest of the components of the coupled system that includes the oceanic entrainment zone (the link to the thermocline), the ocean mixed layer, the wave boundary layer, the atmospheric surface layer, the outer layer (major part of the boundary layer which is generally referred to as the boundary layer), and the entrainment zone of the atmospheric boundary layer (the link to the free atmosphere). This is different from an observational study in which one can measure the mean surface layer quantities and focus on refining the exchange coefficients, roughness length, etc. It is also differs from the common observational approach that uses direct observation (e.g., from a surface mooring) as model input to develop and run a 1D surface layer model (such as the profile structure predicted by the TOGA COARE algorithm) or a 1D ocean mixed layer model. That is, the mean quantities in surface flux parameterization are model results and may be very sensitive to the boundary layer parameterizations used in the model. This feedback between the mean quantities provided by the model and the turbulence provide by parameterizations results in unrealistic characterization or forecasts if there are any systematic biases.

It is therefore important to consider the role of larger scale boundary layer processes to accurately simulate a coupled system. The atmospheric and oceanic boundary layers (not just their surface layers) taken as a whole are essential in the air-sea interaction issues. The variability of surface fluxes is a result of coupled atmosphere-ocean system. We can not separate the surface layer processes that directly affect air-sea interaction from the boundary layer processes in a coupled model. The boundary layer above the surface layer responses to the surface fluxes and other boundary layer forcing and modifies turbulence transport and the thermodynamic structure of the entire boundary layer, including the air-ocean interface.

The current atmospheric boundary layer parameterizations are far from adequate for the state-of-the-art operational coupled model that the navy hopes to develop. Model simulations of surface fluxes and boundary layer structure are very sensitive to different boundary layer parameterizations under the same atmospheric and oceanic conditions. This has been demonstrated in recent simulations of Japan/East Sea region using MM5 (S. Chen, personal communication). Similarly, Glendening and Doyle (1995) found an interesting positive feedback between the surface wind and heat flux through the deep boundary layer circulation in an idealized COAMPS simulation. In both cases if the boundary layer is not predicted correctly, we do not expect to get accurate surface fluxes even with the most accurate exchange coefficients. The sensitivity of surface fluxes to both boundary layers and vice versa will be inevitably amplified in a coupled model.

Research Issues: We need to understand the entire ocean and atmospheric boundary layer (i.e., not just the interfacial processes) systems in order to correctly represent the air-sea interaction in a coupled model. There have been very little systematic evaluation of the atmospheric boundary layer parameterizations used in current mesoscale models even in the uncoupled mode. At the same time we are trying to understand the physical processes directly affecting various components of air-sea interaction, we should also obtain sufficient and coherent observations from the atmospheric boundary layer, the air-sea interface, and the ocean mixed layer to allow systematic evaluation of the various surface and boundary layer parameterizations and develope improved parameterizations.

Lastly, coupling the boundary layers in a global ocean-atmosphere model is expected to improve our skill in 5-10 day forecasts. This expectation is based on many years of atmospheric and oceanic modeling that have shown that improved model initialization and model physics generally result in improved forecasts. To actually test this expectation, the Navy's research and operational centers must take the first step and actually couple an operational forecast model. Improvements can then be quantified by comparing the model against atmospheric and oceanic metrics. A successful model would also provide improved boundary conditions for higher resolution models, which would facilitate the development of a coupled mesoscale model that could be quickly set up in the desired location.

17. Remote Sensing

18. Assets for Process and Model Studies

A. Research Fleet

B. Discus Buoys

Direct observation of the air-sea interface for long periods is notoriously difficult and limited to a few specialized platforms. One of the most successful of these platforms includes the 3-m discus buoys that have been moored at various depths around the world. Surface mooring technology is used to deploy meteorological and oceanographic instrumentation from buoys to measure the key marine parameters needed to estimate the air-sea exchange of heat, freshwater and momentum. The sensors and 3-m discus buoy platforms perform reliably even in severe conditions and are typically deployed for periods of 6-9 months per setting. These buoys measure wind speed and direction, incoming short-wave radiation, incoming long-wave radiation, relative humidity, air temperature, sea temperature, barometric pressure, and precipitation. Recently, turbulence wind measurements made using a sonic anemometer deployed on a 3-m discus buoy have yielded direct covariance fluxes for extended periods.

Below the water line, instrumentation is deployed on the mooring line to monitor both physical and optical marine parameters. Data are both telemetered and recorded on board. Significant improvements in surface buoy technology and bulk flux formulae made over the last 15 years have resulted in the ability to measure monthly mean net heat flux to better than 10 Wm^{-2} (ref, 199X). Recent ONR sponsored deployments of such buoys have demonstrated their ability to perform well in severe environments such as the Arabian Sea and near the track of hurricanes in the Middle Atlantic Bight. The data are used to identify significant problems in the surface meteorology and fluxes from numerical weather predictions models and better understand the coupled air-sea boundary layer system.

Deployment of even larger discus buoys have a number of attractive features for air-sea interaction studies. These large buoys were originally developed for the NOAA National Data Buoy Center to obtain surface meteorological data in very severe conditions. Two platforms were developed: a 12-m discus buoy and a 10-m discus buoy. Advances in buoy technology and sensor design has enabled NDBC to use smaller buoys to the same effect, freeing up the large discuss buoys for new applications that require the hull surface area and large interior space of these platforms. Two of the 10-m buoys have been refurbished by researchers at SIO with funds from ONR. They are currently being use to provide a marine observational capability in southern California to test the concept of sustained multi-disciplinary measurements and real-time data communication.

In principle, the buoys can be deployed almost anywhere with radio modems replaced with broadband width satellite communications. A diesel generator provides back up power to batteries that provide 500W continuous power at 24 volts. This is sufficient for a wide array of sensors operating simultaneously. In special circumstances and for short periods, 115 volts AC is available from the 9.3kVA 12 horsepower generator. The buoys maintain an orientation into the wind using two large airfoils, which work except in the lightest winds. This ensures good exposure for sensitive instrumentation such as turbulent sensors. Two masts can support atmospheric sensors anywhere between 1 m and 10 m above sea level. In water sensors can be deployed within two 36-inch diameter wells, which connect directly with the interior laboratory space, or directly over the side of the hull. Present operations require refueling of the buoys once per year.

One major advantage is the possibility of deploying sensors for long periods to obtain statistically significant samples of the appropriate environmental conditions. The two buoys deployed by SIO have operated almost continuously for more than twelve months. Their present locations enable the collocation of other measurement systems including, wave rider buoys, subsurface sensors and atmospheric profilers.

C. Air-Sea Interaction Spar Buoy (ASIS)

The ASIS buoy provides a stable platform to measure surface fluxes and high-resolution directional wave spectra ranging in scales from centimeter waves to the dominant wind-waves interface (Graber et al. 1995; 1999a; 1999b). The buoy follows the design of a short spar. Instead of intersecting the surface as a single stout column, we use a pentagonal cage of slender cylinders arranged at a radius of ~1 m. This design concept distributes the buoyancy of the members around the perimeter rather than in a single pole, thereby providing some additional stiffness to rotational motion. The five spar elements are joined to a central spar element approximately 2 m below the mean surface, and this central spar is terminated with a drag plate. The overall length of the buoy is 13 m inclusive a mast.

This multi-column spar design is an overdamped system with increased stability to pitch and roll. Pitch and roll motions of ASIS are about one third those of a typical 3-m discus buoy. In addition, the smaller cylinder dimensions serve to reduce flow distortion in the vicinity of the buoy (Zdravkovich 1981), in contrast to the larger simple spars which have diameters of several meters. The ASIS buoy could be deployed in a moored configuration, tethered to a secondary buoy so as to isolate additional downward forces or in a drifting mode. Based on transfer functions determined from the initial deployment, it has been estimated that the buoy could be exposed to waves with significant height of 10 m, before 1% of the waves would overtop the cage. This is due to the buoy system being a surface-follower for long waves, those with periods T > 8 sec. The surface following capability of ASIS allows for the placement of equipment much closer to the surface than is possible with other platforms. It is this surface following property of ASIS which makes it valuable for near surface measurements both on the atmospheric and oceanic side.

The ASIS buoy is typically equipped with sonic anemometers and several levels of wind, temperature and humidity sensors along with an array of capacitance wave gauges mounted along the outer perimeter and interior of the buoy for measuring the directional wave spectrum. In order to make eddy correlation and wave array measurements from a nonstationary platform, the motion of the platform must be accurately recorded. The ASIS buoy is equipped with a 'strapped down' motion package located along with the data aquisition system in watertight cans at the base of the buoy. The three orthogonal components of linear acceleration are measured accelerometers, while the three components of rotational motion are measured with solid state angular rate. Since the performance of the rate gyros declines at low frequencies, low frequency (<0.04 Hz) angular motion was determined using either a compass (for yaw) or the tilt angles derived from the appropriate linear accelerometers (for pitch and roll). The high and low frequency angular motions are combined using complementary filtering. Details of the algorithms are available in Anctil *et al*. (1994) for eddy correlation and Drennan *et al*. (1994; 1998) for wave array measurements. Other waterside sensors for turbulence, void fraction, bubbles, etc. are easily mounted on the buoy's frame. Similarly, radiation sensors can easily be mounted on the mast.

The nearby tether buoy is an additional platform where instrumentation such as current meters, ADCPs, temperature strings, biological sensors, etc can be deployed. The tether buoy is capable of providing power and satellite communications for routine monitoring.

D. R/P FLIP

The Research Platform FLIP (Floating Laboratory Instrument Platform) is a unique 108m long spar buoy designed and operated by the Marine Physical Laboratory of the Scripps Institution of Oceanography. It is towed to the site of the experiment in the horizontal position and "flips" to the vertical position by flooding ballast tanks. When vertical, FLIP is quite stable. Personnel and equipment are in the 17m section above the water line. Various booms and platform space are available for the deployment of oceanographic and atmospheric sensors. Oceanographic sensors can also be mounted on the hull. FLIP can be moored or drifting, depending on the scientific needs and location, for up to about 30 days without replenishment of supplies.

FLIP has room for 16 personnel, including the crew of 5. Laboratory space can house three to four 3-bay relay racks in the main lab and a 2-bay rack in the radio room. Storage space is limited. FLIP's gyro heading can be recorded, and there is a gyro-thruster control system to maintain a set heading in conditions of low to moderate currents and winds. Transfer on and off FLIP is possible in low seas. The usual mode however is for all personnel to ride FLIP on the tow to and from the experimental site. Towing and mooring can be arranged through MPL. Use of Navy tugs greatly lowers the cost of an experiment. A view of FLIP with a meteorological mast deployed is shown in Figure 1.

E. Offshore Towers

F. Research Aircraft

Research aircraft have been used in a wide variety of atmospheric and oceanic experiments. They are limited in endurance (12 hours maximum is typical for a P3-class aircraft), but can sample a large volume of the atmosphere and/or deploy a variety of airborne expendable oceanic probes (e.g., AXBTs). For remote areas of the oceans, they are about the only way to map the vertical and horizontal structure of the marine atmospheric boundary layer. Some experiments have been run with multiple aircraft in formation to better map the atmospheric structure than just one aircraft flying in a line. Meteorological instrumentation includes dropsondes to measure the vertical profile equivalent to a balloon-borne rawindsonde over land. The addition of GPS-derived winds to the sondes gives detailed wind structure down to the ocean surface. In situ measurements include winds, turbulence, aerosols, fluxes, radiation, and cloud physics parameters in addition to the aircraft's position, speed and attitude as measured from inertial navigation units corrected with GPS. A limitation is the lower altitude of aircraft flight tracks, usually 30m in good to moderate weather in daylight. Severe weather and nighttime raises the minimum altitude to 100 m or more.

1. LongEZ

NOAA's experimental Long-EZ airplane (N3R) has been instrumented for high fidelity boundary-layer turbulence measurements. Its aerodynamic characteristics are well suited for long-duration flights. The aerodynamic configuration of the Long-EZ allows for safe low-speed and low-altitude flight within the constant flux layer. Flights around instrumented platforms (e.g., ships, buoys, R/P Flip) can be conducted to provide a necessary linkage between aircraft and surface-based measurements for assessment of air-sea exchange.

The Long-EZ relies on differential Global Positioning System (DGPS) technology that allows the measurement of position, velocity and attitude at a sampling rate of 10 Hz. The aircraft is instrumented with a suite of various sensors for the measurement of horizontal and vertical wind velocity, pressure, air temperature, humidity, and net (long and short) radiation. Fluxes of heat, moisture, momentum, and trace species can be derived through eddy correlation techniques from the data acquired by this instrument suite.

In addition to turbulence and radiation measurements, the Long-EZ can be configured for a number of remote sensing applications. In previous experiments, a pod was mounted below the airplane that housed a Ka-band radar and a laser altimeter. With two additional laser altimeters under the wings, the amplitude and slope of the sea surface can be measured. Digital cameras, visible and infrared radiometers, and other instruments that can simulate Thematic Mapper, SPOT, or other satellite measurement can be mounted on the aircraft. The precision of the GPS-based measurements of position, velocity, and attitude of the airplane that are required for turbulence measurement, also allows accurate registration of remotely sensed information.

2. CIRPAS Twin Otter

A picture of the NPS CIRPAS Twin Otter aircraft is shown in Figure 2 with instrumentation for winds and turbulence (radome and nose area), aerosol inlet (on the nose strut), and particle imaging (wing pods).

3. Aerosondes

Dropwinsondes

XBTs

19. Required Sensor, Instrument, and Platform Development

20. Suggestions for Coordinated Research Initiatives

21. References

Agrawal, Y.C. et al., 1992: Enhanced dissipation of kinetic energy beneath surface waves. *Nature*, **359**, 219-220.

Anctil, F., M.A. Donelan, W.M. Drennan and H.C. Graber, 1994: Eddy correlation measurements of air-sea fluxes from a Discus buoy. *J. Atmos. Ocean. Technol.*, **11**, 1144-1150.

Anderson, S. and A. Lohrmann, 1995: Open water test of the SonTek acoustic Doppler velocimeter. Proceedings of the *IEEE Fifth Working Conference on Current Measurement*, February 7-9, St. Petersburg Florida, 188-192.

Anderson, S. P., R. A. Weller, and R. B. Lukas, 1996: Surface buoyanycy forcing and the mixed layer of the western Pacific warm pool: Observations and 1D model results. *J. Climate*, **9**, 3056-3085.

Anderson, S. P., A. Hinton, R. A. Weller, 1998: Moored observations of precipitation temperature. *J. Atmos. Oceanic Technol.*, **15**, 979-986.

Andreas, E. L., 1990: Time constants for the evolution of sea spray droplets. *Tellus*, **42B**, 481-497.

Andreas, E. L., 1992: Sea spray and the turbulent air-sea heat fluxes. *J. Geophys. Res.*, **97**, 11,429-11,441.

Andreas, E. L., 1994: Reply. J. Geophys. Res., 99, 14,345-14,350.

Andreas, E. L., and J. DeCosmo, 1999: Sea spray production and influence on air-sea heat and moisture fluxes over the open ocean. *Air-Sea Fluxes: Momentum, Heat, and Mass Exchange*, G. Geernaert, Ed., Kluwer, Dordrecht, to appear.

Andreas, E. L., and K. A. Emanuel, 1999: Effects of sea spray on tropical cyclone intensity. Preprint volume, 23rd Conference on Hurricanes and Tropical Meteorology of the

American Meteorological Society, Dallas, TX, 10-15 January 1999, 22-25.
Andreas, E.L., J.B. Edson, E.C. Monahan, M.P. Rouault, and S.D. Smith, 1995: The spray contribution to net evaporation from the sea: A review of recent progress. *Bound.-Layer Meteor.*, **72**, 3-52.
Annis, A., and J. N. Moum, 1992: The superadiabatic surface layer of the ocean during convection. *J. Phys. Oceanogr.*, **22**, 1221-1227.
Annis, A., and J. N. Moum, 1995: Surface wave-turbulence interactions: Scaling $\epsilon(z)$ near the sea surface. *J. Phys. Oceanogr.*, **25**, 2025-2045.
Asselin, R., 1972: Frequency filter for time integration. *Mon. Wea. Rev*., **100**, 487-490.
Banner, M. L., and W. K. Melville, 1976: On the separation of air-flow over water waves. *J. Fluid Mech.*, **77**, 825-842.
Bao, J.-W., J. M. Wilczak, J.-K. Choi, and L. Kantha, 1999: Numerical simulations of air-sea interaction under high wind conditions using a coupled model: A study of hurricane development. *Mon. Wea. Rev*., to appear.
Bauer, E., S. Hasselmann, K. Hasselmann and H.C. Graber, 1992: Validation and assimilation of SEASAT altimeter wave heights using the WAM wave model. *J. Geophys. Res*., **97**, 12,671-12,682.
Beardsley, R. C., C. E. Dorman, C. A. Friehe, L. K. Rosenfeld, and C. D. Winant, 1987: Local atmospheric forcing during the Coastal Ocean Dynamics Experiment: A description of the marine boundary layer and atmospheric conditions over a Northern California upwelling region. *J. Geophys. Res.*, **92**, 1467-1488.
Belcher, S. E., and J. C. R. Hunt, 1993: Turbulent shear flow over slowly moving waves. *J. Fluid Mech.*, **251**, 109-148.
Beljaars, A.C., 1995: The parameterization of surface fluxes in large scale models under free convection. *Quart. J. Roy. Met. Soc.*, **121**, 255-270.
Bender, L.C., 1996: Modification of the physics and numerics in a third-generation ocean wave model. *J. Phys. Oceanogr.*, **13**, No. 3, 726-750.
Bender, M. A., I. Ginis and Y. Kurihara, 1993: Numerical simulations of tropical cyclone-ocean interaction with a high resolution coupled model. *J. Geophys. Res*., **98**, 23245-23263.
Blanc, T.V., 1986: The effect of inaccuracies in weather-ship data on bulk-dervied estimates of flux, stability and sea-surface roughness. *J. Atmos. Oceanic Technol.*, **3**, 12-26.
Blanchard, D. C., 1963: The electrification of the atmosphere by particles from bubbles in the sea. *Progress in Oceanography*, Vol. 1, M. Sears, Ed., MacMillan, New York, 71-202.
Blumberg A.F. and G.L. Mellor, 1987: A description of a three-dimensional coastal ocean circulation model. *Three-Dimensional Coastal Ocean Models*, Coastal Estuarine Sci., **4**, edited by N.S. Heaps, AGU, 1-16.
Bridger, A. F. C., W. C. Brick, and P. F. Lester, 1993: The structure of the marine inversion layer off the central California coast: Mesoscale conditions. *Mon. Wea. Rev.*, **121**, 335-351.
Burk, S. D. and W. T. Thompson, 1996: The summertime low-level jet and marine boundary layer structure along the California coast. *Mon. Wea. Rev.*, **124**, 668-686.
Burk, S. D., , T. Haack, and R. M. Samelson, 1999: Mesoscale simulation of supercritical, subcritical, and transcritical flow along coastal topography. *J. Atmos. Sci.*, **56**, 2780-2795.
Caldwell, D. R., and W. P. Elliott, 1971: Surface stresses produced by rainfall. *J. Phys. Oceanogr.*, **1**, 145-148.

Caldwell, D. R., and W. P. Elliott, 1972: The effect of rainfall on the wind in the surface layer. *Bound.-Layer Meteorol.*, **3**, 146-151.
Cardone, V.J. and D. Szabo, 1985: Impact of uncertainty in specification of offshore wind on accuracy of wave hindcasts and forecasts. Proc. Int. Workshop on Offshore Winds and Icing, Nova Scotia, 7-11 October, 1985. Publ. Environment Canada, Downsview, Ontario.
Cardone, V.J., H.C. Graber, R.E. Jensen, S. Hasselmann, and M. Caruso, 1995: In search of the true surface wind field in SWADE IOP-1: Ocean wave modelling perspective. *Global Atmos. Ocean Sys*., **3**(2-3), 107-150.
Cavaleri, L., L. Bertotti, and P. Lionello, 1991: Wind wave cast in the Mediterranean Sea. *J. Geophys. Res*., **96**, 10,739-10,764.
Cavaleri, L. and G.J.H. Burgers, 1992: Wind gustiness and wave growth. KNMI Afdeling Oceanografisch Onderzoek memo, OO-92-18, DeBilt, 38pp.
Chalikov, D. V., and M. Y. Belevich, 1993: One-dimensional theory of the wave boundary layer. *Bound.-Layer Meteor*., **63**, 65-96.
Chalikov, D., and V. Makin, 1991: Models of the wave boundary layer. *Bound.-Layer Meteor.*, **56**, 83-99.
Charnock, H.,1955: Wind stress on a water surface. *Quart. J.Roy. Meteor. Soc.,* **81**, 639-640.
Cherukat, P., Y. Na, T.J. Hanratty, and J.B. McLaughlin, 1998: Direct numerical simulation of a fully developed turbulent flow over a wavy wall. *Theoret. Comput. Fluid Dynam.*, **11**, 109-134.
Choi, H., P. Moin, and J. Kim, 1992: Direct numerical simulation of turbulent flow over riblets. *CTR manuscript 137*, Center for Turbulence Research Stanford University.
Cook, J., 1991: A sensitivity study of weather data inaccuracies on evaporation duct height algorithms. *Radio Science*, **26(3)**, 731-746.
Craig, P. D. and M. L. Banner, 1994: Modeling wave-enhanced turbulence in the ocean surface layer. *J. Phys. Oceanogr.*, **24**, 2546-2559.
Craig, P. D., 1996: Velocity profiles and surface roughness under breaking waves. *J. Geophys. Res*, **101**, 1265-1277.
Craik, A. D.D. and S. Leibovich, 1976: A rational model for Langmuir circulations. *J. Fluid Mech.* **73**, 401-426.
Crawford, G. B. and W. G. Large, 1996: A numerical investigation of resonant inertial response of the ocean to wind forcing. *J. Phys. Oceanogr.*, **26**, 873-891.
D'Asaro, E. A., D. M. Farmer, J. T. Osse, G. T. Dairiki, 1996: A Lagrangian Float. *J. Atmos. Oceanic Technol.*, **13**, 1230-1246
D' Asaro, E.A., and G.T. Dairiki, 1997: Turbulence intensity measurements in a wind-driven mixed layer. *J. Phys. Oceanogr*., **27**, 2009-2022.
De Angelis, V., P. Lombardi, and S. Banerjee, 1997: Direct numerical simulation of turbulent flow over a wavy wall. *Phys. Fluids*, **9**, 2429-2442.
Deardorff, J.W., 1967: Aerodynamic theory of wave growth with constant wave steepness. *J. Oceanographical Soc. Japan*, **23**:6, 278-297.
Deardorff, J.W., 1970: A numerical study of three-dimensional turbulent flow at large Reynolds's numbers. *J. Fluid Mech.*, **41**, 453-480.
DeCosmo, J., K. B. Katsaros, S. D. Smith, R. J. Anderson, W. A. Oost, K. Bumke and H. Chadwick, 1996: Air-sea exchange of water vapor and sensible heat: The Humidity

Exchange over the Sea (HEXOS) results. *J. Geophys. Res.*, **101**, 12,001-12,016.
De Leeuw, G., 1986: Vertical profiles of giant particles close above the sea surface. *Tellus*, **38B**, 51-61.
De Leeuw, G., 1986: Size distributions of giant aerosol particles close above sea level. *J. Aerosol Sci.*, **17,** 293-296.
De Leeuw, G., 1987: Near-surface particle size distribution profiles over the North Sea. *J. Geophys. Res.*, **92C,** 14631-14635.
De Leeuw, G., 1990: Profiling of aerosol concentrations, particle size distributions, and relative humidity in the atmospheric surface layer over the North Sea. *Tellus*, **42B,** 342-354.
De Leeuw, G., 1990: Comment on "Vertical distribution of spray droplets near the sea surface of jet drop ejection and surface tearing". *J. Geophys. Res*., **95**, 9779-9782.
Denbo, D.W., and E.D. Skyllingstad, 1996: An ocean large-eddy simulation model with application to deep convection in the Greenland Sea. *J. Geophys. Res*., **101**, 1095-1110.
Dillon, J.M., 1982: Vertical Overturns: A comparison of Thorpe and Ozmidov Length Scales. *J. Geophys. Res.*, **87**, 9601-9613.
Donelan, M.A, 1990: Air-Sea Interaction. *The Sea: Ocean Engineering Science*, vol. 9A, LeMehaute, B. and D.M. Hanes, eds., New York: John Wiley, 239-292.
Donelan, M. A. and W. J. Pierson, 1987: Radar scattering and equilibrium ranges in wind-generated waves with application to scatterometry. *J. Geophys. Res.*, **92**, 4971-5029.
Donelan, M.A., F.W. Dobson, S.D. Smith, and R.J. Anderson, 1993: On the dependence of sea surface roughness on wave development. *J. Phys. Oceanogr.*, **23**, 2143-2149.
Donelan, M. A., W. M. Drennan, and A. K. Magnusson, 1996: Nonstationary analysis of the directional properties of propagating waves. *J. Phys. Oceanog*., **26**, 1901-1914.
Donelan, M.A., W.M. Drennan, and E.A. Terray, 1999a: Wavenumber spectra of wind waves in the range of 1-50m. *Proc. 4th Int'l Symp. on "The Air-Sea Interface"*, Sydney, Jan. 1999.
Donelan, M. A., W. M. Drennan, and E.A. Terray, 1999b: Wavenumber spectra of wind-generated waves, (in preparation).
Dorman, C., D. Rogers, W. Nuss, and W. Thompson, 1999: Adjustment of the summer marine boundary layer around Point Sur, California. *Mon. Wea. Rev.*, in press.
Doyle, J. D., 1995: Coupled ocean wave/atmosphere mesoscale model simulations of cyclogenesis. *Tellus*, **47A**, 766-778.
Drennan, W.M., M.A. Donelan, N. Madsen, K.B. Katsaros, E.A. Terray and C.N. Flagg, 1994: Directional wave spectra from a Swath ship at sea. *J. Atmos. Ocean. Technol.*, **11**, 1109-1116.
Drennan, W. M., M. A. Donelan, E. A. Terray, and K. B. Katsaros, 1996: Oceanic turbulence dissipation measurements in SWADE. *J. Phys. Oceanogr.*, **26**, 808-815.
Drennan, W.M., H.C. Graber, M.A. Donelan and E.A. Terray, 1998: Directional wave measurements from the ASIS (Air-Sea Interaction Spar) buoy. *Proc. OCEANS98*, Nice, France, 414-418.
Edson, J. B., and C. W. Fairall, 1994: Spray droplet modeling 1. Lagrangian model simulation of the turbulent transport of evaporating droplets. *J. Geophys. Res.*, **99**, 25,295-25,311.
Edson, J. B., S. Anquentin, P. G. Mestayer and J. F. Sini, 1996: Spray droplet modeling 2. An interactive Eulerian-Lagrangian model of evaporating spray droplets. *J. Geophys. Res*., **101**, 1279-1293.
Edson, J.B., and C.W. Fairall, 1998: Similarity relationships in the marine atmospheric surface

layer for terms in the TKE and scalar variance budgets. *J. Atmos. Sci.*, **55**, 2311-2328.
Edson, J. B., A. A. Hinton, K. E. Prada, J. E. Hare, and C. W. Fairall, 1998: Direct covariance flux estimates from mobile platforms at sea. *J. Atmos. Oceanic Tech.*, **15**, 547-562
Edson, J., S. Wetzel, C. Friehe, S. Miller, and T. Hristov, 1997: Energy flux and dissipation profiles in the marine surface layer. Proceedings of the *12th Symp. on Bound. Layers and Turb.*, Amer. Meteorol. Soc., Boston, MA., 314-315.
Emanual, K. A., 1986: An air-sea interaction theory for tropical cyclones. Part I: Steady-state maintenance. *J. Atmos. Sci.*, **43,** 585-604.
Emanuel, K. A., 1991: The theory of hurricanes. *Ann. Rev. Fluid Mech.*, **23,** 179-196.
Emanuel, K. A., 1995: Sensitivity of tropical cyclones to surface exchange coefficients and a revised steady-state model incorporating eye dynamics. *J. Atmos. Sci.*, **52**, 3969-3976.
Enriquez, A. G., and C. A. Friehe, 1995: Effects of wind stress and wind stress curl variability on coastal upwelling. *J. Phys. Ocean.*, **25**, 1651-1671.
Fairall, C. W., E. F. Bradley, D. P. Rogers, J. B. Edson, and G. S. Young, 1996: Bulk parameterization of air-sea fluxes for Tropical Ocean-Global Atmosphere Coupled-Ocean Atmosphere Response Experiment. *J. Geophys. Res.*, **101**, C2, 3747-3764.
Fairall, C.W., E.F. Bradley, J.S. Gopdfrey, G.A. Wick, J.B. Edson, and G.S. Young, 1996: Cool-skin and warm-layer effects on sea surface temperature. *J. Geophys. Res.*, **101**, 1296-1308.
Fairall, C. W., J. D. Kepert, and G. J. Holland, 1994: The effect of sea spray on surface energy transports over the ocean. *Global Atmos. Ocean Sys*., **2**, 121-142.
Farmer, D. M., and D. D. Lemmon, 1984: The influence of bubbles on ambient noise in the ocean at high wind speeds. *J. Phys. Oceanogr.*, **14**, 1762-1778.
Feingold, G., B. Stevens, W.R. Cotton, and R.L. Walko, 1994: An explicit microphysics/LES model designed to simulate the Twomey Effect. *Atmos. Res.*, **33**, 207-233.
Finnigan, J.J., F. Einuadi, and D. Fua, 1984: The interaction between an internal gravity wave and turbulence in the stably-stratified nocturnal boundary layer. *J. Atmos. Sci.*, **41**, 2409-2436.
Flament, P., and M. Sawyer, 1995: Observations of the effect of rain temperature on the surface heat flux in the intertropical convergence zone. *J. Phys. Oceanogr.*, **25**, 413-419.
Frank, W. M., 1984: A composite analysis of the core of a mature hurricane. *Mon. Wea. Rev.*, **112,** 2401-2420.
Franklin, J. L., and M. DeMaria, 1992: The impact of Omega dropwinsonde observations on barotropic hurricane track forecasts. *Mon. Wea. Rev.*, **120**, 381-391.
Frenzen, P., and C. A. Vogel, 1992: The kinetic energy budget in the surface layer: A review and an experimental reexamination in the field. *Bound.-Layer Meteorol.*, **60**, 49-76.
Gathman, S. G., 1983: Optical properties of the marine aerosol as predicted by the Navy aerosol model. *Opt. Eng.*, **22**, 57-63.
Geernaert, G.L., 1990: Bulk Parameterizations for the wind stress and heat fluxes. *Surface Waves and Fluxes: Volume I - Current Theory*, G.L. Geernaert and W.L. Plant, eds., Netherlands: Kluwer Academic Publishers, 91-172.
Geernaert, G. L., K. B. Katsaros, and K. Richter, 1986: Variation of the drag coefficient and its dependence on sea state. *J. Geophys. Res., 91,* 7667-7679.
Geernaert, G.L., and Smith, J.A.: 1998, On the fetch dependent drag coefficient over coastal and inland seas. *NERI Report 227*, National Environmental Research Institute, Roskilde,

Denmark, 10 pp.
Gent, P. R., and P. A. Taylor, 1976: A numerical model of the air flow above water waves. *J. Fluid Mech.*, **77**, 105-128.
Gnanadesikan, A. , 1994: Dynamics of Langmuir cireculations in oceanic surface layers. PhD. MIT/WHOI Joint Program. WHOI Tech Rep. 94-23, 354 pp.
Godfrey, J. S. and A. C. M. Beljaars, 1991: On the turbulent fluxes of buoyancy, heat and moisture at the air-sea interface at low wind speeds. *J. Geophys. Res.*, **96**, 22043-22048.
Gong, W., P.A. Taylor, and A. Dornbrack, 1996: Turbulent boundary-layer flow over fixed aerodynamically rough two-dimensional sinusoidal waves. *J. Fluid Mech.*, **312**, 1-37.
Graber, H.C., M.J. Caruso and R.E. Jensen, 1991: Surface wave simulations during the October storm in SWADE. Proc. *MTS '91* Conf., Marine Technology Society, New Orleans, LA, 159-164.
Graber, H.C., M.A. Donelan, S. Ataktürk, W.M. Drennan and K.B. Katsaros, 1999: Marine flux-profile relations from an air-sea interaction spar buoy. *Proc. of the Air-Sea Interface Symposium*, Sydney, Australia.
Graber, H.C., E.A. Terray, M.A. Donelan, J. VanLeer and W. M. Drennan, 1995: A lightweight multi-spar buoy - Design and sea trials. Technical Report, **RSMAS 95-009**, University of Miami, 38pp.
Graber, H.C., E.A. Terray, M.A. Donelan, W.M. Drennan, J.C. Van Leer and D.B. Peters, 1999: ASIS -- a new air-sea interaction spar buoy: Design and performance at sea. *J. Atmos. Oceanic Tech.*, accepted for publication.
Grachev, A. A., Fairall, C. W. and Larsen, S. L., 1998: On the determination of the neutral drag coefficient in the convective boundary layer. *Bound. Layer Meteorol.*, **86**, 423-439.
Hare, J.E., T. Hara, J.B. Edson, and J.M. Wilczak, 1997: A similarity analysis of the structure of air flow over surface waves. *J. Phys. Oceanogr.*, **27**, 1018-1037.
Hasselmann, D. and J. Bösenberg, 1991: Field measurements of wave-induced pressure over wind-sea and swell. *J. Fluid Mech.*, **230**, 391-428.
Hasselmann, S. and Hasselmann, K., 1985: Computations and parameterizations of the nonlinear energy transfer in a gravity wave spectrum, part 1: A new method for efficient computations of the exact nonlinear transfer integral. *J. Phys. Oceanogr.*, **15**, 1369-1377.
Holland, G. J. 1997: The maximum potential intensity of tropical cyclones. *J. Atmos. Sci.*, **54,** 2519-2541.
Holt, T. R., 1996: Mesoscale forcing of a boundary layer jet along the California coast. *J. Geophys. Res.*, **101**, 4235-4254.
Holton, J. R., 1979: *An Introduction to Dynamic Meteorology*. Academic Press, 391 pp.
Hristov, T., and C. Friehe, 1999: Linear time-invariant compensation of cup anemometer inertia. *Proc. 13th Symp. on Boundary Layers and Turbulence*, Dallas, TX, AMS, Boston, MA.
Hristov, T., S. Miller, C. Friehe, J. Edson, and S. Wetzel, 1998: Structure of the atmospheric surface layer over open ocean waves: Representation in terms of phase averages. *Wind-Over-Waves Couplings: Perspectives and Prospects*, Southend-on-sea, Essex, UK, in press.
Hsu, C.-T., E.Y. Hsu, and R.L. Street, 1981: On the structure of turbulent flow over a progressive water wave: theory and experiment in a transformed, wave-following coordinate system. *J. Fluid Mech.*, **105**, 87-117.
Hsu, C.-T and E.Y. Hsu, 1983: On the structure of turbulent flow over a progressive water wave: theory and experiment in a transformed, wave-following coordinate system. Part 2. *J.*

Fluid Mech., **131**, 123-153.

Hubbert, G. D., G. J. Holland, L. M. Leslie, and M. J. Manton, 1991: A real-time system for forecasting tropical cyclone storm surges. *Wea. Forecasting,* **6,** 86-97.

Hwang, P. A., D. W-C. Wang, E. J. Walsh, W. B. Krabill, and R. N. Swift, 1999: Directional wavenumber spectra of ocean surface waves. Part 1. Spectral slope and dimensionless spectral coefficient. (Submitted to *J. Phys. Oceanog.*).

Janssen, P. A. E. M., 1989: Wave induced stress and the drag of the air flow over sea waves. *J. Phys. Oceanogr.*, **19**, 745-754.

Janssen, P.A.E.M., 1991: Quasi-linear theory for wind-wave generation applied to wave forecasting. *J. Phys. Oceanogr.*, **21**, 1631-1642.

Janssen, P.A.E.M., 1994: Results with a coupled wind wave model. ECMWF Res. Dept. Techn. Rep. 71, ECMWF, Reading, 58pp.

Janssen, P. A. E. M., 1999: On the effect of ocean waves on the kinetic energy balance and consequences for the inertial dissipation technique. *J. Phys. Oceanogr.*, **29**, 530–534.

Janssen, P.A.E.M., G.J. Komen, and W.J.P. de Voogt, 1984. An operational coupled hybrid wave prediction model. *J. Geophys. Res.*, **89**(C3), 3635-3654.

Janssen, P.A.E.M., P. Lionello, M. Reistad, and A. Hollingsworth, 1989: Hindcasts and data assimilation studies with the WAM model during the Seasat period. *J. Geophys. Res.*, **94**(C1), 973-993.

Janssen, P. A. E. M., B. Hansen, and J.-R. Bidlot, 1997: Verification of the ECMWF wave forecasting system against buoy and altimeter data. *Wea. Forecasting*, **12**, 763-784.

Jeffreys, H., 1924: On the formation of waves by wind. *Proc. Roy. Soc. London, Ser. A*, **107**, 189-206.

Jeffreys, H., 1925: On the formation of waves by wind. II. *Proc. Roy. Soc. London, Ser. A*, **110**, 341-.

Jerlov, N. G., 1968: *Optical Oceanography*. Elsevier, 194pp.

Jerlov, N. G., 1976: *Marine Optics*. Elsevier, 229pp.

Jessup, A. T., C. J. Zappa, and H. H. Yeh, 1997: Defining and quantifying microscale wave breaking with infrared imagery. *J. Geophys. Res*., in press.

Johnson, H. K., and H. J. Vested, 1992: Effects of water waves on wind shear stress for current modeling. *J. Atmos. Oceanic Tech.,* **9**, 850-861.

Johnson, H. K., J. Højstrup, H. J. Vested, and S. E. Larsen, 1998: On the dependence of sea surface roughness on wind waves. *J. Phys. Oceanogr.*, **28**, 1702-1716.

Kahma, K. K. and M .A. Donelan, 1987: Laboratory studies of the minimum wind speed for wave generation. *J. Fluid Mech*.

Kaimal, J.C., J.C. Wyngaard, Y. Izumi, and O.R. Coté, 1972: Spectral characteristics of surface-layer turbulence. *Quart. J. Roy. Meteor. Soc.*, **98**, 563-589.

Källstrand, B. and A.-S. Smedman, 1997: A case study of the near-neutral coastal internal boundary-layer growth: Aircraft measurements compared with different model estimates. *Bound. Layer Meteorol.*, **85**, 1-33.

Kantha, L.H. and C.A. Clayson, 1994: An improved mixed layer model for geophysical applications. *J. Geophys. Res*., 99, **25**, 235-25,266.

Katsaros, K. B., J. DeCosmo, R. J. Lind, R. J. Anderson, S. D. Smith, R. Kraan, W. Oost, K. Uhlig, P. G. Mestayer, S. E. Larsen, M. H. Smith, and G. de Leeuw, 1994: Measurements of humidity and temperature in the marine environment during the HEXOS Main Experiment. *J. Atmos. Oceanic Technol.*, **11**, 964-981.

Kepert, J.D., and C.W. Fairall, 1999: Modelling the interaction between the atmospheric boundary layer and evaporating sea spray droplets. Presented at *13th Conference on Boundary Layers and Turbulence,* Dallas, Texas, Jan 10 - 15 1999.

Kepert, J.D., C.W. Fairall and J-W Bao, 1999: Modelling the interaction between the atmospheric boundary layer and evaporating sea spray droplets. In *Air-Sea Fluxes of Momentum, Heat and Chemicals.* ed Gary Geernaert. Kluwer. To appear.

Kahma, K.K. and M.A. Donelan, 1988: A laboratory study of the minimum wind speed for wind wave generation. *J. Fluid Mech.*, **192**, 339-364.

Klemp, J. and D. Durran, 1983: An upper boundary condition permitting internal gravity wave radiation in numerical mesoscale models. *Mon. Wea. Rev*., **111**, 430-444.

Komen, G.J., S. Hasselmann and K. Hasselmann, 1984: On the existence of a fully developed wind-sea spectrum. *J. Phys. Oceanogr*., **14**, 1271-1285.

Komen, G.J., Cavaleri, L., Donelan, M., Hasselmann, K., Hasselmann, S., and Janssen, P.A.E.M., 1994: *Dynamics and Modelling of Ocean Waves,* Cambridge University Press.

Konstanzer, G. C., 1996: Sensitivity of AN/SPY-1B propagation to evaporation duct heights. JHU/APL Tech. Rep. F2F-94-U-4-012, 34 pp.

Kraus, E.B. and J.S. Turner, 1967: A one-dimensional model of the seasonal thermocline. II. The general theory and its consequences. *Tellus*, **19**, 98-105.

Kraus, E.B. and J. A. Businger, 1994: *Atmosphere-Ocean Interaction*. Oxford University Press, 362 pp.

Krettenauer, K and U. Schumann, 1992: Numerical simulation of turbulent convection over wavy terrain. *J. Fluid Mech.*, **237**, 261-299.

Kurihara, Y., R. E. Tuleya, and M. A. Bender, 1998: The GFDL hurricane prediction system and its performance in the 1995 hurricane system. *Mon. Wea. Rev.,* **126,** 1306-1322.

Large, W. G., and S. Pond, 1981: Open ocean momentum flux measurements in moderate to strong winds. *J. Phys. Oceanogr.,* **11**, 324-336.

Large, W.G., and P.R. Gent, 1999: Validation of vertical mixing in an equatorial ocean model using large eddy simulations and observations. *J. Phys. Oceanogr*., **29**, 449-464.

Large, W. G., J.C. McWilliams, and S.C. Doney, 1994. Oceanic vertical mixing: A review and a model with a nonlocal boundary layer parameterization. *Rev. Geophys*. **32**, 363-403.

Lesieur, M and O. Métais, 1996: New trends in large-eddy simulations of turbulence, *Annu. Rev. Fluid Mech.*, **28**, 45-82.

Levy, G. and D. Vickers, 1999: Surface fluxes from satellite winds: Modeling air-sea flux enhancement from spatial and temporal observations. To appear in *J. Geophys. Res*.

Lewis, M. R., J. J. Cullen and T. Platt. 1983: Phytoplankton and thermal structure in the upper ocean: consequences of nonuniformity in chlorophyll profile. *J. Geophys. Res*., **88**, 2565-2570.

Lewis, M. R., M.-E. Carr, G.C. Feldman, W Esaias and C. McClain. 1990: Influence of penetrating soar radiation on the heat budget of the equatorial Pacific Ocean, *Nature*, **347**, 543-544.

Li, M. and C. Garrett, 1997: Mixed layer deepening due to Langmuir circulation. *J. Phys. Ocean.*, **27**, 121-132.

Lin, C.-L., J.C. McWilliams, C.-H. Moeng, and P. P. Sullivan, 1996: Coherent structures and dynamics in a neutrally stratified planetary boundary layer flow. *Phys. Fluids,* **8**, 2626-2639.

Lin, R.Q. and Huang, N.E., 1996: The Goddard coastal wave model. Part I: Numerical method. *J. Phys. Oceanogr.,* **26**, No. 6, 833-847.
Lin, R.Q., Perrie, W. and Huang, N.E., 1997: A new coastal wave model. Part III. Nonlinear wave-wave interaction. *J. Phys. Oceanogr.*
Ling, S. C., 1993: Effect of breaking waves on the transport of heat and water vapor fluxes from the ocean. *J. Phys. Oceanogr.*, **23**, 2360-2372.
Lionello, P., P. Malguzzi, and A. Buzzi, 1998: Coupling between the atmospheric circulation and the ocean wave field: An idealized case. *J. Phys. Oceanogr.*, **28**, 161-177.
Lionello, P., K. Hasselmann, and G.L. Mellor, 1996: On the coupling between a surface wave model and a model of the mixed layer in the ocean. *The Air-Sea Interface: Radio and Acoustic Sensing, Turbulence and Wave Dynamics*, M.A. Donelan, W. H. Hui and W.J. Plant, Eds, University of Toronto Press, 195-201.
Liu, W. T., K. B.Katsaros, and J. A. Businger, 1979: Bulk parameterization of air-sea exchanges of heat and water vapor including the molecular constraints at the interface. *J. Atmos. Sci.*, **36**, 1722-1735.
Louis, J. F., 1979: A parametric model of vertical eddy fluxes in the atmosphere. *Bound.-Layer. Meteor.*, **17**, 187-202.
Lumley, J. L., and H. A. Panofsky, 1964: *The Structure of Atmospheric Turbulence*. J. Wiley and Sons, 229 pp
Lynch, D.R., J.T.C. Ip, C.E. Naimie, F.E. Werner, 1996. Comprehensive coastal circulation model with application to the Gulf of Maine. *Continental Shelf Res.*, **16**, 875-906.
Maass, C. and U. Schumann, 1994: Numerical simulation of turbulent flow over a wavy boundary. *Proc. First ERCOFTAC Workshop on Direct and Large-Eddy Simulation*, 287-297.
Makin, V. K., 1998: Air-sea exchange of heat in the presence of wind waves and spray. *J. Geophys. Res.*, **103**, 1137-1152.
Makin, V.K., V.N. Kudryavtsev, and C. Mastenbroek, 1995: Drag of the sea surface. *Bound. Lay. Meteor.*, **73**, 159-182.
Mahrt, L., and J. Sun, 1995: The subgrid velocity scale in the bulk aerodynamic relationship for spatially averaged scalar fluxes. *Mon. Wea. Rev.*, **123**, 3032-3041.
Mahrt, L., D. Vickers, J. Edson, J. Sun, J. Højstrup, J. Hare and J. Wilczak, 1998: Heat flux in the coastal zone. *Bound. Layer Meteorol.*, **86**, 421-446.
Marmorino, G. O., and C. L. Trump, 1996: High-resolution measurements made across a tidal intrusion front. *J. Geophys. Res.*, **101**, 25661-25674.
Mastenbroek, C., G. Burgers, and P.A.E.M. Janssen, 1993: The dynamical coupling of a wave model and a storm surge model through the atmospheric boundary layer. *J. Phys Oceanogr*., **23,** 1856-1866.
Mastenbroek, C., V.K. Makin, M.H. Garat, and J.P. Giovanangeli, 1996: Experimental evidence of the rapid distortion of turbulence in the air flow over water waves. *J. Fluid Mech.,* **318**, 273-302.
McWilliams, J.C., C-H. Moeng, and P. P. Sullivan, 1999: Turbulent fluxes and coherent structures in marine boundary layers: Investigations by large-eddy simulation. *Air-Sea Exchange: Physics, Chemistry, Dynamics, and Statistics*, G. Geernaert, ed. in press.
McWilliams, J.C., P.P. Sullivan, and C-H. Moeng, 1997: Langmuir turbulence in the ocean. *J. Fluid Mech.*, **334**, 1-30.

McWilliams, J.C., P.C. Gallacher, C.-H. Moeng, and J.C. Wyngaard, 1993: Modeling the oceanic planetary boundary layer. *Large-Eddy Simulations of Turbulent Flows, Lecture Notes in Engineering*, Cambridge University Press, 441-454.

Mellor, G.L. and T. Yamada, 1982. Development of a turbulent closure model for geophysical fluid problems. *Rev. of Geophys. and Space Phys*, **20**, 851-875.

Melville, W. K., 1977: Wind stress and roughness length over breaking waves. *J. Phys. Oceanogr.*, **7**, 702-710.

Mestayer, P.G., A.M.J. Van Eijk, G. De Leeuw, and B. Tranchant, 1996: Numerical simulation of the dynamics of sea spray over the waves. *J. Geophys. Res.*, **101**, 20771-20797.

Miles, J. W., 1957: On the generation of surface waves by shear flows. *J. Fluid Mech.*, **3**, 185-204.

Miller, S. D., 1998: The Structure of Turbulent and Wave-Induced Wind Fields Over Open Ocean Wave, Ph.D. Thesis, University of California, Irvine, Department of Mechanical and Aerospace Engineering, 221 pp.

Moeng, C.-H., 1984: A large-eddy-simulation model for the study of planetary boundary-layer turbulence. *J. Atmos. Sci.*, **41**, 2052-2062.

Moeng, C.-H. and J.C. Wyngaard, 1989: Evaluation of turbulent transport and dissipation closures in second-order modeling. *J. Atmos. Sci.*, **46**, 2311-2330.

Moeng, C.-H. and P. P. Sullivan, 1994: A comparison of shear- and buoyancy-driven planetary boundary layer flows. *J. Atmos. Sci.*, **51**, 999-1022.

Moeng, C.-H., P. P. Sullivan, and B. Stevens, 1999: Including radiative effects in an entrainment-rate formula for buoyancy-driven PBLs. *J. Atmos. Sci.*, **56**, 1031-1049.

Moin, P. and K. Mahesh, 1998: Direct numerical simulation: A tool in turbulence research. *Annu. Rev. Fluid Mech.*, **30**, 539-578.

Monahan, E. C., D. E. Spiel and K. L. Davidson, 1986: A model of marine aerosol generation via whitecaps and wave disruption. *Oceanic Whitecaps and Their Role in Air-Sea Exchange*, E. C. Monahan and G. Mac Niocaill, Eds., D. Reidel, Dordrecht, 167-174.

Monin, A.S., and Obukhov, A.M., 1954: Basic laws of turbulent mixing in the surface layer of the atmosphere. *Tr. Akad. Nauk SSSR, Geofiz Inst.*, **151**, 163-87.

Munk, W. H. and M. A. Traylor, 1947: Refraction of ocean waves: A process linking underwater topography to beach erosion. *J. of Geology*, **55**, 1-26.

Nieuwstadt, F.T.M., P.J. Mason, C-H. Moeng, and U. Schumann, 1993: Large-eddy simulation of the convective boundary layer: A comparison of four computer codes. *Turbulent Shear Flows*, **8**, Durst et al. (eds.), Springer-Verlag, 431 pp.

Nordeng, T. E., 1991: On the wave age dependent drag coefficient and roughness length at sea. *J. Geophys. Res*, **96**, 7167-7174.

O' Brien, J.J., 1970. A note on the vertical structure of the eddy exchange coefficient in the planetary boundary layer. *J. Atmos. Sci.*, **27**, 1213-1215.

Obukhov, A.M., 1946: Turbulence in an atmosphere with a non-uniform temperature. *Tr. Akad. Nauk.USSR, Inst. Teoret. Geofiz*, **1**. Translated and published in *Bound.-Layer Meteor.*, **2**, 7-29, 1971.

Oncley, S. P., C. A. Friehe, J. C. Larue, J. A. Businger, E. C. Itsweir, and S. S. Chang, 1996: Surface-layer fluxes, profiles, and turbulence measurements over uniform terrain under near-neutral conditions. *J. Atmos. Sci*, **53**, 1029-1044.

Ooyama, K., 1969: Numerical simulation of the life-cycle of tropical cyclones. *J. Atmos. Sci.*,

26, 3-40.
Overland, J. E., 1984: Scale analysis of marine winds in straits and along mountainous coasts. *Mon. Wea. Rev.*, **112**, 2530-2534.
Pacanowski, R.C., and S.G.H. Philander, 1981: Parameterization of vertical mixing in numerical models of the tropical oceans. *J. Phys. Oceanogr.*, **11**, 1443-1451.
Paluszkiewicz, T., and R. D. Romea, 1997: A one-dimensional model for the parameterization of deep convection in the ocean. *Dyn. Atmos. Oceans,* **13**, 513-547.
Panofsky, H. A., and J. A. Dutton, 1984: *Atmospheric Turbulence*. J. Wiley and Sons, 397 pp.
Perrie, W. and Toulany, B., 1990: Fetch relations for wind-generated waves as a function of wind-stress scaling. *J. Phys. Oceanogr.*, **20**, 1666-1681.
Phillips, O. M., 1977: *The Dynamics of the Upper Ocean*, 2d. Ed., Cambridge University Press, 336 pp.
Pickard, G. L., and W. J. Emery, 1990: *Descriptive Physical Oceanography: An Introduction*. Pergamon Press, 320 pp.
Plant, W. J., 1982: A relationship between wind stress and wave slope. *J. Geophys. Res,* **87**, 1961-1967.
Plueddemann, A.J., J.A. Smith, D.M. Farmer, R.A. Weller, W.R. Crawford, R. Pinkel, S. Vagle and A. Gnanadesikan, 1996: Structure and variability of Langmuir circulation during the Surface Wave Processes Program. *J. Geophys. Res.*, **101** (C2), 3525-3543.
Pollard, R.T., 1977. Obserfations and theories of Langmuir circulations and their role in near surface mixing. In *A voyage of discovery: George Deacon 70th Anniversary,* Volume, M. Angel, Eds. Pargamon, 235-251.
Powers, J.G., and M.T. Stoelinga, 1999: A coupled air-sea mesoscale model: Experiments in atmospheric sensitivity to marine roughness. Submitted to: *Mon. Weather Rev.*
Price, J., R. Weller and R. Pinkel, 1986: Diurnal Cycling: Observations and Models of Upper Ocean Response to Diurnal Heating, Cooling and Wind Mixing., *J. Geophys. Res.,* **91**, 8411-8427.
Ramp, S. R., R.W. Garwood, C.O. Davis and R.L. Snow. 1991: Surface heating and patchiness in the coastal ocean off central California during a wind relaxation event, *J. Geophys. Res.* **96(C8)**, 14,637-12,647.
Resio, D.T., 1993: Full boltzmann discrete spectral wave model, implementation and nondimensional tests. Contract Report **CERC-93-1**, USAE Waterways Experiment Station, Vicksburg, MS.
Rogallo, R.S. and P. Moin, 1984: Numerical simulation of turbulent flows. *Annu. Rev. Fluid Mech.*, **16**, 99-137.
Rogers, D. P. *et al.*, 1998: Highlights of Coastal Waves 1996. *Bull. Amer. Meteor. Soc.*, **79**, 1307-1326.
Romeiser, R., 1993: Global validation of the wave model WAM over a one-year period using GEOSAT wave height data. *J. Geophys. Res*., **98**, 4713-4726.
Rosenthal, S.L., 1971: The response of a tropical cyclone model to variations in boundary layer parameters, initial conditions, lateral boundary conditions and domain size. *Mon. Wea. Rev.*, **99**, 767-777.
Rotunno, R., and K. A. Emanuel, 1987: An air-sea interaction theory for tropical cyclones. Part II. *J. Atmos. Sci*., **44**, 542-561.
Samelson, R.M., 1992: Supercritical marine-layer flow along a smoothly varying coastline. *J.*

Atmos. Sci., **49**, 1571-1584.
Sanford, T. B., and R.-C. Lien, 1999: Turbulent properties in a homogeneous tidal bottom boundary layer. *J. Geophys. Res.*, **104**, 1245-1257.
Sathyendranath, S, A. D. Gouveia, S. R. Shetye, P. Ravindran, and T. Platt. 1991: Biological control of surface temperature in the Arabian Sea. *Nature*, **349**, 54-56.
Shay, L. K., 1999. Near-inertial wave energy flux forced by Hurricane Gilbert. *J. Phys. Oceanogr.*, submitted.
Siegal, D. A., J. C. Ohlmann, L. Washburn, R. R. Bidigare, G. T. Nosse, E. Fields, and Y. Zhou, 1995: Solar radiation, phytoplankton pigments and the radiant heating of the equatorial Pacific warm pool. *J. Geophys. Res.*, **100**, 4885-4891.
Skyllingstad, E.D. and D.W. Denbo, 1995: An ocean large eddy simulation of Langmuir circulations and convection within the surface mixed layer. *J. Geophys. Res.*, **100**, 8501-8522.
Skyllingstad, E. D., T. Paluszkiewicz, D. W. Denbo, and W. D. Smyth, 1996: Nonlinear vertical mixing processes in the ocean: modeling and parameterization. *Physica D*, **98**, 574-593.
Skyllingstad, E.D., W.D. Smyth, J.N. Moum, and H. Wijesekera, 1999: Upper-ocean turbulence during a westerly wind burst: A comparison of large-eddy simulation results and microstructure measurements. *J. Phys. Oceanogr.*, **29**, 5-28.
Skyllingstad, E.D., W.D. Smyth, and W.G. Crawford, 1999: Resonant wind-driven mixing in the ocean boundary layer. *J. Phys. Oceanogr.*, submitted.
Smagorinsky, J.,1963: General circulation experiments with the primitive equations. I. The basic experiment. *Mon. Wea. Rev.*, **91**, 99-164.
Smedman, A.-S. And C. Johansson, 1997: Modifications of Monin-Obukhov theory in unstable conditions. Proceedings of the *12th Symp. on Bound. Layers and Turb.*, Amer. Meteorol. Soc., Boston, MA., 283-284.
Smedman, A-S., Bergström, H. and Högström, U., 1995: Spectra, variances and length scales in a marine stable boundary layer dominated by a low level jet. *Bound. Layer Meteorol.*, **76**, 211-232.
Smith, S. D., 1988: Coefficients for sea surface wind stress, heat flux, and wind profiles as a function of wind speed and temperature. *J. Geophys. Res.*, **93**, 15467-15472.
Smith, S.D. and E.G. Banke, 1975: Variation of the sea surface drag coefficient with wind speed. *Quart. J. Roy. Meteor. Soc.*, **101**, 665-673.
Smith, S. D., 1980: Wind stress and heat flux over the ocean in gale force winds. *J. Phys. Oceanogr.*, **10**, 709-726.
Smith, S. D., R. J. Anderson, W. A. Oost, C. Kraan, N. Maat, J. DeCosmo, K. B. Katsaros, K. L. Davidson, K. Bumke, L. Hasse, and H. M. Chadwick, 1992: Sea surface wind stress and drag coefficients: The HEXOS results. *Bound.-Layer Meteor.*, **60**, 109-142.
Snyder, R.L., F.W. Dobson, J.A. Elliot, and R.B. Long, 1981: Array measurements of atmospheric pressure fluctuations above surface gravity waves. *J. Fluid Mech.*, **102**, 1-59.
Song, Y. and D.B. Haidvogel, 1994: A semi-implicit ocean circulation model using a generalized topography following coordinate system. *J. Comput. Phys.*, **115**, 228-244.
Stull, R. B., 1988: *An Introduction to Boundary Layer Meteorology*. Kluwer Academic Publishers, 666 pp.
Sullivan, P.P., J.C. McWilliams, and C.-H. Moeng, 1994: A subgrid-scale model for large-eddy simulation of planetary boundary-layer flows. *Bound.-Layer Meteor.*, **71**, 247-276.
Sullivan, P.P., J.C. McWilliams, and C.-H. Moeng, 1996: A grid nesting method for large-eddy

simulation of planetary boundary-layer flows. *Bound.-Layer Meteor*., **80**, 167-202.
Sullivan, P. P., C.-H. Moeng, B. Stevens, D. H. Lenschow, and S. D. Mayor, 1998: Structure of the entrainment zone capping the convective atmospheric boundary layer. *J. Atmos. Sci*., **55**, 3042-3064.
Sullivan, P.P., J.C. McWilliams, and C.-H. Moeng, 1999: Simulation of turbulent flow over idealized water waves. submitted to *J. Fluid Mech*.
Terray, E.A., M.A. Donelan, Y.C. Agrawal, W.M. Drennan, K.K. Kahma, A,J. Williams III, P.A. Hwang, and S.A. Kitaigorodskii, 1996: Estimates of kinetic energy dissipation under breaking waves. *J. Phys. Oceanogr.*, **26**, 792-807.
The WAMDI Group: Hasselmann, S., K. Hasselmann, E. Bauer, P.A.E.M. Janssen, G.J. Komen, L. Bertotti, P. Lionello, A. Guillaume, V.C. Cardone, J.A. Greenwood, M. Reistad, L. Zambresky and J.A. Ewing, 1988: The WAM model - a third generation ocean wave prediction model. *J. Phys. Oceanogr*., **18**, 1775-1810.
Thompson, W. T., T. Haack, J. D. Doyle, and S. D. Burk, 1997: A nonhydrostatic mesoscale simulation of the 10-11 June 1994 coastally trapped wind reversal. *Mon. Wea. Rev*., **125**, 3211-3230.
Thorpe, S.A., 1997: Interactions between internal waves and bounadary layer vortices. *J. Phys. Ocean.*, **27**, 62-71.
Thorpe, S. A., P. Bowyer, and D. K. Woolf, 1997: Some factors affecting the size distributions of oceanic bubbles. *J. Phys. Oceanogr.*, **22**, 382-389.
Tolman, H.L., 1992: Effects of numerics on the physics in a third-generation wind-wave model. *J. Phys. Oceanogr.*, **22**, No. 10, 1095-1111.
Townsend, A. A., 1972: Flow in a deep turbulent boundary layer over a surface distorted by water waves. *J. Fluid Mech*., **55**, 719-735.
Troen, I.B., and L. Mahrt, 1986: A simple model of the atmospheric boundary layer; Sensitivity to surface evaporation. *Bound.-Layer Meteorol.,* **37**, 129-148.
Trowbridge, J. H. 1998: On a technique for measurement of turbulent shear stress in the presence of surface waves. *J. Atmos. Oceanic Technol.,* **15**, 290-298.
Tuleya, R.E., 1994: Tropical storm development and decay: sensitivity to surface boundary conditions. *Mon. Wea. Rev.,* **122**, 291-304.
Uang, C.-L., 1999: Impacts of sea spray and oceanic response on the development of tropical cyclones. Preprint volume, 23rd Conference on Hurricanes and Tropical Meteorology of the American Meteorological Society, Dallas, TX, 10-15 January 1999, 30-31.
Vickers, D. and L. Mahrt, 1997: Fetch limited drag coefficients over shallow water. *Bound.-Layer Meteorol.*, **89**, 53-79.
Vickers, D. and L. Mahrt, 1999: A gleam in the authors eyes. To appear somewhere.
Vickers, D. and S. K. Esbensen, 1998: Subgrid surface fluxes in fair weather conditions during TOGA COARE: Observational estimates and parameterization. *Mon. Wea. Rev*., **126**, 620-633.
Volkov, Y. A., 1969: The spectra of velocity and temperature fluctuations in the airflow above the agitated sea surface. *Izv. Atmos. Ocean. Phys.,* **5**, 723-730.
Wallace, J. M., and P. V, Hobbs, 1977: *Atmospheric Science*. Academic Press, 467 pp.
Walsh, E. J., D. W. Hancock, D. E. Hines, R. N. Swift, and J. F. Scott, 1985: Directional wave spectra measured with the surface contour radar. *J. Phys. Oceanog.*, **15**, 566-592.
Wang, D., W.G. Large, and J.C. McWilliams, 1996: Large-eddy simulation of the equatorial ocean boundary layer: Diurnal cycling, eddy viscosity, and horizontal rotation. *J.*

Geophys. Res., **101**, 3649-3662.
Wang, D., J.C. McWilliams, and W.G. Large, 1998: Large-eddy simulation of the diurnal cycle of deep equatorial turbulence. *J. Phys. Oceanogr*., **28**, 129-148.
Wang, Y., J. D. Kepert and G. J. Holland, 1999: The impact of sea spray evaporation on tropical cyclone intensifcation. Preprint volume, 23rd Conference on Hurricanes and Tropical Meteorology of the American Meteorological Society, Dallas, TX, 10-15 January 1999, 26-29.
Weber, S.L., 1991: Bottom friction for windsea and swell in extreme depth-limited situations. *J. Phys. Oceanogr.,* **21**, 149-172.
Weber, S.L., H. von Storch, P. Viterbo, and L. Zambresky, 1993: Coupling an ocean wave model to an atmospheric general circulation model. *Clim. Dyn*. **9**, 63-69.
Weller, R.A., J.P. Dean, J. Marra, J.F. Price, E.A. Francis and D.C. Boardman, 1985: Three-Dimensional flow in the upper ocean. *Science*, **227**, 1552-1556.
Weller, A.R. and J.F. Price, 1988: Langmuir circulation within the oceanic mixed layer. *Deep-Sea Research*, **35** (5), 711-747.
Weller, R. A., and S. P. Anderson, 1996: Surface meteorology and air-sea fluxes in the western equatorial Pacific warm pool during TOGA Coupled Ocean-Atmosphere Response Experiment. *J. Climate*, **9**, 1959-1990.
Wetzel, S.W., 1996: An investigation of wave-induced momentum flux through phase averaging of open ocean wind and wave fields. *M.S. Thesis*, Massachusetts Institute of Technology, Cambridge, MA and the Woods Hole Oceanographic Institution, Woods Hole, MA, **93**.
Wittmann, P.A. and R.M. Clancy, 1995: Operational wave forecasting at Fleet Numerical Meteorology and Oceanography Center. 4^{th} Int. Workshop on Wave Hindcasting and Forecasting, Banff, Alberta, Canada, 335-343.
Wijesekera, H. W., C. A. Paulson, and A. Huyer, 1999: The effect of rainfall of the surface layer during a westerly wind burst in the western equatorial pacific. *J. Phys. Oceanogr.*, **29**, 612-632.
Woolf, D. K., E. C. Monahan and D. E. Spiel, 1988: Quantification of the marine aerosol produced by whitecaps. Preprint volume, Seventh Conference on Ocean-Atmosphere Interaction of the American Meteorological Society, Anaheim, CA, 31 January - 5 February 1988, 182-185.
Wu, J., 1975: Wind induced drift currents. *J. Fluid Mech.*, **68**, 49-70.
Wu, J., 1990: Vertical distribution of spray droplets near the sea surface: Influence of jet drop ejection and surface tearing. *J. Geophys. Res.*, **95,** 9775-9778.
Wu, X. and R.A. Flather, 1992: Hindcasting waves using a coupled wave-tide-surge model. Third Int. Workshop on Wave Hindcasting and Forecasting., Montreal, Quebec, 19-22 May; Environment Canada, Ontario, 159-170.
Wyngaard, J.C., 1984: Large-eddy simulation: Guidelines for its application to planetary boundary layer research. U.S. Army Research Office Contract 0804, 122 pp.
Zang, Y., R.L. Street, and J. R. Koseff, 1994: A non-staggered grid, fractional step method for time-dependent incompressible Navier-Stokes equations in curvilinear coordinates. *J. Comput. Phys.*, **114**, 18-33.
Zdravkovich, M.M., 1981: Review and classification of various aerodynamic and hydrodynamic means for suppressing vortex shedding. *J. Wind Eng. Industr. Areodyn*., **7**, 145-189.
Zemba, J., and C.A. Friehe, 1987: The marine atmospheric boundary layer jet in the Coastal Ocean Dynamics Experiment. *J. Geophys. Res.*, **92**, 1489-1496.